Review

Low Molecular Weight Fluorescent Probes (LMFPs) to Detect the Group 12 Metal Triad

Ashley D. Johnson, Rose M. Curtis and Karl J. Wallace *

The Department of Chemistry and Biochemistry, The University of Southern Mississippi, Hattiesburg, MS 39406, USA; Ashleydjohnson@usm.edu (A.D.J.); Rose.curtis@usm.edu (R.M.C.)
* Correspondence: karl.wallace@usm.edu; Tel.: +1-601-266-4715

check for
updates

Abstract: Fluorescence sensing, of d-block elements such as Cu^{2+}, Fe^{3+}, Fe^{2+}, Cd^{2+}, Hg^{2+}, and Zn^{2+} has significantly increased since the beginning of the 21st century. These particular metal ions play essential roles in biological, industrial, and environmental applications, therefore, there has been a drive to measure, detect, and remediate these metal ions. We have chosen to highlight the low molecular weight fluorescent probes (LMFPs) that undergo an optical response upon coordination with the group 12 triad (Zn^{2+}, Cd^{2+}, and Hg^{2+}), as these metals have similar chemical characteristics but behave differently in the environment.

Keywords: chemosensors; fluorescence; recognition; sensing; group 12 metals (zinc; cadmium; and mercury)

1. Introduction

Sensors are used in every aspect of modern life; for example, many modern households have a carbon monoxide sensor or a smoke detector installed. In industry, fiber-optic sensors are used for monitoring process variables, such as temperature, pressure flow, and the level of a liquid. The environment requires sensors to monitor toxic gases and air pollution, and in clinical applications for the detection of medical conditions, i.e., Type 1 diabetes.

The field of sensor technology has rapidly been expanding over the last several decades, and the field can be categorized into two broad areas (1) chemical sensors and (2) biosensors. Chemical sensors measure, monitor, and identify chemical compounds, whereas biosensors combine a biological component, for example, microorganisms, tissue, cells, organelles, nucleic acids, enzymes, or antibodies [1]. Both types of sensors have the same purpose; to measure an analyte, either qualitatively or quantitatively. Some excellent reviews have covered recent advances in biosensors, and these have been omitted in this article [2–14].

The word sensor has become more ambiguous over time, and there is no universal definition of the term chemical sensor; the term is highly debated in the scientific community. Therefore, there has been much confusion over the two broad definitions of "chemical sensors" and "biosensor." One definition states that "chemical sensors are miniaturized devices which can deliver real-time and online information in the presence of a specific compound or ions in complex samples" [15]. This definition itself is not concise, as the term device is also unclear. Interestingly, the International Union of Pure and Applied Chemistry (IUPAC) does not have a specific definition of "chemical sensor" defined in the Compendium of Chemical Terminology: "Gold Book" [16]. The term "biosensor" is also broad, but the IUPAC does define a biosensor "as a device that uses specific biochemical reactions mediated by isolated enzymes, immune systems, tissues, organelles or whole cells to detect chemical compounds usually by electrical, thermal or optical signals" [16].

The focus of this review is to highlight how Low Molecular Weight Fluorescent Probes (LMFP), act as chemical sensors. These molecules are defined as a small organic or inorganic molecule that has a molecular weight that is no more than a 1,000 Daltons [17]. The molecules are used to monitor metal ions (chemical analytes). Sensors that contain any biological component as defined by IUPAC or containing proteins and amino acids as part of the receptor (the device) unit are not considered, as the authors argue that a molecular receptor containing a "biological" component should be considered to be a biosensor.

Based on our interpretation of a chemical sensor described above, chemical sensors can be described as devices that convert the response into a measurable signal, which can either be related to the concentration of the analyte [18] or provide a binary "on" or "off" signal [15]. The signal can be a change in magnetic or electrical fields [19], resistance [20], capacitance [21], inductance [22], frequency [23] or optical response [24]. Monitoring and measuring metal ions can be carried out using analytical techniques, including atomic absorption spectroscopy (AAS) [25], atomic emission spectroscopy (AES) [26], inductively coupled plasma mass spectrometry (ICP-MS) [27], electrochemical techniques [28], surface plasmon resonance [29], and X-ray spectroscopic methods (e.g., X-ray fluorescence (XRF), X-ray photoelectron spectroscopy (XPS), and X-ray absorption spectroscopy (XAS)) [30]. Each technique has its specific advantages and disadvantages, but all suffer from similar problems, including signal-to-noise ratio, drift, sensitivity, selectivity, specificity, stability, reusability, cost of the specialized technique, the preparation of the samples, and fouling/clogging of instruments. Measuring analytes at low concentrations offers additional challenges too. For example, high sensitivity detection, and false positives can arise. As a consequence, a professionally trained technician is needed to prepare samples, operate (and maintain) instrumentation, and interpret the results. The techniques also need to be tailored to different settings (for different metal ions), and some of these techniques cannot monitor every metal ion, due to interferences. Many of the instruments required are big and bulky, and samples have to be sent back to the lab for analysis, therefore, conducting onsite analysis can be problematic. Nevertheless, these techniques have their uses and will continue to play important roles in the analysis of metal ions.

There has been a push to develop analytical methods that are simple, fast, and reliable to detect metal ions in the field. Optical spectroscopy is of particular interest as it provides the basis for sensitive and inexpensive methods of detection. Optical spectroscopy comprises a group of spectroscopic analytical techniques that measure the intensity and wavelength of radiation absorbed and emitted by the sample. Luminescence is a spontaneous emission of radiation from an electronically or vibrationally excited species, not in thermal equilibrium with its environment, the resulting emission is either in the form of fluorescence or phosphorescence. Luminescence covers several techniques that involve the emission of radiation (emissive or non-emissive) by either atoms or molecules, but varies in the manner in which the emission is induced. Optical spectroscopy, for example, UV-Vis and fluorescence, are of particular interest to the sensor community. Fluorescence spectroscopy is particularly attractive, as the scientist can take advantage of manipulating different fluorescent mechanisms. The theoretical aspects of optical spectroscopy and the mechanisms that initiate a recognition event have been covered in reviews, including those by de Silva [31] and Wang [32], which are of particular relevance. The mechanisms involved include—photoinduced electron transfer (PET) [33], intramolecular charge transfer (ICT) [34], the heavy atom (metal) effect [35], the destabilization of nonemissive n-σ* excited states, metal-to-ligand charge transfer (MLCT) [36], Dexter (exchange mechanism), and Förster (coulombic) resonance energy transfer (FRET) [37], excimer/exciplex formation [38], twisted intramolecular charge transfer (TICT), electronic energy transfer (EET), aggregation-induced emission (AIE) [39], excited-state intramolecular proton transfer (ESIPT) [40], and chelation enhancement fluorescence (CHEF) [41].

These mechanisms can be tuned to prepare the fluorescent supramolecular probes for metal ion detection, monitoring, and remediation. In addition to these mechanisms, the underlying principles of molecular recognition and disclosure of analytes have also been extensively reviewed [42–52]. The review articles can be broad, covering a range of metals or probes, or could be very specific,

highlighting the work on one particular cation, such as Fe^{3+} [53], a specific fluorescent mechanism, such as excimer formation [54], or a specific type of chromophore, for example, squaraine dyes [55]. Alternatively, reviews might highlight the different probes within a given period [56]. In this review, we have highlighted some of the most recent work on the development of low molecular weight fluorescent probes for the group 12 metal ions (Zn^{2+}, Cd^{2+}, and Hg^{2+}). We have chosen to focus on these specific metal ions because they play significant roles in biology and the environment, for better or worse [57–66]; these analytes are optically silent, whereby an outside source is required for monitoring; to the best our knowledge this is the first time a review focuses on this specific triad. Most reviews focus on either the biologically important metal ions (Zn^{2+}, Cu^{2+}, Fe^{2+}, and Fe^{3+}) or environmentally important ions (Hg^{2+}, Pb^{2+}, and Cd^{2+}), that have very little, if any, biological roles. There are a handful of reviews that cover the optical response of a number of different metal ions, but they seem to lack focus. Moreover, the year 2019 is the 150th year since Dimitri Mendeleev has been credited for the development of the periodic law, thus, focusing on a specific group is a modest way to honor the achievement by Mendeleev.

The goal of this review is to highlight some of the more recent developments of low molecular weight fluorescent probes that quench the initial fluorescence signal, but the fluorescence signal is switched on upon the addition of metal ions (CHEF) for Zn^{2+} and Cd^{2+} ions, or the metal aids in a chemical reaction that produces a new compound that is fluorescent, commonly reported for Hg^{2+} ion molecular probes. Traditionally, the molecular sensor design has been carried out using two different approaches. The most common method is the intuition method of rational design, from years of experience being in the desired field, using a pen and paper (or chemical drawing software), followed by synthesis, and experimentation. The studies are then usually confirmed (or not) by computational methods, for example density functional theory (DFT) calculations, either to support the fluorescence mechanisms (which cannot be achieved easily by the traditional way) or to propose a binding mode between the analyte and the molecular probe, if a crystal structure cannot be obtained. As computer power is increasing and software is becoming more sophisticated the time required to run a calculation has been reduced. A new strategy in molecular probe design is to initially utilize a computational approach. The advantage of this approach is to investigate the fluorescence mechanisms first, to prepare a more efficient LMFP to improve the limit of detection for the desired analyte. This method has been used successfully for zinc sensors [67–70].

2. Chemosensors for the Group 12 Triad (Zinc, Cadmium, and Mercury)

The group 12 elements, zinc, cadmium, and mercury have a valence shell configuration of $[Ar]3d^{10}4s^2$, $[Kr]4d^{10}5s^2$, and $[Xe]4f^{14}5d^{10}6s^2$, respectively. They are known as the "silent ions" as they lack any intrinsic spectroscopic or magnetic properties and, as a consequence, cannot be monitored directly. The chemistries of zinc and cadmium are similar; however, that of mercury is vastly different. All three elements are found in the +2 oxidation state, they all adopt a range of coordination numbers (2, 4, and 6 being the most common) and form tetrahedral and octahedral complexes [71]. Mercury is found predominantly in a linear (coordination 2) or tetrahedral (coordination 4) geometry [72,73]. The 3d sub-shell for zinc is somewhat polarizable, despite its high charge-to-volume ratio [74]. It is well-known that Zn^{2+} plays pivotal roles in biochemical processes. Over 300 zinc enzymes carry out specific functions and zinc also plays a structural role, helping to stabilize protein binding domains, for example in zinc fingers [75]. Cadmium and mercury have no known biological functions, although there have been reports that cadmium has a limited biological function in marine diatoms [76]. Lane et al. reported that the growth of the diatom *Thalassiosira Weissflogii* is enhanced when there is a limited supply of zinc, suggesting that under extreme conditions, the presence of cadmium can be biologically beneficial [77,78].

All three group 12 elements form alloys with the other d-block elements [79]. For example, brass is a well-known alloy of copper in which the weight ratio between the metal alloys (and Sn and Pb) gives rise to a specific type of brass [80]. Common brass, used to make the Lincoln cent, is made up of 63%

copper and 37% zinc. Since 1982, a copper-coated zinc alloy has been used instead due to increases in the copper price. Amalgams, such as mercury-containing alloys, are often associated with the teeth and the dentistry fields [81]. Tooth fillings consist of mercury, silver, copper, and tin, as the predominant contributors to amalgam. Cadmium alloys are known, but many have had their alloying element replaced with other metals, due to the fear of leeching into the environment, where it is readily absorbed through the roots and shoots of crops [82]. This impedes the uptake of nutrients required by the plant, disrupting photosynthesis, stunting growth, and resulting in diminished crop yield. Moreover, the bioaccumulation of cadmium in plants, increases the risk of cadmium entering the food chain. This is particularly concerning where extensive agricultural procedures occur, for example, in China [83].

It is often assumed that mercury is "bad", due to misleading public information. Mercury is found in three broad forms, metallic mercury, inorganic mercury salts, and organic mercury and its form dictates its toxicity [84]. For example, inhaled mercury vapor will accumulate in the body mainly in the central nervous system (CNS) [85]. Ingesting metallic mercury under standard conditions poses a negligible risk of severe toxicity. The toxicity of inorganic mercury salts is dependent on their K_{sp} value. For example, the K_{sp} for Hg_2I_2 is 5.2×10^{-29} M^{-1} (+1-oxidation state) and for HgS (+2-oxidation state) is 2×10^{-53} M^{-1}. As salts are non-volatile, inorganic mercury salt poisoning is at a greater risk by oral digestion than inhalation. Additionally, inorganic mercury salts have very low solubility in lipids, so their abilities to cross the blood-brain barrier are significantly reduced [86]. Any ingestion of an inorganic mercury salt that accumulates in the liver, is processed by bile and the kidneys, and then excreted out via urine. Mercury found in its organic form (for example methyl mercury), is the species that the general public refers to as "mercury poising" and is highly toxic [87]. Organic mercurials are formed from elemental mercury through micro-organisms and make their way up the food chain, because methyl mercury is very soluble in lipids and bioaccumulates readily [88]. As mercury is one of the oldest known elements it has extensively been studied and the toxicity of its three forms is well understood. Even though mercury can enter the environment readily, gone are the days of being "mad as a hatter"—mercury poising is rare in the developed world.

As there are various ways in which the group 12 triad of metals can enter a biological or environmental surroundings, all three metal ions are toxic above specific concentrations. For example, the World Health Organization (WHO) and the Environmental Protection Agency (EPA) limit for these metal ions in water should not exceed 0.005, 0.001 and 5.0 mg·L^{-1} for Cd^{2+}, Hg^{2+}, and Zn^{2+} ions, respectively [89,90].

2.1. Zinc Probes

Zinc is arguably the most frequently studied d-block metal, due to its biological importance [91]. The Zn^{2+} ions are predominantly located within the confines of proteins and enzymes where they are essential to many biological functions [92]. The human body contains approximately 2–3 g of zinc; the amount found in the blood is kept constant (12–16 μM), however, higher concentrations (mM) are localized in many parts of the body, for example in the breast [93], prostate [94], brain [95], and pancreas [96]. The association constants range from tightly bound (log K > 11) and moderately bound (log K = 7–9) to loosely bound (log K < 7), and affect the bioavailability of Zn^{2+} ions. Loosely bound zinc is responsible for the dark side of Zn^{2+} ions. For example, free zinc has an active role in neuronal injury [93], and there have since been numerous reports on the acute toxicity of free zinc and its link to neurodegenerative effects in Alzheimer's disease [97] and amyotrophic lateral sclerosis (Lou Gehrig's disease) [98]. Low molecular weight probes that can chelate and monitor Zn^{2+} ions by an optical response are abound [99–108]. The subject matter appears in many authoritative reviews from investigators that have made seminal contributions in this field [109–123].

Whenever a molecular probe is being designed for a particular analyte, three crucial factors need to be considered; (1) high sensitivity (detection limit), (2) high specificity (distinguishing among metal ions), and (3) high selectivity (for the specific ion pool under investigation). Moreover, it might not be necessary to monitor metal ions at low concentrations, but rather over a dynamic range of

concentrations [124,125]. For example, the concentration of intracellular "free" zinc can be as low as 1 nM, whereby, Zn^{2+} ions found in synaptic vesicles in the presynaptic bouton of a neuron can be as high as 300 mM [126–128]. Therefore, developing molecular sensors that can work within this range is very challenging. An elegant example of a molecular receptor that can monitor Zn^{2+} ions over a wide concentration has been prepared by Zhu et al. [129].

The salicylaldehyde motif is a popular organic functional group, often incorporated into molecular probes [130], as it readily undergoes Schiff base reactions, and therefore, introduces the Lewis basic sites to bind metal ions in a stable chelating ring system. Compound **1**, a bis(bidentate) iminophenol ligand was synthesized by Chakraborty et al. (Figure 1A) [131], through the condensation of salicaldehyde and 4-aminobenzylamine in ethanol. The X-ray crystal structure shows that two resonance-assisted hydrogen bonding (RAHB) interactions are present. Therefore, in order for compound **1** to act as a molecular probe, Et_3N was added to the DMF solution to disrupt the intramolecular hydrogen bonding interaction to produce the chelating motif. Upon the addition of Zn^{2+} ions the absorbance wavelength, initially seen at 321 nm, bathochromically shifted to 406 nm. Unfortunately, the X-ray structure of the zinc complex could not be solved as the crystals diffracted weakly, but the analogous Co^{2+} complex was solved, showing a 2:2 binding ratio in the solid state. Based on the Co^{2+} structure (a tetrahedral arrangement around the Co^{2+} ions) and the Zn^{2+} ions UV-Vis titration data, the authors speculated that a 1:1 binding stoichiometry occurs in the solution phase. Their UV-Vis does show a pseudo-isosbestic point at 365 nm, but yet the binding isotherm saturates upon the addition of two equivalences of Zn^{2+} ions. Therefore, the author's interpretation of a 1:1 binding is misleading. No calculated binding constants were reported, presumably due to a number of different species existing in solution, rendering it difficult to calculate a precise binding constant, and their claim of 1:1 binding mode is questionable. The free ligands (**1**) are essentially non-fluorescent ($\phi = 0.025$ in DMF) but on addition of Zn^{2+} ions, a new emission band is observed at 527 nm ($\lambda_{ex} = 406$ nm), Figure 1B,C. This increase did not occur in the presence of the other metals studied (Fe^{3+}, Co^{2+}, Cu^{2+}, Ni^{2+}, Cr^{2+} Mn^{2+}, Cd^{2+}, Hg^{2+}, and Pb^{2+}) and the authors attributed this to a CHEF fluorescence mechanism. Unfortunately, no fluorescence binding isotherms were reported and, upon closer inspection of their titration data, the fluorescence spectra seemed to increase continuously. This could be due to an aggregated fluorescence enhancement, as it is reasonable to assume that other polymeric species are present in solution, and not only in the discrete 2:2 model, which has been suggested from their solid-state studies. This might explain why the binding constants were not calculated, as they could not be easily modeled.
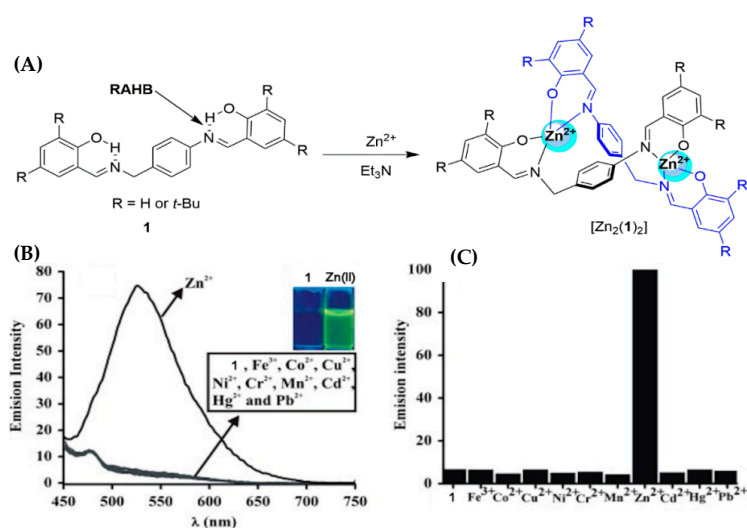

Figure 1. (**A**) The proposed coordination structure (based on the Co^{2+} crystal structure) and (**B**) the emission spectrum of compound **1** (DMF 10 μM and two equivalents of Et_3N, λ_{ex} 422 nm) and (**C**) bar chart highlights the emission intensity at 527 nm, upon the addition of metal salts (1.2 equivalents). Adapted from [131], with permission from Elsevier.

Zhang, Zhao, and Zhou prepared chemosensor **2** (Scheme 1), by incorporating a binding motif to the dye [132]. The optical studies were carried out in a CH_3CN-HEPES buffer (6:4 *v/v*; pH 7.4). On adding the 20 equivalents of metal salts (Na^+, Co^{2+}, Ni^{2+}, Cu^{2+}, Zn^{2+}, Pb^{2+}, Cd^{2+}, Ag^+, Hg^{2+}, Fe^{2+}, Mg^{2+}, and Cr^{3+}), negligible emission enhancement was seen, except for in Zn^{2+} ions. The emission spectra of LMFP **2** was very weak (ϕ = 0.06), and was attributed to the PET quenching by the lone pair of electrons residing on the nitrogen atom on the imine group. A 13-fold increase in the fluorescence intensity was seen at 556 nm (λ_{ex} = 397 nm) when 20 equivalents of Zn^{2+} ions were added. The binding constant K_a for a 1:1 binding model was calculated to be approximately 3×10^3 M^{-1}. The stoichiometry was supported by a Job's plot analysis. As Zn^{2+} was the only species that produced a fluorescent signature, the authors investigated the biological imaging of compoun **2**, with an array of cell lines. These included adenocarcinomic human alveolar basal epithelial cells (A549), bronchial epithelial cell (BEAS-2B), Chinese hamster ovary (CHO), Hela, and human liver cancer cells (HEP G2). Compound **2** showed different fluorescence emission colors in the cell nucleus and in the cytoplasm.
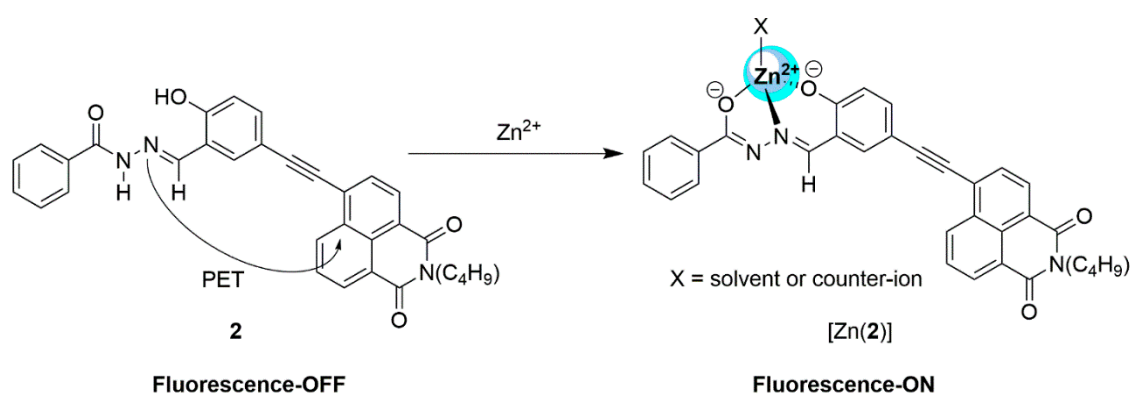

Scheme 1. The proposed binding motif between compound **2** and Zn^{2+} ions. The binding environment was also confirmed by ^{1}H NMR spectroscopy.

It is well-known that UV-visible irradiation can induce isomerization of organic and inorganic compounds [108,133]. This switching mechanism has been extensively used in molecular probe design [134]. The spyiropyran functional group is known to undergo a reversible heterolytic cleavage of the spiro C-O bond. A metastable merocyanine is then formed upon *cis-trans* isomerization. Giordani et al. synthesized a photochromic compound **3** containing a metal binding site, Figure 2A [135]. They utilized a methyl pyridinyl group, often used in zinc selective chromophores and incorporated the pyridinyl group onto the spirochromene indolic nitrogen atom. The stability of the open-closed form of the spiropyrene was affected by the electron withdrawing or electron donating groups attached to it, thus, influencing the feasibility of the open and closed form. Electron donating groups favor the closed system, whereas electron withdrawing groups favor the open form. Therefore, the Giordani team incorporated the electron withdrawing NO_2 group into their molecular probe design, to favor the open form and, thus, making the Lewis basic sites available to coordinate to a metal center. Many metal perchlorate salts were added to a 1×10^{-4} M CH_3CN solution of probe **3**. The $Zn(ClO_4)_2$ salt produced a distinctive color at 504 nm, from which the binding isotherm was obtained, Figure 2B, although these data points were not used to calculate the binding constant. A modified Benesi–Hilderbrand equation was used but the regression line showed curvature so the calculated binding constant ($K = 1.6 \times 10^4$ M^{-1}) should be viewed with a little skepticism. Upon the irradiation of the solution, the absorbance band disappeared. The switching was maintained over 100 second period. ^{1}H NMR studies showed that the *trans* configuration was sustained when the probe coordinated to the metal ion, confirmed by ^{1}H NMR, a large coupling constant was calculated (J = 16 Hz).
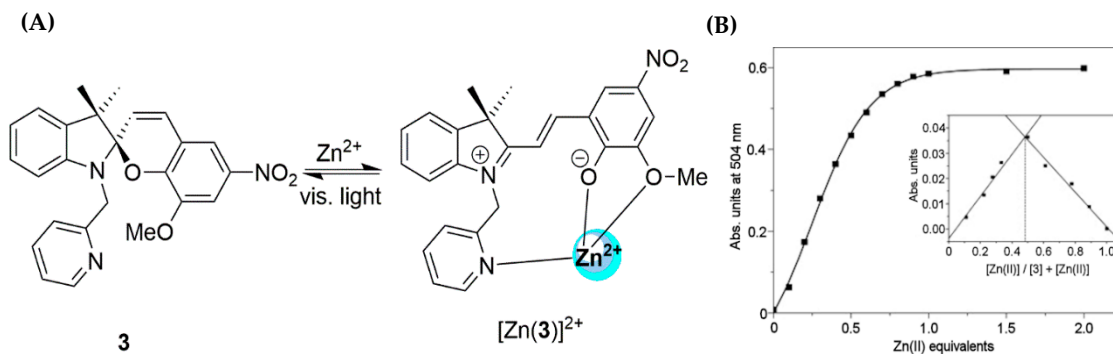
Figure 2. (**A**) The proposed binding of Zn^{2+} and molecular probe **3** (**B**) The absorption binding isotherm obtained, upon the addition of $Zn(ClO_4)_2$ to a 1×10^{-4} M of **3** in CH_3CN solution and Job's plot (insert). Unfortunately, the calculated binding constant was not calculated using the non-linear regression presented. Adapted from [135], with permission from Elsevier.

Another tridentate coordination moiety was incorporated onto a 1,8 naphthyridine scaffold where a protected L-proline was attached to position two on the naphthlyridine ring system, chemosensor **4** [136]. Upon the addition of various metal salts (Li^+, K^+ Cd^{2+}, Mn^{2+}, Fe^{3+}, Cu^{2+}, Mg^{2+}, Fe^{2+}, Ni^{2+}, Co^{2+}, Hg^{2+}, Pb^{2+}, Ag^+, and Zn^{2+}) in MeOH, only the Zn^{2+} ions showed a significant fluorescence enhancement by a factor of 2.5, whereas all other metal ions quenched emission. The authors suggested that the CHEF mechanism was the reason for the fluorescence enhancement observed. The fluorescence signal was saturated after the addition of one equivalent of Zn^{2+} ions and the calculated K_a was approximately 6×10^4 M^{-1}. The coordination environment of compound **4** and the Zn^{2+} complex was investigated by IR spectroscopy and TD-DFT. The natural bond orbital (NBO) calculations suggested that the zinc metal ion preferred to coordinate with the two nitrogen atoms and the oxygen atom (the negative charge density on N(2), N(3), and O(2), were calculated to be −0.403, −0.63, and −0.65, respectively), the final coordination site was occupied by an MeOH molecule. Based on these theoretical calculations and, the IR study, they suggested that the Zn^{2+} ions had a tetrahedral geometry.
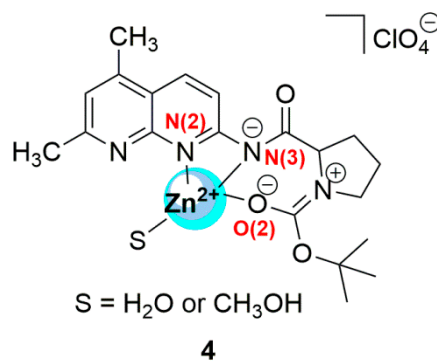

The naphthalene moiety has been used by Kim to prepare two very similar chemosensors, compounds **5** and **6** [137,138]. The hydrazide functional group was utilized, as it readily undergoes a Schiff base condensation reaction, to prepare a tridentate binding site (shown in red). The binding group is shown to be ideal for Zn^{2+} ions and the compounds coordinated in a 2:1 fashion. In both examples, the fluorescent mechanism was due to inhibition of C=N isomerization and ESIPT, upon the addition of Zn^{2+} ions, which drastically increased the emission intensity, via a CHEF mechanism. The calculated β values were 1×10^9 M^{-2} in a DMSO-buffer and DMF-buffer for compounds **5** and **6**, respectively.

[Zn(**5**)₂]　　　　　　　　　　　　　　[Zn(**6**)₂]
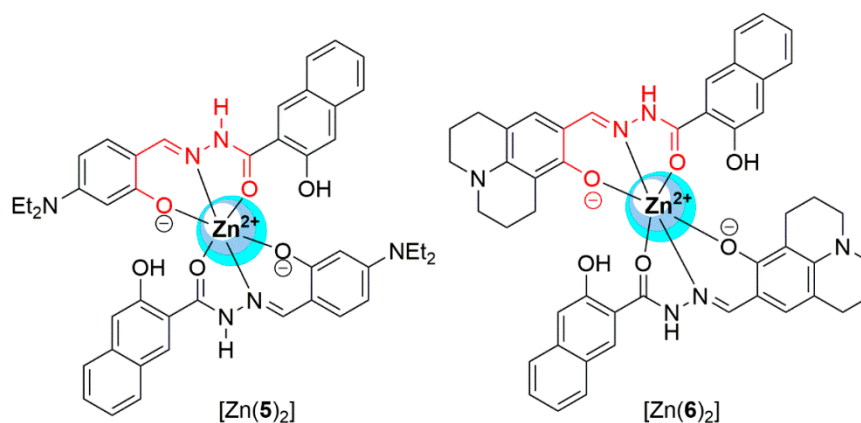
The chemosensor alone had hydrogen bonding donor and acceptor groups. Kim et al. also investigated the anion binding ability of compound **6** in DMF [138]. Upon the addition of AcO⁻ and F⁻, to ligand **6**, a 15 nm red shift was observed. The AcO⁻ anion showed the greatest hyperchromic shift. This was attributed to a stable chelating binding mode between compound **6** and the AcO⁻ anion. The authors proposed a binding stoichiometry of 2:1, whereby, the AcO⁻ molecules were bound on the same side of the ligand, although no evidence was provided to support their claim.

A similar binding motif was used as a tridentate binding environment by Erdemir et al. who prepared a triphenylamine derivative **7** [139]. The absorbance spectrum showed subtle wavelength changes which the authors claimed to represent a 1:1 binding stoichiometry with a binding constant of 6×10^6 in CH₃CN. It is reasonable to assume that a 1:1 complex would exist in solution. If this were true, the Benesi–Hildebrand plot would be a straight line, yet the data reported shows a curvature in the double reciprocal plot, indicative of stoichiometries other than a 1:1. The emission spectrum showed a distinctive enhancement upon the addition of Cd²⁺ and Zn²⁺, when a 1 μM CH₃CN solution was excited at 400 nm.

Interestingly, the λ_{em} for Cd²⁺ and Zn²⁺ was seen at 595 nm and 620 nm, respectively, a large enough difference to discriminate between these two metals. The optical responses between Cd²⁺ and Zn²⁺ ions are usually difficult to differentiate, due to the similarities of these ions. The authors argue that the difference in the metals radius (88 and 109 pm for Zn²⁺ and Cd²⁺, respectively) was enough to influence the binding energy in the maximum wavelength seen. The fluorescence mechanism of compound **7** was due to the C=N isomerization which was inhibited upon the coordination of metal ions, thus, the intensity enhancement was a consequence of CHEF. The fluorescence binding isotherms showed that the onset of curvature occurred at two equivalents of metal ion, suggesting that the binding constant was not 1:1.

7
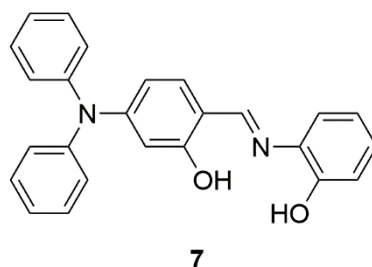
Lippard has made a career by designing and synthesizing molecules to bind Zn²⁺ ions selectively. Over the years, his group has incorporated the dipicoylamine functional group on to different organic scaffolds [140–144], including the rhodamine dyes **8a–c**, Figure 3 [145]. The rhodamine dye itself has been used extensively as an off–on sensor to detect a number of metal ions [146]. These molecules are colorless in organic solvents (DMSO, acetone, MeOH, and CH₃CN) but under simulated physiological conditions (50 mM PIPES, 100 mM KCl pH 7.0), the spirolactam opens upon the addition

of ZnCl$_2$. The absorption band was observed at 569 nm, and the emission wavelength was seen at 569 nm. Once the concentration of Zn^{2+} ions was greater than 1 mM, no further optical response occurred. The φ yield was calculated to be 0.22 for the zinc complex, compared to 0.001 for the molecular probe **8a**. The Zn^{2+} ions could be removed from the chelating motif by the addition of *N,N,N',N'*-tetrakis(2-pyridinylmethyl)-1,2 ethanediamine (TPEN) or ethylenediaminetetra acetic acid (EDTA). Compounds **8b** and **8c** exhibited little zinc binding via the lactone ring. It was highly probable that Zn^{2+} ions did coordinate with the DPA group, but the Zn^{2+} ions were too far away to participate in the coordination of the Lewis basic sites, in the lactone ring. Therefore, no emission signal was observed. This suggested that the lactone group did partake in the binding of the Zn^{2+} ion with **8a**, but no evidence was offered to substantiate this. The other biological relevant ions (Na$^+$, K$^+$, Ca$^{2+,}$ and Mg^{2+}) did not generate the equivalent optical response. The authors calculated the K_t value to be 73 μM, which took into account the zinc dissociation constant and the lactam formation. Despite this calculated value being at the higher concentration range, in comparison to other dipicolylamine molecular probes, it was still in the biological sensing range for neurochemical applications [147]. The ability for probe **8a** to track Zn^{2+} ions in Hela cells was also investigated and successfully showed cell permeability.
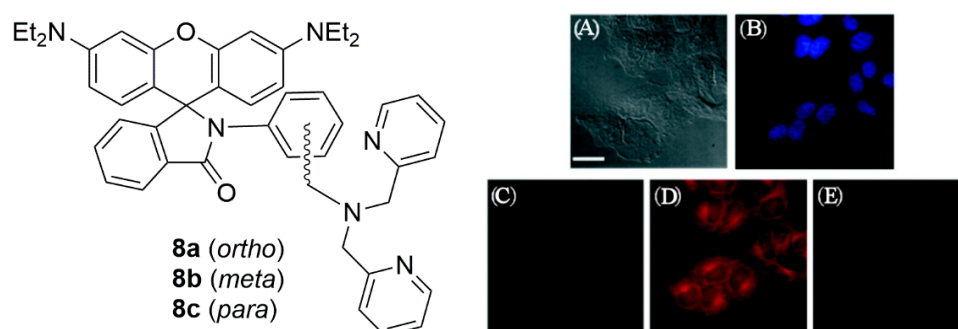
Figure 3. Live cell imaging of Hela cells after incubation with compound **8a** (10 μM) and Hoechst 33258 nuclear stain (blue): (**A**) Bright-field transmission image (**B**) Hoechst 33258 nuclear stain (**C**) fluorescence image without Zn^{2+} ions (**D**) Cells incubated with **8a** for 15 min, washed, and then treated with 50 μM Zn^{2+} pyrithione for 20 min. (**E**) **8a** loaded plus Zn^{2+} (50 μM)-supplemented cells treated with 80 μM TPEN after 10 min. Scale bar = 25 μM. Adapted from [145], with permission from American Chemical Society.

Dipodal receptors have been used extensively in molecular recognition [148]. By incorporating pendent side arms with the appropriate functional groups to bind a guest species, the thermodynamic properties of the host-guest complex can be significantly enhanced, as it wraps itself around the guest. Kim et al. prepared dipodal chemosensor **9** from a piperazine group with two quinoline derivatives attached [149]. Many dipodal receptors are symmetrical but the group chose to synthesize an asymmetric system. On the addition of metal salts (Na$^+$, K$^+$, Mg^{2+}, Ca^{2+}, Al^{3+}, Ga^{3+}, Cr^{3+}, Mn^{2+}, Fe^{2+}, Fe^{3+}, Co^{2+}, Ni^{2+}, Cu^{2+}, Zn^{2+}, and Pb^{2+}), significant optical changes were seen. The Zn^{2+} ions produced a significant intense broad band centered around 500 nm, Figure 4B. The authors claimed that the fluorescence signal was turned off, due to the PET quenching mechanism, which was subsequently inhibited by the coordination of the Zn^{2+} ions.
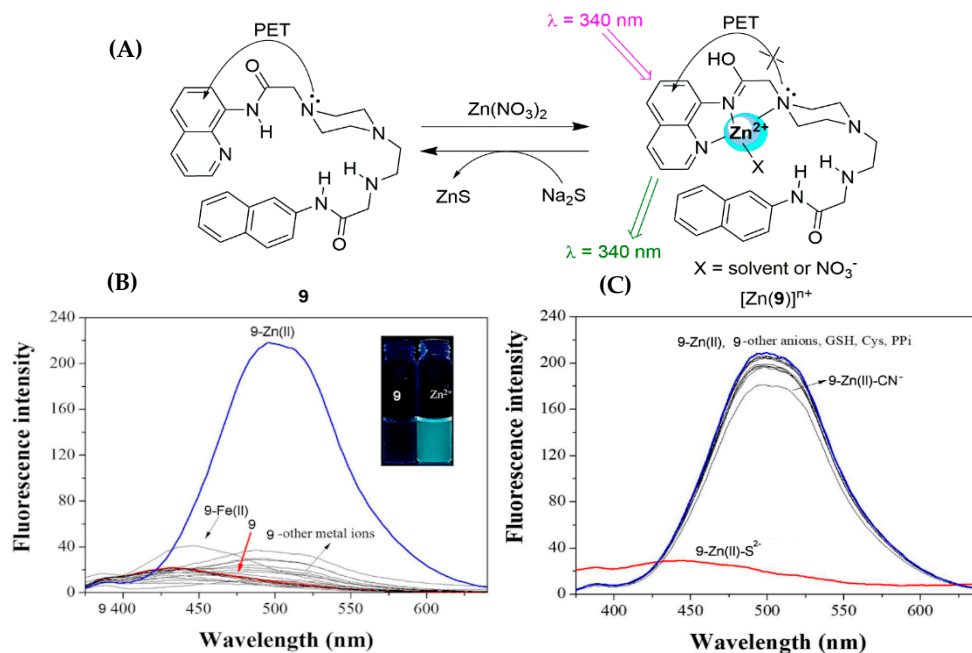
Figure 4. (**A**) Proposed binding mode of compound **9** and Zn^{2+} ions. (**B**) Fluorescence changes observed for compound **9** (5 μM) upon the addition of different metal salts (3.0 equivalents) in bis-tris buffer (10 mM, pH 7.0, λ_{ex} = 340 nm) and (**C**) spectral changes of $[Zn(\mathbf{9})(NO_3)]^+$ upon the addition of different anions added. Br^-, BzO^-, Cl^- ClO^-, CN^-, F^-, $H_2PO_4^-$, I^-, N_3^-, NO_2^-, OAc^-, SCN^- SO_4^{2-}, HSO_4^-, pyrophosphate (PPi), cysteine, and glutathione (thiol containing amino acids). Adapted and reprinted from [149], with permission from Elsevier.

On closer inspection, the broad band was more reminiscent of an excimer band (Figure 4B). It seemed that, in solution, the two naphthalene units in the dipodal system came closer together to produce this band. It just so happened that the Zn^{2+} ion was the correct size to bring the units together and maximize the excimer signal. Molecular modeling calculations, however, showed that the two fluorophores were significantly further apart, suggesting that this band was not an intramolecular excimer formation. An excimer band might be formed between molecules at concentrations greater than 1 μM [38] and these studies were at 5 μM. Intermolecular excimer formation could have been ruled out by dilution experiments and intramolecular excimer formation could have been ruled out by a model compound with a single fluorophore. Other metals also showed broad bands but of significantly lower intensity. The emission bands were difficult to assess as the band for Zn^{2+} ions saturated the other metals' optical responses. Additionally, it was claimed that the Zn^{2+} molecular probe was reversible by adding S^{2-}, yet the titration conditions did not seem to be conducive to sulfide chemistry. The studies were in 10 mM bis-tris buffer at pH 7, but at this pH there was an equilibrium between H_2S and HS^-, and it was not until the pH reached 13 that the sulfide could exist in solution. There is no doubt that the authors showed that upon the addition of Na_2S to their receptor, drastic spectral changes were observed (Figure 4C), but the K_{sp} for ZnS was approximately 2×10^{-25} M^{-1} [150]. Thus, the onset of ZnS precipitation drove the equilibrium towards the formation of the salt under their conditions.

Photochromic sensors have been used in many applications. The development of ratiometric fluorescent sensors utilizing a UV-Vis switch to sense metal ions is a unique way to prepare logic gates, in which a unimolecular fluorescent probe was designed to bind a metal that could be removed by a competing ligand, such as EDTA. Photoisomerization by UV-Vis could act as an input and the fluorescence emission could act as the output. Pu et al. synthesized two similar molecular switches compounds **10** and **11**, which were utilized as a logic circuit based on the truth table that could be constructed from four different inputs and one output (Table 1 and Figure 5) [151,152].
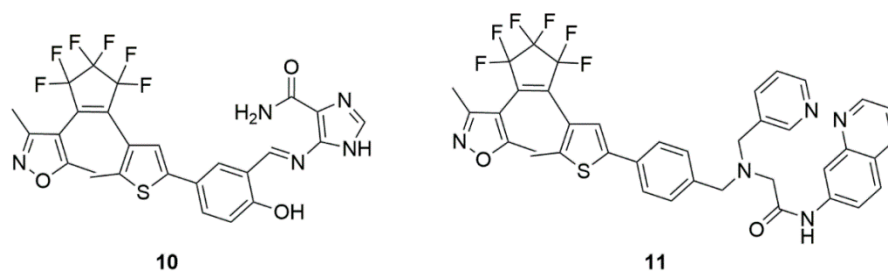
The absorption band assigned to the open isomers is seen at 243 nm and a new band at 534 nm is seen upon irradiation in a 2.0×10^{-5} M solution of CH_3CN. The purple color is a consequence of the rigid conjugation of alternated double bonds, across the backbone of the organic molecule, when the molecule is in its closed state. This was shown to be reversible and was supported by the difference in quantum yields (φ) of 0.03 and 0.17 for the open and closed states, respectively. The spectroscopic signatures were different for the ring opening and closing, and upon interaction with Zn^{2+} by EDTA, dual-controlled-switching behavior of compound **10** and **11** was shown, Scheme 2.
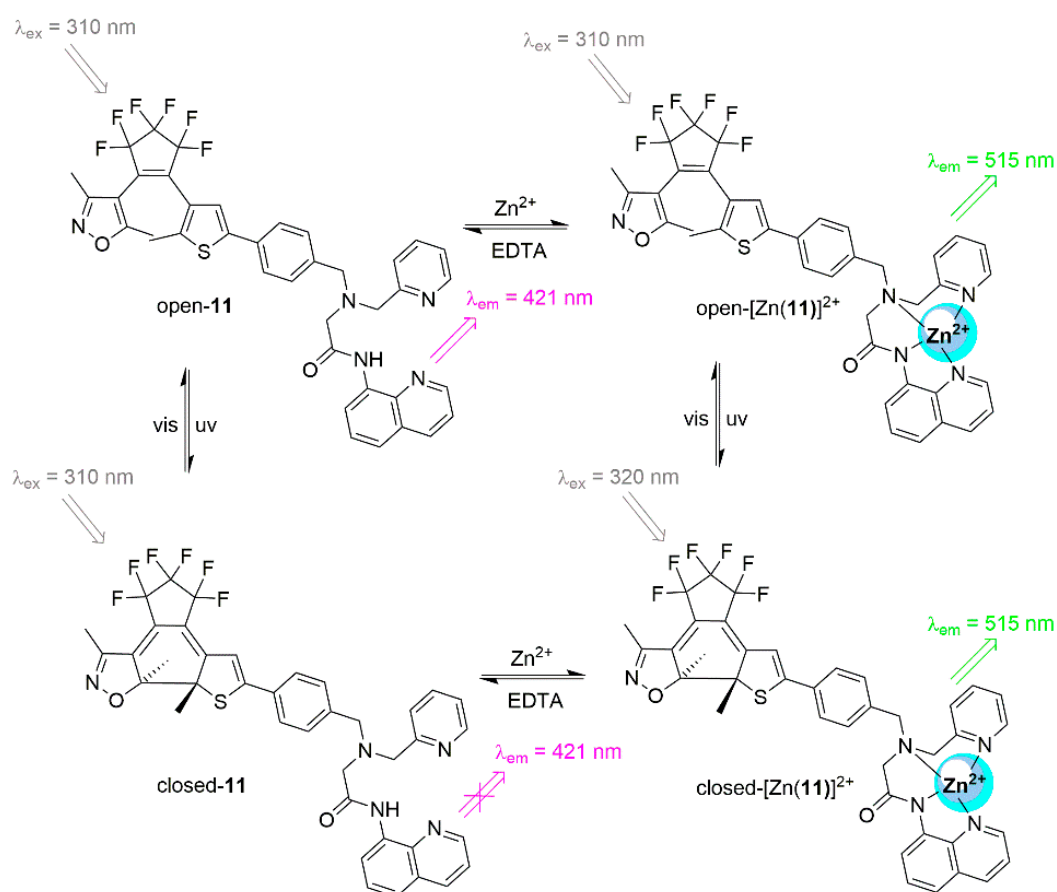
Scheme 2. The molecular switching behavior of molecular probe **11** with the interaction of Zn^{2+} ions/EDTA and UV-Vis stimuli.

Table 1. Truth table highlighting the possible binary inputs and the corresponding digital output.

Input				Output *
In (1) UV	In (2) Vis	In (3) Zn^{2+}	In (4) EDTA	λ_{em} = 515 nm
0	0	0	0	0
1	0	0	0	0
0	1	0	0	0
0	0	1	0	1
0	0	0	1	0
1	1	0	0	0
1	0	1	0	0
1	0	0	1	0
0	1	1	0	1
0	1	0	1	0
0	0	1	1	0
1	1	1	0	1
1	1	0	1	0
1	0	1	1	0
0	1	1	1	0
1	1	1	1	0

* when the emission band at 515 nm is seven times larger than the initial band at 421 nm, the output is "on", this is assigned a "1". Otherwise a "0" is assigned, i.e., the "off" state.
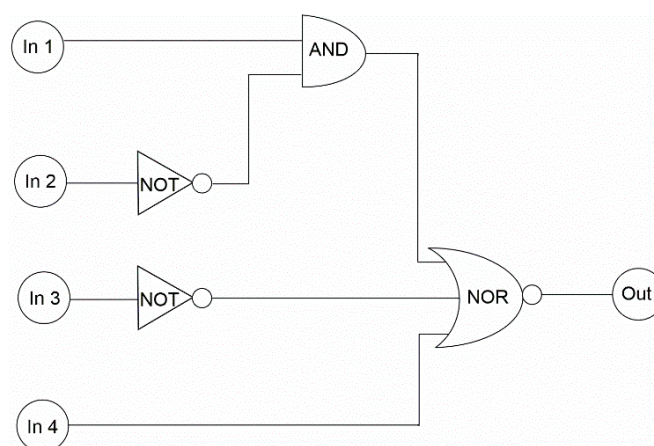
Figure 5. The logic circuit representing the Truth Table 1 (In 1 (UV), In 2 (Vis), In 3 (Zn^{2+}), In 4 (EDTA)).

Zhu et al. systematically changed the linker groups and fluorophores to improve the fluorescent output [153]. Zhu employed the PET switch mechanism to quench the fluorescence signal in a number of chemical fluorophores, which include the di(2-dicolyl) amino group (DPA) [154–156]. This functional group is known to bind Zn^{2+} ions and has been attached to anthracene [157], fluorescein [158], and rhodamine [159] groups, directly or via short linker groups, such as the methylene group. Zhu's team utilized the triazole functionality, to "click" the DPA binding site. Their early molecular probes relied on fluorophores that were excited around 400 nm, but this visible wavelength region was not conducive if the fluorophore was to be used in fluorescence microscopy for cell imaging, whereby, fluorophores that emit in the near IR region were more desirable. Therefore, they prepared molecular probes **12** to **14** that used the visible region to excite the fluorophore. All of their compounds were evaluated as zinc sensors and studied for their cell imaging capabilities, and all but one was shown to report zinc ion concentration at 50 µM in the Hela cells, by exciting the fluorophores at either 405 (compound **12** and compound **13**) or 488 nm (compound **14**). The anilino-DPA group was found to be the key to shift the excitation wavelength for the fluorophores and selectively coordinate the Zn^{2+} ions.
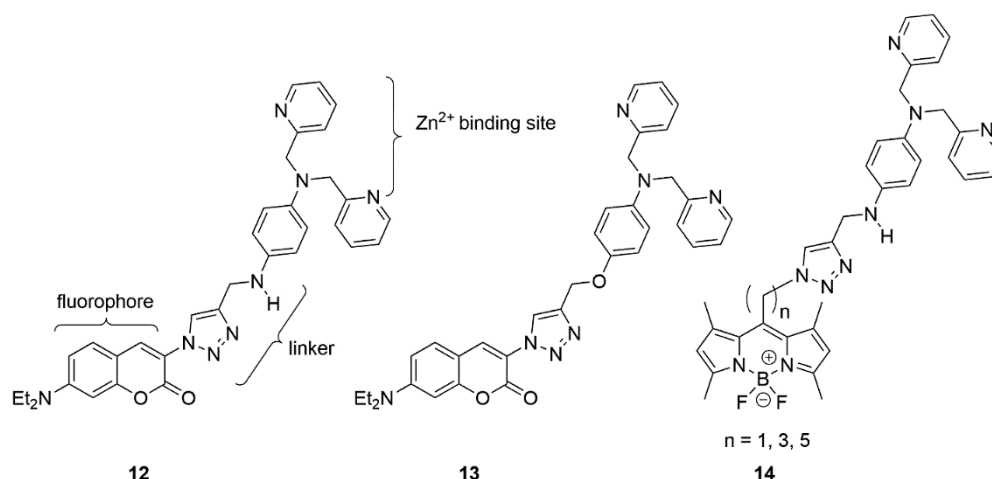
Another dipodal system was developed by Yang et al. who prepared a mixed fluorophore receptor (coumarin-naphthalene) which contained a very elaborate chelating motif, compound **15**, Scheme 3 [160]. The absorbance spectra showed a hypochromic shift at 335 nm and a hyperchromic shift at 430 nm, through a pseudo-isosbestic point at 307 nm. The binding isotherm was sigmoidal, which is indicative of cooperative binding. The fluorescence spectrum in EtOH (50 μM) showed a very strong emission band at 498 nm (λ_{ex} = 430 nm). There was a preference to the Zn^{2+} ions, in comparison to the other metal ions studied (Al^{3+}, Ba^{2+}, Ca^{2+}, Cu^{2+}, Hg^{2+} Co^{2+}, K^+, Mg^{2+}, Mn^{2+}, Na^+, Cr^{3+}, Li^+, Pb^{2+}, Cd^{2+}, Ag^+ and Fe^{3+}), however, competition experiments showed that both Cu^{2+} and Fe^{3+} significantly quenched the fluorescence intensity, when added to a $[Zn(\mathbf{15})]^{2+}$ solution. The binding constant was calculated to $K_a = 2.0 \times 10^4$ M^{-1}, using the Benesi–Hildebrand method and the stoichiometry was confirmed by a Job's plot. The fluorescence signal was off in the initial state, as a consequence of the C=N isomerization and PET quenching. On addition of the Zn^{2+} ions, the fluorescence was turned on via the CHEF mechanism. The limit of detection (LoD) was calculated to be 10^{-7} M.
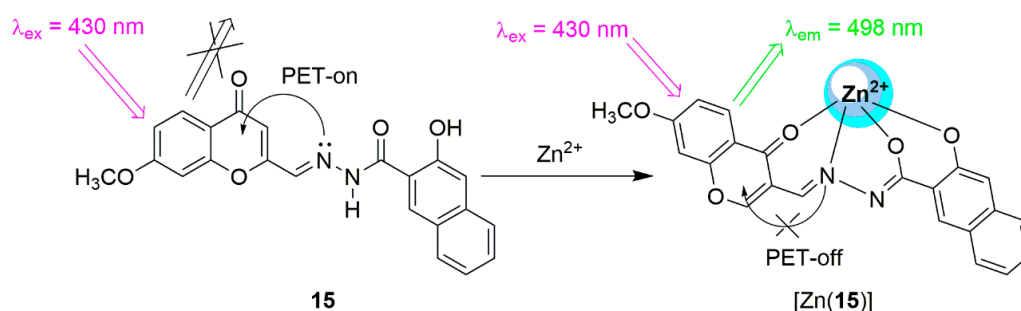
Scheme 3. Proposed binding motif between probe **15** and Zn^{2+} ions.

Another dual fluorescence mechanism used in sensor technology is the PET and ICT quenching approach, which is inhibited by the addition of Zn^{2+} ions. Molecular probe **16**, Scheme 4, was synthesized by Wang et al. [161] based on a (1,4 diketo-3,6-diphenyl-pyrrolo[3,4-c]pyrrole derivative, which is known to be a brilliant red and strongly fluorescent dye. Additionally, this organic fluorophore is stable to heat with high photostability and shows a large Stokes shift, which makes it an excellent choice in sensor design. Compound **16** shows a weak emission band at 630 nm (ϕ = 0.07), in the absence of Zn^{2+} ions, but upon the addition of Zn^{2+} ions to compound **16**, a blue shift to 560 nm (ϕ = 0.85) was observed; no other metal ion showed this enhancement. The optical studies (absorbance and fluorescence), and the NMR studies showed that no further optical or structural changes occurred after the addition of two equivalents of Zn^{2+} ions. A binding constant of 4.69×10^7 M^{-2} was determined

using the fluorescence data and the stoichiometry was confirmed as a 2:1 metal:probe complex formation, through MS studies.
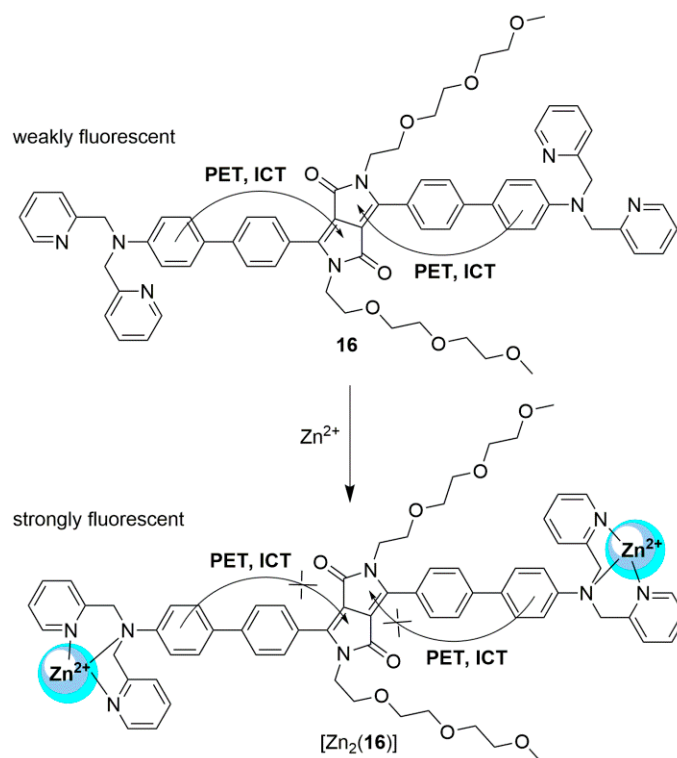
Scheme 4. Proposed binding motif between probe **16** and Zn^{2+} ions.

Throughout this section there have been examples of molecular probes for the detection of Zn^{2+} ions, but very few papers also discuss the counter-ion effect in their systems. Zinc complexes (in particular $ZnCl_2$) also play an important role, as a moderate strength Lewis acid, in Friedel–Crafts acylations. Our own group has prepared pyrene-based molecular probes **17** and **18** [162]. Compound **17** was shown to simultaneously bind the cation and anion, in a self-assembled process. Self-assembly occurred in the presence of ZnX_2 salts (X = F^-, Cl^-, Br^-, I^-, BF_4^-, $CH_3CO_2^-$, $H_2PO_4^-$, ClO_4^-, CN^-, NO_3^-) and $ZnSO_4$. The optical response was due to a strong excimer band observed at 410 nm in the presence of $ZnCl_2$ in acetonitrile. DFT calculations supported the proposed structure (Scheme 5). The intensity of the excimer signal was dependent on the proximity of the two pyrene units. In absence of the Zn^{2+} ion, the excimer signal was not observed, as was confirmed by the analogous spectroscopic studies with tetrabutylammonium salts, i.e., the metal was required for the self-assembly process to occur. This suggests that the Zn^{2+} halide was templating the pyrene units. The geometry around the Zn^{2+} ion was tetrahedral and the pyrene moieties adopted a *syn* configuration. The fluorescence titrations were in good agreement with the NMR studies, which showed a 2:1 binding mode calculated by non-linear regression with a calculated binding constant (K_{21}) of 1.8×10^6 M^{-2} for $ZnCl_2$. This example was a good example of size-selective self-assembled recognition and was carried out at a low concentration, to rule out intermolecular excimer formation.
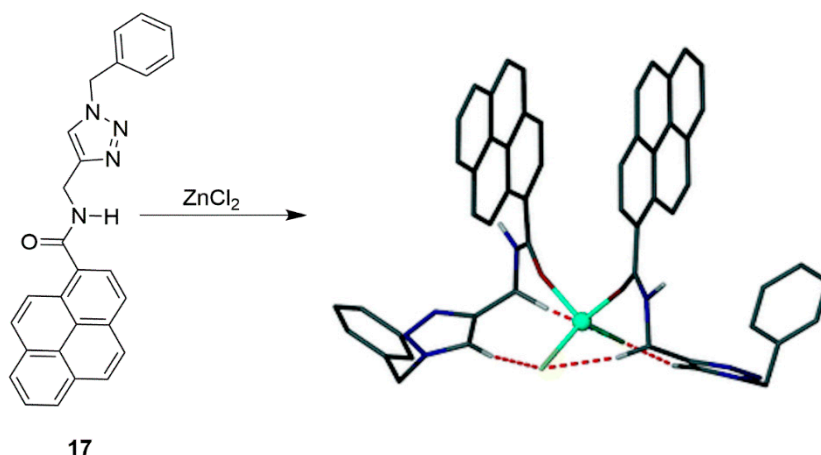
Scheme 5. A simultaneous ion pair recognition event. Adapted from [160] with permission from The Royal Society of Chemistry.

The next step our group took was to tether two of the pyrene units, shown in compound **17**, onto an organic backbone, to prepare a dipodal receptor. Three molecular probes containing an amide functional group and a triazole moiety was attached to a benzene scaffold (**18a-c** *ortho, meta and para* respectively) [163].

18a (ortho)
18b (meta)
18c (para)
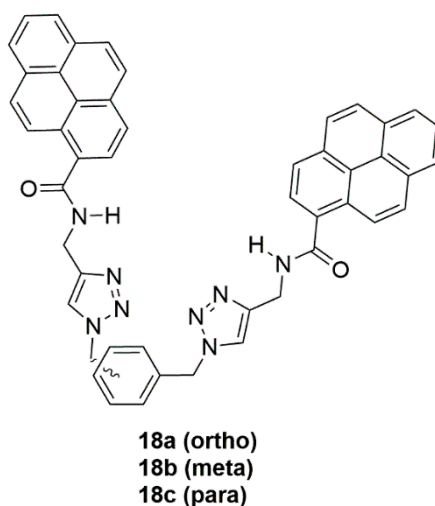
Fluorescence analysis of compounds **18a** and **18b** with different metal ions (Zn^{2+}, Mg^{2+}, Cd^{2+}, Al^{3+}, Hg^{2+}, Ni^{2+}, Cu^{2+}, Fe^{2+}, Fe^{3+} and Na^+) as either their chloride or perchlorate salts were initially tested, with the addition of 10 equivalents of metal salts in CH_3CN and excited at 325 nm. The fluorescence signal of the free receptors showed the typical monomer bands at 380 and 400 nm, characteristic of the unique electronic transitions in the pyrene-derived compounds, which were assigned to the π-π^* electron transitions. A very broad band at 495 nm was also seen, which was assigned to the intramolecular excimer formation, upon excitation at 325 nm. On inspection of the fluorescence spectrum, quenching was observed for all metals except Zn^{2+} (and to a lesser degree Cd^{2+} and Mg^{2+}), and a new band was seen to increase at 400 nm. It was evident that the Zn^{2+} salts showed significantly greater fluorescence at 400 nm for **18b** than for **18a**, for which a small increase in intensity was observed at 400 nm. The fluorescence intensity at 400 nm for **18a** was a consequence of the two pyrene units in **18a** adopting an anti-orientation, which gave a greater pyrene–pyrene separation than was available to **18b**. It was shown that the binding affinity for $Zn(ClO_4)_2$ was a magnitude greater for **18a** than for **18b**, even though the fluorescence change at 400 nm was not observed to be as dramatic. In fact this trend was seen for all the other analytes studied, we argued that the more favorable chelating

motif was the reason for the observed calculated binding constant. To understand the binding mode, extensive IR and molecular modeling studies were carried out. It is known that significant infrared spectral changes occur when perchlorate coordinates with a metal ion through different modes [164]. Determination of the changing symmetry of the ClO_4^- ion, upon binding, from T_d (ionic) to C_{3v} (unidentate) and C_{2v} (bidentate or bridging), could help identify if the binding mode proposed model was consistent with IR data reported. Molecular mechanics calculations for **18a** and **18b** and their corresponding $Zn(ClO_4)_2$ complexes were carried out (Figure 6). Both of the free receptors showed very different π stacking interactions. The *ortho*-isomer, **18a**, showed that the aromatic scaffold of the molecular probes participates in π-stacking and one of the pyrene arms seemed to intercalate and form an intramolecular sandwich interaction Figure 6A. This intercalation was not observed in the *meta*-isomer, **18b**, which showed the π-π distance between the two pyrene units to be 4.77 Å. The distance was measured between the pyrene centroids (Figure 6C) and the CH hydrogens on the triazole rings orientated towards the center of the molecular probes. This is in excellent agreement with the interactions expected to generate the excimer band seen in the fluorescence spectrum. Both of the Zn^{2+} complexes showed drastically different optimized geometries. The Zn^{2+} ion was bound in a tetrahedral arrangement, coordinated to the oxygen atom of the carbonyl functional group, and a nitrogen atom in the triazole ring, forming a seven-membered chelating ring. The distance between the two pyrene units in $[Zn(\mathbf{18a})]^{2+}$ was 10.8 Å, whereas the distance between the two pyrene units in $[Zn(\mathbf{18a})]^{2+}$ was 5.5 Å. This was in excellent agreement with the fluorescence data in which a broad excimer band was seen at 400 nm for the **18b** complex; the same band was significantly less intense for the **16a** complex.
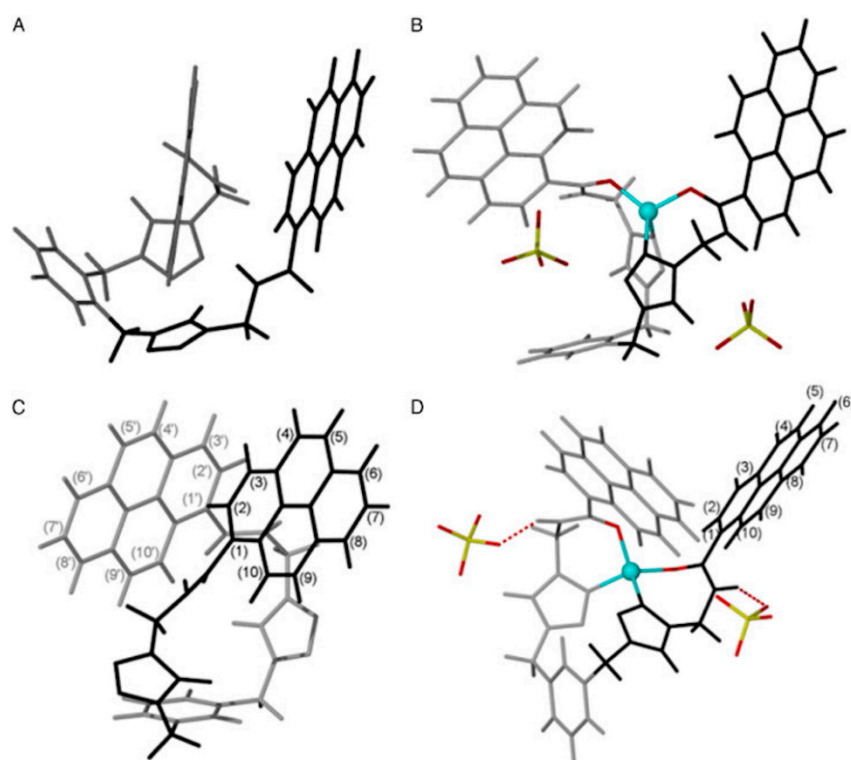
Figure 6. Fully optimized structures (DFT) in the gas phase of (**A**) compound **18a**, (**B**) [Zn·**18a**](ClO$_4$)$_2$, (**C**) compound **18b**, and (**D**) [Zn·**18b**](ClO$_4$)$_2$. Adapted From [163], with permissiom from Taylor & Francis Ltd.

2.2. Cadmium Probes

As cadmium has essentially no biological use and the bioaccumulation of Cd^{2+} ions in the environment is a real threat, there is an increasing need to remove cadmium from wastewater from an industrial process. Cadmium has been ranked as one of the top 10 priority lists from the top

275 hazardous materials that have been identified by The Comprehensive Environmental Response, Compensation, and Liability Act in the USA [165], therefore, detection and remediation of Cd^{2+} ions in the environment are imperative. A review by El-Safty outlined the importance of cadmium in the environment, discussed common techniques to remediate Cd^{2+} ions, and highlighted the chemosensors used for cadmium monitoring [166]. The chemistry and structural similarities of cadmium is similar to zinc. Both the tetrahedral and octahedral forms are known. The type of Lewis basic atom plays a role in the geometry. For example, Parkin et al. showed that Zn^{2+} ions preferred a tetrahedral environment when the donor atom was sulfur, whereas the Cd^{2+} complex showed a six-coordinate environment [167]. Selenolato complexes are known to coordinate to Zn^{2+} and Cd^{2+} in a distorted tetrahedral environment [168]. A review published by Sigel and Martin state that the Cd^{2+} ion could be found in 4, 5, and 6 coordination environments, 20%, 8%, and 56% of the time, respectively [169].

Therefore, it is not surprising that the LMFP reported for the detection of Cd^{2+} ions is similar to the probes for zinc ions. Additionally, the fluorescence mechanism is alike. For example, Pu et al. synthesized a closely related molecule to probes **10** and **11** and subtly changed their binding motif to prepare a sensor for Cd^{2+} ions [170].

A rhodamine-based conjugated dyad probe (**19**) has been synthesized by Stalin and coworkers (Scheme 6) [171]. The authors claimed that the FRET mechanism between the rhodamine and pyridine conjugated dyad is responsible for the emission observed upon the coordination of Cd^{2+} ions in the organic–aqueous system (CH$_3$CN:HEPES buffer 2:8, *v/v*, pH 7.2, 10 mM). However, upon inspection of their molecular probe, it is difficult to justify the authors claim. For FRET to occur, several criteria must be met: (i) the fluorescence emission spectrum of the donor molecule must overlap the absorption or excitation spectrum of the acceptor chromophore, (ii) the two fluorophores (donor and acceptor) must be in close proximity to one another (typically 1 to 10 nm), (iii) the transition dipole orientations of the donor and acceptor must be approximately parallel to each other, and (iv) the fluorescence lifetime of the donor molecule must be of sufficient duration to allow the FRET to occur. The pyridine unit alone is not usually considered a fluorophore. It is more reasonable to assume that the mechanism is an off–on fluorescence mechanism, based on the spirolactam ring opening. However, the authors did show high selectivity and sensitivity towards Cd^{2+} ions in the presence of other competing metal ions, which was indicated by the appearance of a new fluorescence band at 590 nm, due to Cd^{2+} coordination. Spectroscopic studies were used to determine a LoD of 1×10^{-8} M, which is well below the WHO acceptable limit of 1.85 mM for Cd^{2+} ions in drinking water. Both the association constant and binding ratio were determined from the absorption spectra. The absorption titration was used to calculate an association constant of 4×10^4 M^{-1} and, from the Job's plot data, the binding ratio was found to be 1:1. In the presence of sulfide ions CdS was formed, which resulted in decomplexation and the disappearance of the emission band observed at 590 nm. The results described above suggest that the sensor was recycled during the detection of S^{2-} ions.
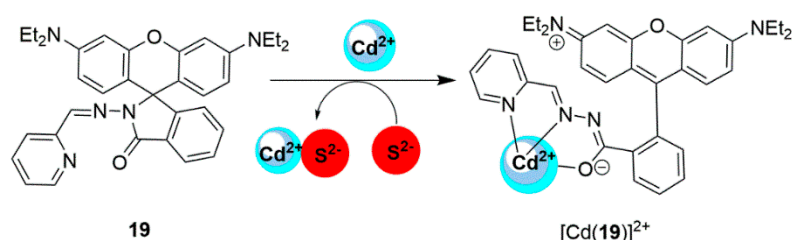
**Scheme 6.** The proposed binding of Cd^{2+} ions and chemosensor **19**.

A FRET molecular probe incorporating rhodamine was synthesized by Goswami et al. Chemosensor **20** was shown to be selective for Cd^{2+} ions, with the sensor acting as an 'off–on' FRET sensor capable of detecting Cd^{2+} ions in a mixed organic–aqueous solvent system. Additionally, a distinctive color change was seen, typical of rhodamine dyes. A quinoline–benzothiazole functional group (FRET donor) was tethered to the rhodamine molecule (FRET acceptor), via a nonconjugated

spacer, Scheme 7 [172]. As the emission spectra of the quinoline benzothiazole group overlapped significantly with the absorption spectra of the ring-opened rhodamine B dye, it was possible to observe the transfer of energy from donor to acceptor, once the sensor interacted with the Cd^{2+} ions. Both the quantum yield and FRET efficiency of the sensor were calculated from fluorescence studies carried out in MeOH/H_2O (1:4, *v/v*, pH 7.2, 10mM HEPES buffer solution) and were found to be ϕ = 0.37 and 48%, respectively. These experimental conditions were optimized for the water content. They reported that when the percentage of water was increased above 80%, the intensity ratio (I_{585}/I_{470}) of the emission band decreased significantly, whereas less water content showed modest changes in the emission intensity. From the fluorescence titration, Aich and coworkers found that the lowest concentration of Cd^{2+} ions detectable by the sensor was 3×10^{-7} M and the association constant (determined using a nonlinear least-squares fit) was found to be 1×10^5 M^{-1}. The other metal ions studied (K^+, Ca^{2+}, Ni^{2+}, Mn^{2+}, Zn^{2+}, Cu^{2+}, Fe^{3+}, Cr^{3+}, Hg^{2+}, and Pb^{2+}) did not show the same optical response. The 1:1 binding mode was confirmed both in solution and in the solid state. The X-ray crystal structure confirmed that the Cd^{2+} binds in an octahedral environment with five of the donor groups from compound **20** and a chloride ion in the remaining coordination site.
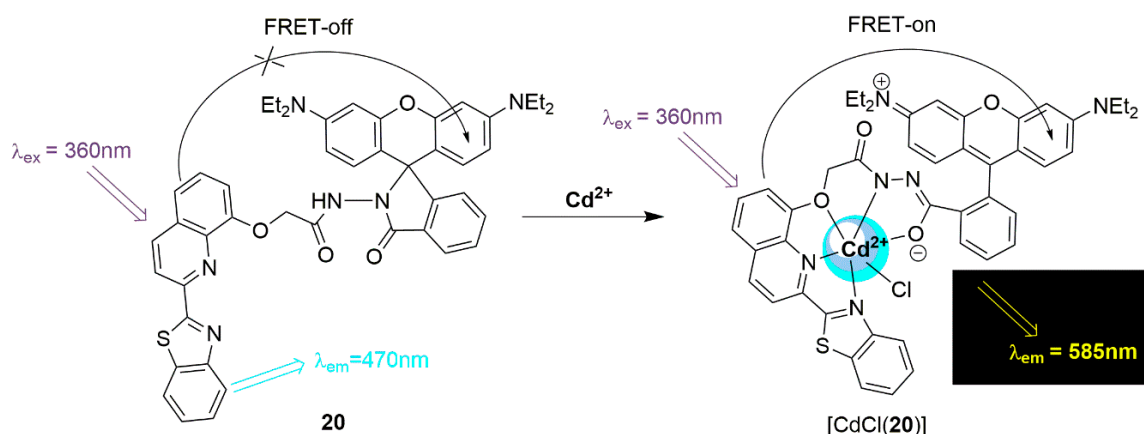

Scheme 7. The binding mode of Cd^{2+} ions to chemosensor **20** MeOH/H_2O (1:4, *v/v*, pH 7.2, 10mM HEPES buffer solution).

As Cd^{2+} ions are hazardous to the environment the preparation of portable sensing kits is attractive. Goswami immersed thin layer chromatography (TLC) plates soaked with **20** in MeOH solution (2×10^{-4} M), removed excess MeOH and placed the probe coated plates into a MeOH solution of cadmium ions (2×10^{-3} M), which showed distinctive color changes (Figure 7).
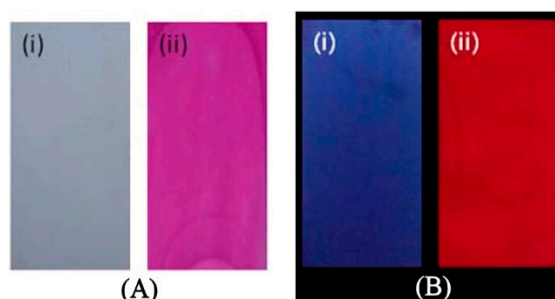
Figure 7. (**A**) Photographs of TLC plates after the immersion of molecular probe **20** into a MeOH solution (**i**) after the addition of Cd^{2+} ions (**ii**) under ambient light; and (**B**) under hand-held UV-light at 365 nm, (**i**) after the addition of Cd^{2+} ions, (**ii**) under hand-held UV-light at 365 nm, Adapted from [172], with permission from American Chemical Society.

Another popular fluorescent mechanism that is being used in molecular probe design is aggregation induced emission (AIE), a similar mechanism to excimer formation. Wang et al. employed this by tethering a hydrophobic tetraphenylethene (TPE) moiety (hydrophobic part) onto a β-cyclodextrin (hydrophilic part), via a click reaction to give compound **21**. Therefore, by varying the ratios of water and organic solvent the mechanism could be turned on and off. The triazole moiety was used as the Lewis basic site to coordinate the Cd^{2+} ions [171]. In solutions containing ≤50% water, the sensor gave no significant emission when the probe was excited at 330 nm. However, upon the addition of Cd^{2+} ions, a noticeable emission band emerged around 476 nm. This could be attributed to the overlap of the tetraphenylethene groups as a result of the 2:1 coordination between the sensor and Cd^{2+} ions. This same behavior was observed as the water content of the solvent system was increased up to 98%. In higher concentrations of water, the solution of the sensor becomes strongly emissive at 476 nm, and this emission was visible with the naked eye, Figure 8. This strong emission was due to the formation of aggregates in solution, owing to the decreased solubility of the sensor. Zhang et al. observed that in a solution of $DMSO/H_2O$ (1:1, *v/v*) the sensor only responded to Cd^{2+} ions and no other metal ions and they were able to detect Cd^{2+} ions at concentrations as low as 1×10^{-8} M.
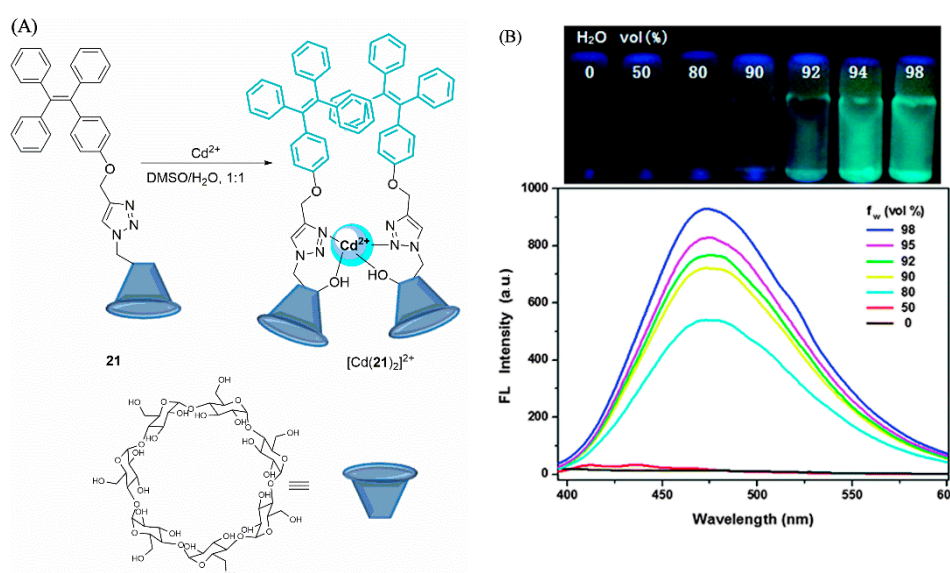

Figure 8. (**A**) The proposed binding mode of chemosensor **21** and Cd^{2+} ions and (**B**) the emission turn-on in 50 μM solution of **21** with a different ratio of DMSO-H_2O (λ_{ex} = 330 nm). Aggregation could be seen by the naked-eye once the water content was greater than 90%. Adapted from [173] with permission from The Royal Society of Chemistry.

Many LMFPs have been adsorbed (physisorption or chemisorption) onto surfaces to improve sensitivity. This is done to increase the number of binding sites, by incorporating a number of the desired molecular probes onto a single platform. Commonly used scaffolds are mesoporous silica materials. These materials are rigid and porous and have been used to support a number of molecular sensors. An advantage of these materials is that they are optically transparent in the visiable range, therefore, the signal generated is genuinely from the receptor and the analyte. These types of materials have been used in sensor applications and for remediation purposes [119,129,174,175]. A reusable fluorescent sensor capable of detecting Cd^{2+}, Hg^{2+}, and Pb^{2+} ions in aqueous solutions was synthesized by Zhu et al. by physidorption, of a 2,2-dipicoylamine modified naphthalimide fluorophore, **22**, onto the surface of a silica microsphere [176]. It is inherently hydrophilic and capable of metal detection and adsorption (Scheme 8), as indicated by increases in its fluorescence intensity. Control studies indicated that, in the absence of the silylpropylamine linkers on the microspheres, no adsorption of metal ions had occurred. Under optimal conditions (low concentration of metal ions and **22** at pH 4.5–10), compound **22** had an adsorptivity greater than 95%. In acidic media (pH < 4.5), the

adsorption capability of the sensor was greatly diminished, which allowed the desorption of metal ions from the sensor. Presumably, the nitrogen atoms become protonated, removing the ability of the molecular probe to form a Lewis acid-base adduct, before the acidic medium removes the metal ions. This allows microspheres coated with **22** to be recycled multiple times, by washing them with an acidic solution, then readjusting the pH by adding base. Fluorescence studies determined that the LoD of **22** was in the nM concentration range with an association constant of 2.3×10^7 M^{-1} for Cd^{2+} ions.

Interestingly, this molecular probe was able to remove Cd^{2+} (and Hg^{2+} and Pb^{2+}) from tap water, lab wastewater, and simulated biological fluid. Samples were spiked with 2.0 mg·L^{-1} Cd^{2+} salts and 99%, 98%, and 96% of the metal was recovered from tap water, wastewater, and biological fluid, respectively, indicating that the molecular probe is a good candidate for cadmium remediation, but it remains to be seen if the probe can selectively remove metals from a mixture of metal ions in the samples.
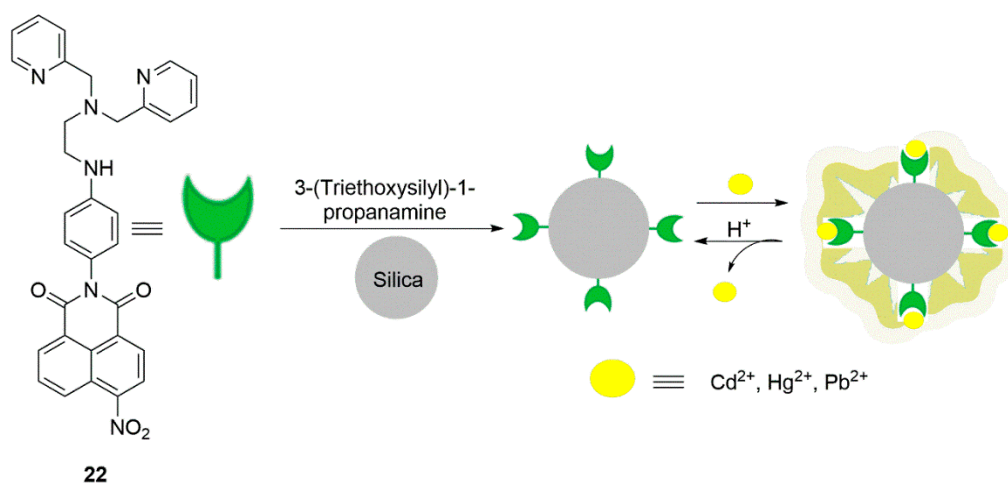

Scheme 8. Chemosensor **22**, attached to silica, is able to undergo a fluorescence turn on, upon the addition of Cd^{2+}, Hg^{2+}, and Pb^{2+}. The removal of the metal was achieved by the addition of acid.

Lv and Shen synthesized a ratiometric porphyrin-based fluorescent probe (**23**) for detecting Cd^{2+} ions in aqueous systems from pH 6.5 to 10 [177]. The incorporation of sulfonic groups enhances the probe's water solubility of the porphyrin ring system. The 2,2′-dipyridylamine (DPA) possesses remarkable binding ability towards Cd^{2+} ions; therefore two DPA groups were attached to coordinate the Cd^{2+} ions. The porphyrin fluorophore serves as an ideal signaling unit owing to its large conjugated π plane. Upon the coordination of DPA to Cd^{2+} ions, a ratiometric fluorescent change to the emission spectra of the probe was observed. The fluorescence mechanism is based on an intramolecular charge transfer (ICT). Compound **23** shows a good solubility in aqueous solutions without the addition of an organic solvent. Spectroscopic studies were carried out in HEPES buffer solution (pH 7.4). Upon the addition of Cd^{2+} ions to a solution of the probe, the emission wavelength shifted from 653 to 611 nm (ϕ = 0.15). The noticeable hypsochromic shift of 42 nm was indicative of a reduction in the electron donating ability of the DPA moieties, upon Cd^{2+} ions coordination, as the Cd^{2+} ion is electron-withdrawing. Moreover, as the Cd^{2+} ions are coordinated to the DPA molecule through the nitrogen atom, the porphyrin ring system is perturbed subtly, therefore, decreasing the conjugation, and shifting the wavelength in the blue direction. Direct fluorimetric titration as a function of Cd^{2+} ion concentration was used to calculate a dissociation constant (K_d) value of 31 μM, and a Job's plot showed a 1:2 binding ratio between the sensor and Cd^{2+} ions. Often signaling systems that depend on fluorescence changes (increases or decreases) at a fixed wavelength, suffer from uncertainty in absolute fluorescence measurements; however, a ratiometric fluorescence response enhances the reliability of the signaling from a quantitative viewpoint. Through linear regression of the calibration plot ($[F_{611}/F_{653}]$ vs $[Cd^{2+}]$), the detection limit was calculated to be 0.032 μM. Furthermore, the Cd^{2+} ions could be

removed from the DPA groups by the addition of EDTA. As compound **23** showed good aqueous solubility studies in Hela cells and A549 (adenocarcinomic human alveolar basal epithelial) cells, the two cancer lines remained 87% viable, implying that the sensor exhibited minimal cytotoxicity and is likely safe for use in bioimaging.


23
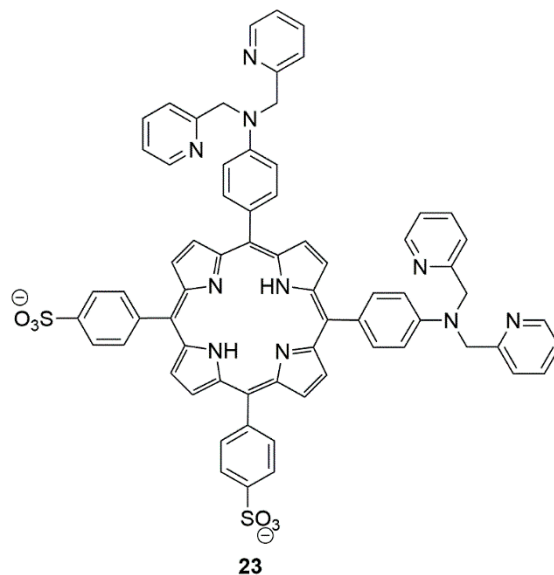
Siva and Chellapa synthesized a ratiometric benzimidazole tagged coumarin probe **24**. Compound **24** could selectively detect Cd^{2+} and F^- ions in a CH_3CN/H_2O (1:9, *v/v*) HEPES-buffered solutions at pH 7.52, Scheme 9 [178]. The UV-Vis absorption spectrum showed three distinct bands at 292, 342, and 401 nm. The addition of Cd^{2+} ions led to a hyperchromic shift at 292 and 343 nm, and a hypochromic shift at 401 nm, through an isosbestic point at 367 nm, indicative of metal complexes in solution. Upon exciting probe **24** at 340 nm, two distinct emission bands at 410 and 530 nm were observed. The addition of Cd^{2+} ions led to a blue emission band at 410 nm and an increase in emission intensity, at 530 nm, through an isoemissive point 518 nm. From these spectral changes the association constant was calculated to be 3.5×10^3 M^{-1}, using a modified Benesi−Hildebrand method and the LoD was determined to be 1.5×10^{-10} M. The addition of the Cd^{2+} ions inhibited the intermolecular charge transfer (ICT) between the lone pair on the secondary amine in the imidazole ring system and the carbonyl group on the coumarin unit. It is reasonable that the molecular probe would chelate the metal ions in a tridentate fashion, via the three Lewis basic sites (Scheme 9, red bonds). Additionally, the authors carried out an extensive anion study which showed very little spectral changes for a number of tetrabutylammonium salts (TBAX, where $X = F^-$, Cl^-, Br^-, I^-, OAc^-, NO_3^-, $H_3PO_4^-$, CN^-). Fluoride was the only anion to produce a small changes in the fluorescence spectrum, which was also shown to inhibit the ICT mechanism, by forming a hydrogen bonding interaction with the NH group in the benzimidazole group.
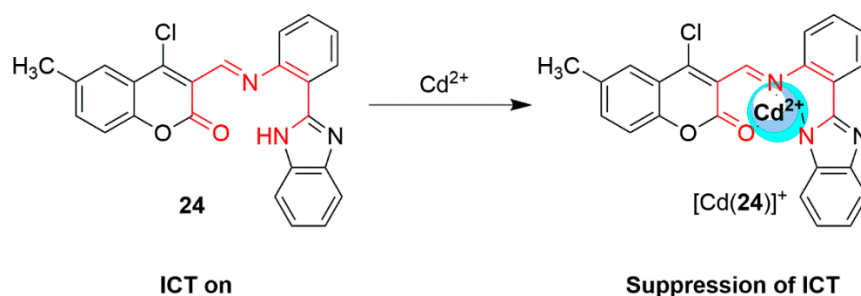
Scheme 9. Proposed binding of molecular probe **24** and Cd^{2+} ions.

Another LMFP coumarin dyad, **25**, was prepared by Kumar and Ahmed [179]. The molecular probe served as, both, a colorimetric sensor and a fluorescent sensor, through chelation-enhanced fluorescence (CHEF), Figure 9. Upon the addition of Cd^{2+} ions in a HEPES-buffered solution (20 mM, CH_3CN:H_2O, 3:7, *v/v*, pH 7.0) of probe **25**, the solution changed from yellow to colorless, whereas there were no color changes observed upon the addition of the other metal ions studied (Na^+, K^+, Ba^{2+}, Ca^{2+}, Mg^{2+}, Cr^{3+}, Mn^{2+}, Fe^{3+}, Co^{2+}, Ni^{2+}, Cu^{2+}, Zn^{2+}, Pb^{2+}, Ag^+, Al^{3+}, Hg^{2+}, Hg^+, and Sn^{2+}). On the addition of Cd^{2+} ions to a solution of **25**, there was a blue shift in the absorbance band from 387 nm to 370 nm, whereas the addition of other metal ions resulted in no notable changes to the absorbance spectra. Titration studies were carried out to further study the interactions between **25** and Cd^{2+} ions. The gradual changes in the absorbance bands suggests that a new species was produced during the titration. A Job's plot was used to verify the formation of a 1:1 complex between the sensor and cadmium ions and a Benesi–Hilderbrand plot was used to calculate an association constant of 1.8×10^6 M^{-1}. Furthermore, the LoD was calculated to be 6.3×10^{-8} M. The fluorescence data of the sensor with different metal ions was analogous to the absorbance data, as there were only notable spectroscopic changes in the presence of Cd^{2+} ions. Under the same solution conditions as the absorbance experiments, **25** was non-fluorescent. However, in the presence of Cd^{2+} ions, a gradual increase in the emission band at 495 nm was observed and the absolute fluorescence quantum yield (ϕ) increased by a factor of nine, upon coordination with the Cd^{2+} ions. A fluorescence lifetime decay was observed from 0.217 to 1.97 ns, after the addition of Cd^{2+} ions, indicative of the strong coordination between the sensor and Cd^{2+} ions. In an attempt to prepare a workable probe, test strips were prepared, which changed color upon the immersion into a Cd^{2+} solution (5×10^{-4} M), Figure 9.
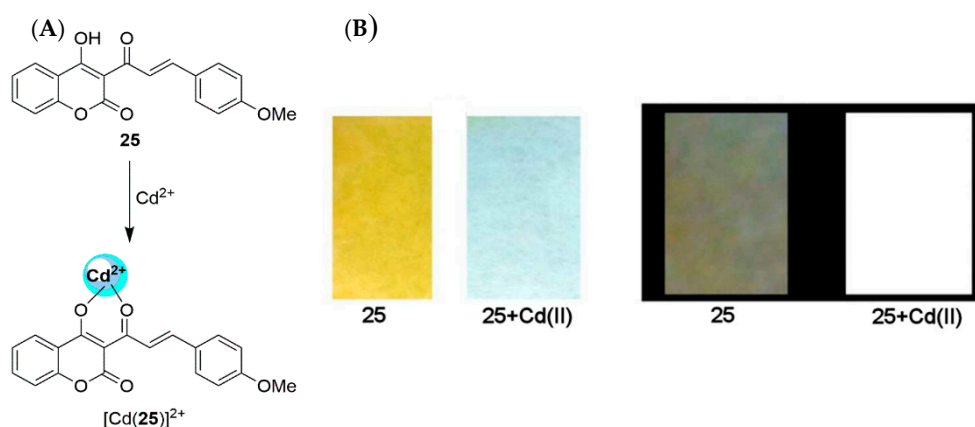
Figure 9. (**A**) Proposed binding between compound **25** and Cd^{2+} ions and (**B**) photographs of colorimetric (**left**) and fluorometric (**right**) test kits. The filter papers were coated with **25** (0.1 mM) and then immersed into a HEPES-buffered solution (20 mM, CH_3CH-H_2O 3:7, *v/v*, pH 7). Adapted from [179] with permission from the Centre National de la Recherche Scientifique (CNRS) and the Royal Society of Chemistry.

Interestingly, the authors used their probe to monitor the amount of Cd^{2+} in lipstick, hair dye, and makeup cream as Cd^{2+} is a common ion found in the preparation of these cosmetics. Spectrofluorometry and AAS analysis showed the amount of Cd^{2+} ions in the samples to be very similar (Table 2).

Table 2. The calculated concentration of Cd^{2+} ions in cosmetics and personal care samples by fluorometric and atomic absorption spectroscopy (AAS) [179].

Sample	Amount of Cd^{2+} in $mol \cdot L^{-1}$)	
	Fluorometric with Probe 25	**AAS**
Lipstick	2.07×10^{-6}	1.96×10^{-6}
Hair color	1.12×10^{-6}	1.06×10^{-6}
Makeup cream	7.92×10^{-6}	7.20×10^{-6}

Many molecular probes designed to bind cadmium can also bind zinc ions and it is often difficult to distinguish between the two. The binding ratio between the metal and the probe can be enough to discriminate between two metal ions. For example, LMWP **26** was synthesized by Rajak et al. Scheme 10 [180]. Fluorene–pyridine were coupled together via an imine bond. Compound **26** served as both a colorimetric sensor, producing noticeable color changes in the presence of both zinc and cadmium, and a turn-on fluorescence sensor. As Cd^{2+} ions were added to a CH_3CN:H_2O solution (8:2, *v/v*, 10 mM HEPES, pH 7.4) of **26**, the solution changed from pale yellow to deep orange, whereas a deep pink color was observed in the presence of Zn^{2+} ions. The UV-Vis titration data showed the emergence of several new bands, upon the addition of Cd^{2+} ions to a solution of the sensor, with a noticeable difference to that of the Zn^{2+} ion titration. Fluorescence titrations further highlighted the probe's selectivity for Cd^{2+} and Zn^{2+} ions.

Decomplexation of the [CdCl(**26**)] complex and subsequent emission turn off could be accomplished with the addition of S^{2-} ions to a solution of the complex. The fluorescence turn-off also served as a means of distinguishing between Zn^{2+} and Cd^{2+} ions, as decomplexation of the Zn^{2+} ion's complex did not occur in the presence of S^{2-} ions. A Job's plot verified the binding stoichiometry of the sensor for Cd^{2+} ions as 1:1 with an association constant of 6.4×10^4 M^{-1}, calculated from a Benesi–Hildebrand plot using the data from UV-Vis titrations. The weak fluorescence band seen around 430 nm is due to the lone pair on the nitrogen atom on the imine group quenching the intensity. However, on chelation of Cd^{2+} ions with the sensor, the PET process is prevented and the molecule becomes less flexible, as the free rotation of the azomethine carbon is also restricted. The coordination environment was further validated by studying the ^1H NMR titration of Cd^{2+} ions into a solution of the sensor which showed a clear disappearance of the phenolic proton and a downfield shift of the azomethine proton. From the fluorescence titration, an LoD of 0.53 μM for Cd^{2+} ions was calculated and a fluorescence quantum yield of 0.996 was observed, whereas the fluorescence quantum yield of **26** was calculated to be 0.042. As Zn^{2+} and Cd^{2+} produced different optical inputs with one output, a binary logic gate function could be produced Table 3). This selective behavior mimics an OR binary logic gate (Figure 10).
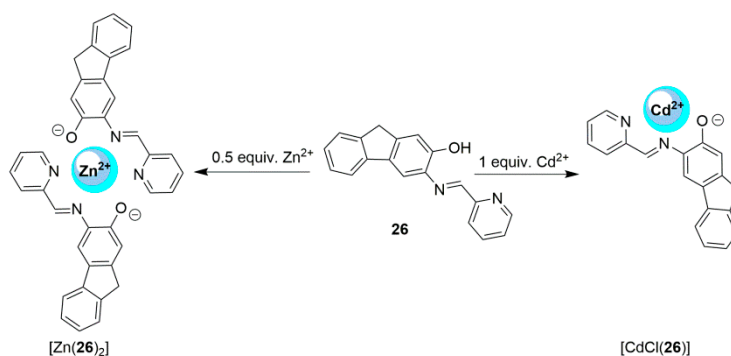
Scheme 10. Schematic representation the binding behavior of probe **26** and Cd^{2+} and Zn^{2+} ions.
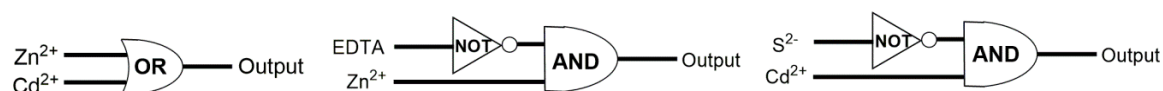
Figure 10. Logic schemes prepared from the binary inputs/outputs in the Truth tables [180].

Table 3. Truth table highlighting the binary inputs and the corresponding digital output [180].

(A)			(B)			(C)		
Input		Output *	Input		Output *	Input		Output *
Zn^{2+}	Cd^{2+}	λ_{em} 485 or 495 nm	Zn^{2+}	EDTA	λ_{em} 485 nm	Cd^{2+}	S^{2-}	λ_{em} 495 nm
0	0	0	0	0	0	0	0	0
1	0	1	1	0	1	1	0	1
0	1	1	0	1	0	0	1	0
1	1	1	1	1	0	1	1	0

* (**A**) OR logic gate, the output "1" is assigned to Zn^{2+} and Cd^{2+} when the emission bands appears at 485 and 495 nm, respectively and "0" in the absence of metal i.e., no emission. (**B**) and (**C**) logic gates operate as an INHIBIT function (a combination of an AND function plus an additional event, in this xample NOT). Addition of the metal produces the output "1" and the inverter (EDTA for Zn^{2+} or S^{2-} for Cd^{2+}) switches off the emission, output "0".

A simple cleft-shaped fluorescent chemosensor, **27**, was prepared by Qian and Yang, Scheme 11 [181]. Originally prepared to bind group 1 and group 2 metal ions, NH_4^+ ions and heavy metal salts in methanol and at high concentrations (1.9×10^{-2} M) by Maass and Vögtle [182–184], the molecular cleft did not discriminate between different metal ions. The fluorescence spectra for 10 µM of compound **27** (20 mM Tris-HCl, pH 7.4) with Cd^{2+} ions showed a significant fluorescence band at 417 nm. The other metals studied did not show any response (Ba^{2+}, Mn^{2+}, Hg^{2+}, Ni^{2+}, Ca^{2+}, Cu^{2+}, Co^{2+}, Pb^{2+}, Mg^{2+}, Zn^{2+}, Cd^{2+}, Fe^{2+}, Fe^{3+}, Cr^{3+}, Ag^+, Li^+, Na^+, and K^+). The PET mechanism quenched the initial fluorescence intensity, via the lone pairs on the nitrogen atom. On the addition of Cd^{2+} ions, the flexible molecular cleft became rigid and the fluorescence increased, due to CHEF, and the π-π* transitions gave rise to the emission band observed. The association constant calculated by the nonlinear least square analysis was found to be 5.3×10^7 M^{-1}.
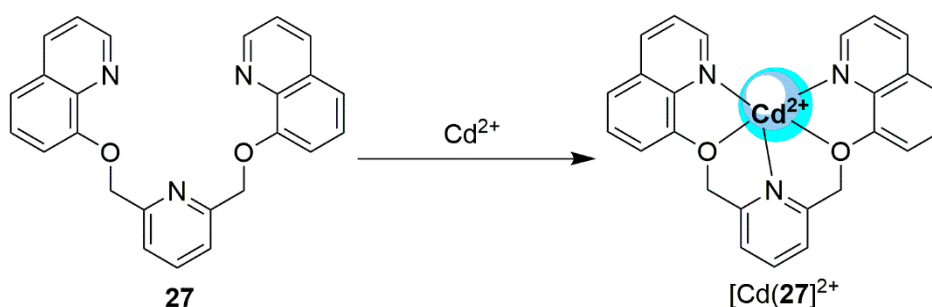

Scheme 11. Proposed binding mode of **27** and Cd^{2+} ions.

Liu and Wang took advantage of the encapsulating and adsorbing capabilities of cationic surfactant hexadecyl trimethyl ammonium bromide (CTAB) and the selectivity of thymine-squaraine based fluorescent chemosensor **28**, to develop a system capable of sensing and capturing Cd^{2+} ions, Figure 11 [185]. The thymine moiety of **28** efficiently bound to Cd^{2+} ions, while the squaraine moiety served as a signaling unit whose spectroscopic performances could be tuned by changing its solution environments. The CTAB micelles could induce aggregation of the squaraine dyes, reducing the likelihood of any intermolecular electron transfer. On the addition of Cd^{2+} ions, the fluorescence intensity of compound **28** increased. Optimal conditions for the system were observed when the concentration of CTAB was less than 1 mM. At higher concentrations, the CTAB micelles made it difficult for the Cd^{2+} ions to access the thymine moiety via an adsorption process into the cell. Under these conditions, a 5-fold increase in the emission band at 660 nm was observed for compound **28**

in the presence of Cd^{2+} ions. There was no notable emission change observed for any other metal ions that were studied (K^+, Zn^{2+}, Li^+, Fe^{3+}, Hg^{2+}, Fe^{2+}, Ag^+ Co^{2+} Na^+ Ca^{2+}, and Cu^{2+}). The sensor was also found to be very sensitive, demonstrating an LoD in the nM range. The binding constant was determined using a Benesi–Hildebrand plot and found to be 2×10^3 M^{-1}. Additionally, a Job's plot revealed that the binding stoichiometry between the squaraine moiety and Cd^{2+} ions was 1:1. Competition studies did not highlight any notable inhibition, due to the presence of other metal ions. However, the presence of some anionic and non-ionic surfactants (sodium dodecyl sulfate (SDS), Dodecylbenzene sulfonic acid sodiym salt (SDBS), and Triton X-100) did diminish the probe's ability to detect Cd^{2+} ions. The micelle was found to be stable to photobleaching, as decomplexation did not occur when the soft material was exposed to constant irradiation for 6 h.
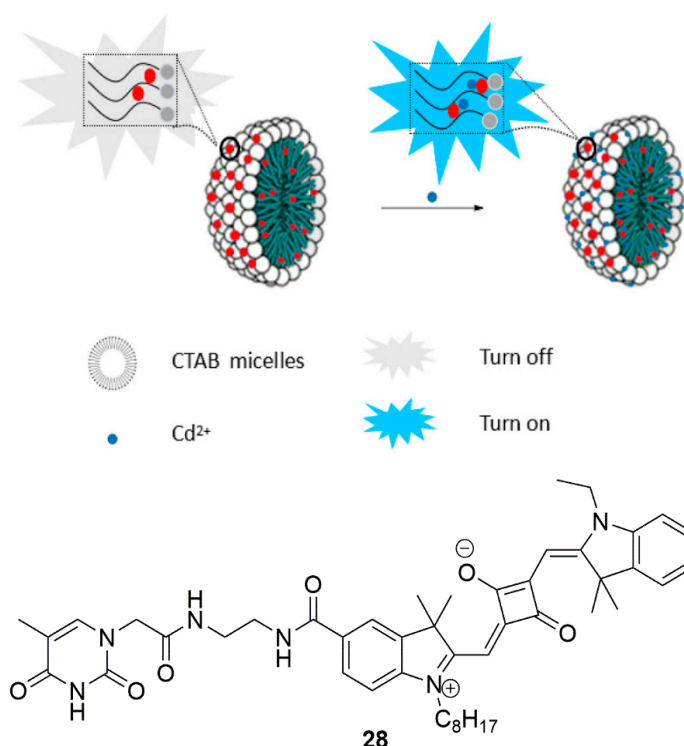

Figure 11. The proposed intermolecular interaction between compound **28** and the Cd^{2+} ions encapsulated in the micelle. Adapted and reprinted from [183], with permission from Elsevier.

Two turn-"on" fluorescent sensors compounds **29a** and **29b** were synthesized by Xu and coworkers, Scheme 12 [186]. Both compounds could bind both Zn^{2+} and Cd^{2+} ions in a CH_3OH/H_2O solution (1:1, *v/v*, Tris, 10 mmol·L^{-1}, pH 7.4). These molecular probes displayed a weak fluorescence emission band, however, in the presence of Zn^{2+} and Cd^{2+} ions, an eight-fold increase in the emission intensity, due to CHEF mechanism, was observed at 430 nm. Data obtained from the fluorescence titrations and Job's plots, suggested a 1:1 complex formation. This was supported by NMR studies. The calculated association constants of compounds **29a** and **29b** to Cd^{2+} ions were 1.5×10^7 M^{-1} and 1.0×10^6 M^{-1}, respectively. Competition studies were carried out using other metal ions but there were no notable interferences observed in the fluorescence spectra. There were however interferences from biologically relevant anions, namely adenosine triphosphate (ATP), adenosine diphosphate (ADP), and other phosphate ions. Complete quenching was observed when phosphate ions were introduced to a solution of the complex demonstrating the complex's ability to serve as an on–off sensor for phosphate ions.
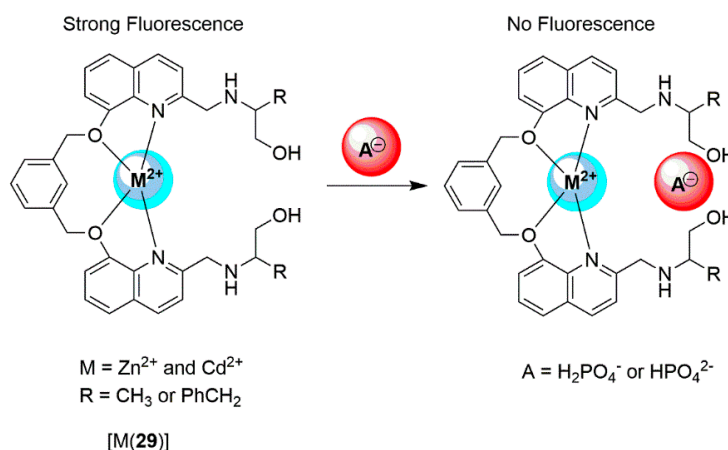
Scheme 12. The proposed interaction between the molecular sensors and the metal ions. The binding cavity size was ideal to chelate Cd^{2+} or Zn^{2+} ions. When the phosphate anion was added, the fluorescence intensity was switched off.

Kim and Harrison synthesized a tripodal receptor containing quinoline and pyridyl aminophenol moieties (compound **30**) [187]. It was shown to prefer to coordinate with Zn^{2+} ions in CH_3CN solution but had a preference for Cd^{2+} ions in aqueous solutions. Optical investigations were carried out in the presence of 19 different nitrate metal salts (Na^+, K^+, Zn^{2+}, Cd^{2+}, Mg^{2+}, Ca^{2+}, Al^{3+}, Ga^{3+}, In^{3+}, Pb^+, Hg^{2+}, Cr^{3+}, Mn^{2+}, Fe^{2+}, Fe^{3+}, Co^{2+}, Ni^{2+}, Cu^{2+}, Ag^+) at 10 μM in CH_3CN solution. The addition of Zn^{2+} ions lead to a large fluorescence enhancement ($\phi = 0.001$ to $\phi = 0.24$) at 510 nm. The only other metal ion that produced an emission intensity increase was Cd^{2+} but to a lesser extent, approximately one third of the magnitude seen for Zn^{2+} ($\phi = 0.039$). The other metals did not lead to an increase in fluorescent intensity, but several did interfere with the probe's ability to bind to Zn^{2+}. Similar optical investigations were undertaken in a $CH_3CN:H_2O$ (1:1, *v/v*) HEPES-buffered solution (10 mM, pH 7.4). The fluorescence enhancement seen in the presence of Cd^{2+} remained the same, but the fluorescence enhancement seen in the presence of Zn^{2+} was only 10% of that seen in CH_3CN. Other metal ions did not lead to an increase in intensity, but Zn^{2+}, Cr^{3+}, Cu^{2+}, Co^{2+}, Ni^{2+}, Hg^{2+} interfered with Cd^{2+} binding. The differences in fluorescence intensities between the two solvent systems suggested that the coordination environments for Cd^{2+} ions were similar in both. The Zn^{2+} ion could adopt an equilibrium between tetrahedral and octahedral geometries. The binding environment for $[Cd(NO_3)_2(30)]$ was confirmed by solid-state studies (Figure 12) and supported by NMR studies. The weak fluorescence seen for **30** was a consequence of PET quenching, which was inhibited upon the coordination of Zn^{2+} ions. The binding constants, in CH_3CN were calculated to be 1.4×10^6 M^{-1} and 5.6×10^5 M^{-1}, for Zn^{2+}, and Cd^{2+} respectively, but it is unclear how these binding constants were obtained, as no binding isotherms were reported. It was also claimed that **30** bound Cd^{2+} ions more favorably than Zn^{2+} ions in an organic-aqueous system. No binding constants were reported to back up this claim, only a single fluorescence spectrum showed that the intensity was greater for Cd^{2+} ions.
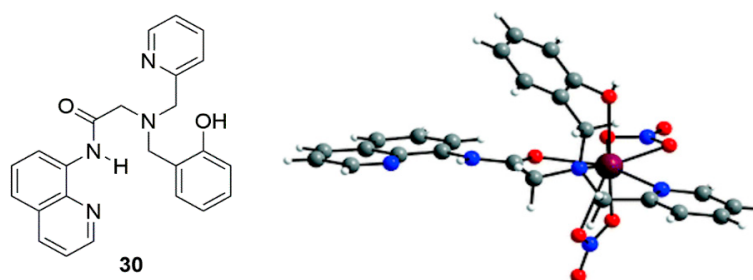
Figure 12. X-Ray crystal structure of $[Cd(NO_3)_2(30)]$. Adapted from [187] with permission from The Royal Society of Chemistry.

　　　Hou and Wang developed a phenylene-acetylene based compound **31** that was capable of selectively detecting Fe^{2+} by colorimetric methods and Cd^{2+} and Zn^{2+} via ratiometric fluorescent detection [188]. Optical studies were carried out in the presence of 23 different chloride or perchlorate metal salts (Li^+, Ba^{2+}, Ca^{2+}, K^+, $Li+$, Mg^{2+}, Mn^{2+}, Na^+, Cr^{3+}, Au^{3+}, Zr^{4+}, Rh^{3+}, Pb^{2+}, Ag^+, Co^{2+}, Cu^{2+}, Ni^{2+}, Hg^{2+}, Cd^{2+}, Zn^{2+}, Fe^{2+}, Fe^{3+}, Pt^{2+}). In an EtOH:H_2O (10 μM, 1:1, *v/v*) solution, **31** showed two π-π^* absorption bands at 286 nm and 327 nm, and the addition of Fe^{2+} ion led to the appearance of a new peak at 573 nm, with a corresponding color change from colorless to purple-red. The other metals did not produce any significant changes in the absorption spectra, and their presence did not interfere with the probe's response to Fe^{2+}. Job's plot and ESI-MS data indicated that the **31**:Fe^{2+} complex had a 2:1 binding stoichiometry and the association constant was calculated to be 3.4×10^7 M^{-1}. The limit of detection for the method was found to be 2.0×10^{-8} M. When excited at 340 nm, **31** showed an emission at 408 nm and the addition of Cd^{2+} ions led to a decrease in the intensity of the emission at 408 nm, the appearance of a new emission at 475 nm, and a change in fluorescent color from blue to cyan. The addition of Zn^{2+} ions led to a decrease in the intensity of the emission at 408 nm, the appearance of a new emission at 498 nm, and a change in fluorescent color from blue to yellow-green. No other metals showed a significant response, and only Fe^{2+} interfered with the probe's response to Cd^{2+} and Zn^{2+}. The ratios of the two emissions (I_{475}/I_{408} and I_{498}/I_{408}) could be used to calculate the LoD for Cd^{2+} and Zn^{2+} of 2.6×10^{-8} M and 2.0×10^{-9} M, respectively. Job's plot and ESI-MS data indicated that the **31**:Cd^{2+} complex had a 1:1 binding stoichiometry and the association constant was calculated to be 0.2×10^6 M^{-1}. The **31**:Zn^{2+} complex had a 2:1 binding stoichiometry, and an association constant of 0.9×10^6 M^{-1}. ^1H NMR data indicated that the metals bound to the nitrogen atoms; the proposed sensing mechanism for the probe toward Fe^{2+}, Cd^{2+}, and Zn^{2+} is presented in Scheme 13.
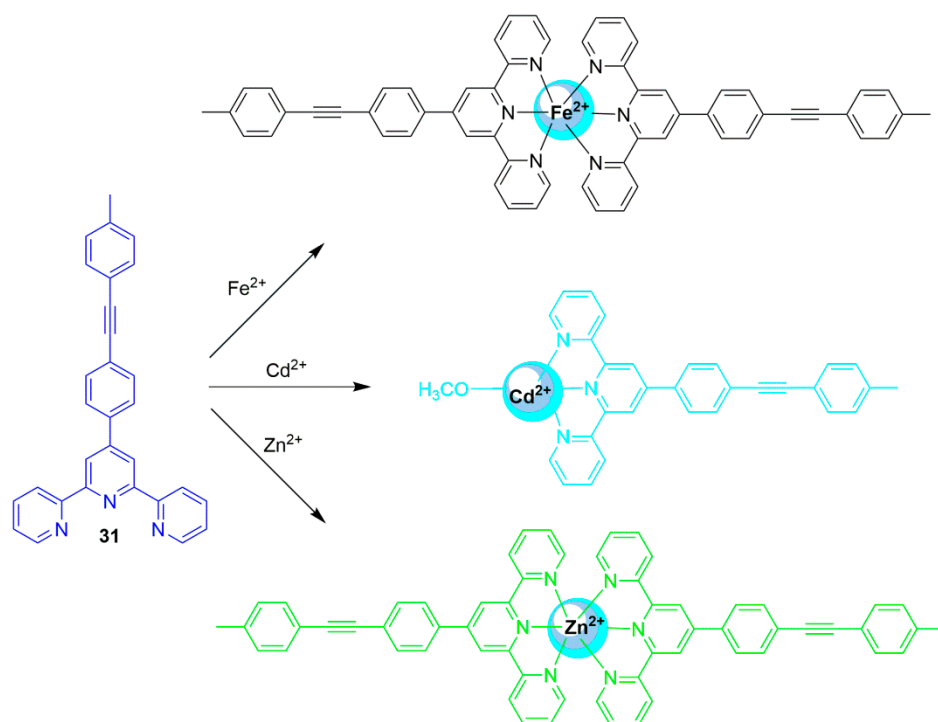
Scheme 13. The binding modes of probe **31** and the different metal ions.

2.3. Mercury Probes

　　　Out of the three metal ions in group 12, mercury in the form of organic mercury is the most toxic. Therefore, designing molecular chemosensors for mercury ions is a very important endeavor, especially in aqueous systems, as certain biological species readily convert metallic mercury into organic mercury. There have been many different types of fluorescent sensors for mercury, recent examples include

quantum dots [189], biosensors [8], carbon dots [190], carbon nanoparticles [191], gold and silver nanoparticles [192,193], but the focus in this final section is on LMFP sensors.

Highly selective off–on optical sensor **32** was synthesized by Ahmed et al. for the detection of mercuric ions in an organic-aqueous, HEPES-buffered ($CH_3CN:H_2O$, 1:2, *v/v*, pH 7.2) system [194], Compound **32** drastically changed color from yellow (340 nm) to purple (550 nm), upon the addition of Hg^{2+} ions and was also found to be highly fluorescent, with an emission band at 430 nm, when the coordination complex was formed in situ. The weak fluorescence emission of **32** was a consequence of PET quenching which was inhibited upon by the coordination of the Hg^{2+} ions. The binding constant was calculated to be 1.9×10^3 M^{-1} using the Benesi–Hildebrand linear regression analysis, which showed a straight line. However on closer inspection of the regression line, the data presented was not a Benesi–Hildebrand plot. The authors plotted an intensity ratio versus concentration of Hg^{2+} ions, therefore, the binding constant reported should be viewed with a little skepticism. The coordination environment was confirmed by IR and NMR studies, as compound **32** had distinct functional groups (carbonyl and hydrazide) that could act as IR labels, the stretching frequencies shifted when coordinated to Hg^{2+} ion, the tridentate binding motif was further supported by DFT calculations. The Hg^{2+} ion was removed from the binding site by the addition of KI ions to precipitate HgI_2, which turned off the emission signal. Therefore, this "off–on–off" approach could be translated into binary code to build an INHIBIT logic gate (a combination function consisting of and AND gate plus one other event, in this example a NOT event), Figure 13.

(A)

(B)

Input		Output
In 1 (Hg^{2+})	In 2 (KI)	Fluorescence enhancement at 429 nm
0	0	0
0	1	0
1	0	1
1	1	0

(C)
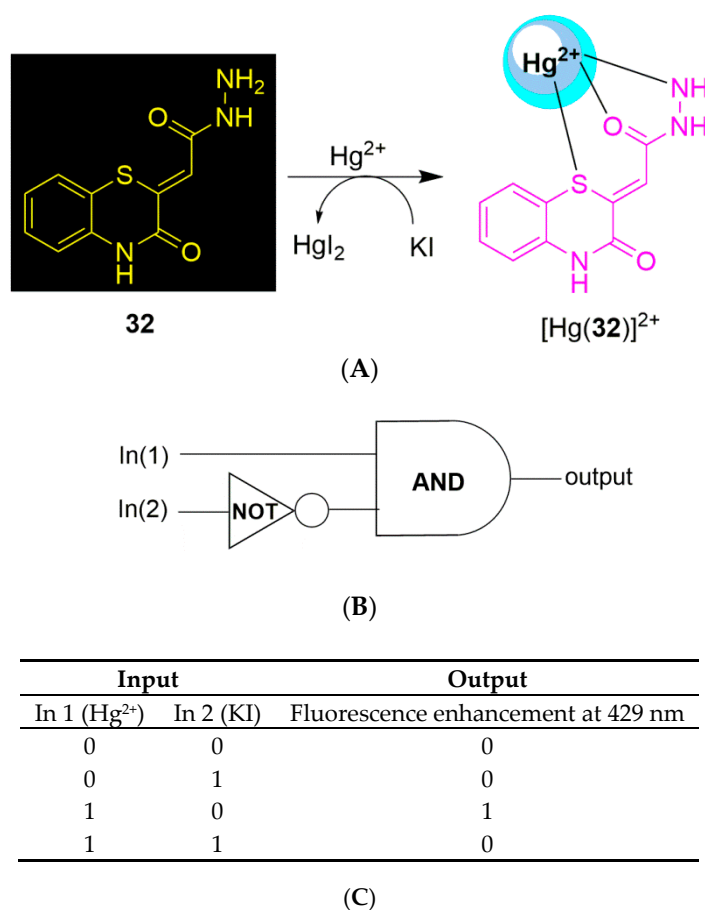
Figure 13. Molecular probe **32**, highlights the proposed binding environment and color and fluorescence changes (**A**) chemical scheme, (**B**) circuit diagram corresponding to the Hg^{2+} and KI inputs and (**C**) truth tabled [194].

Aggregation-induced emission (AIE) has become a popular mechanism exploited for sensors often used in chemodosimeter and chemoreactand type molecular probes. A recent review covers the use of chemodosimeters (non-reversible covalent bonds and chemoreactands with reversible covalent bonds), whereby, the optical properties were different from the bound and unbound chemical adducts [53]. Chatterjee and coworkers have prepared chemodosimeter **33** to detect organic and inorganic Hg^{2+} species, Figure 14 [193]. The probe functions based on a mercury ion-promoted transmetalation reaction between tetraphenylethylene mono-boronic acid **33** and Hg^{2+} ions. For aggregation to occur, the correct working concentration needed to be established, which was found to be 30 μM (H_2O-THF (90:10)). On the addition of $HgCl_2$ to probe **33**, transmetalation occurred to form compound **33a**. As a consequence of the chemical transformation, the planarity of **33a**-HgCl was restored and the onset of AIE occurred. The AIE aggregation was supported by transmission electron microscopy (TEM) and dynamic light scattering (DLS) experiments, which showed average nanoaggregates of 36 nm but, after the addition of $HgCl_2$ to the 30 μM solution of **33**, these grew to 690 nm. No other metal was shown to transmetalate compound **33**, therefore, the molecular chemodosimeter was very specific for Hg^{2+} ions. Interestingly, methylmercury ion was also shown to undergo transmetalation, forming **33b**, which also aggregated and turned on emission. As methylmercury ion readily bioaccumulates in fish, the chemodosimeter was tested using zebrafish embryos. In the presence of methylmercury ion, fluorescence microscopic images showed that a distinctive blue glow occurred. This elegant experiment showed that transmetallation of the C-B bond to C-Hg bond, and aggregation can occur in vivo, making this a highly attractive approach to monitor organomercury species, in higher order fish species.
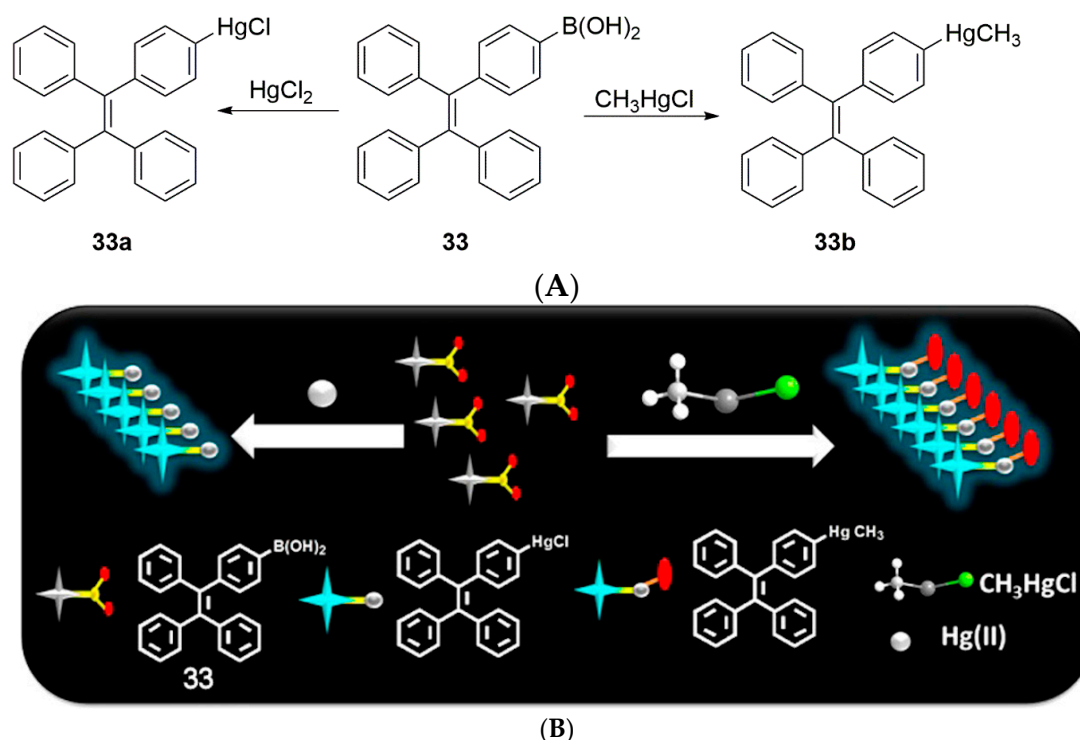
Figure 14. Schematic representation of the sensing process of chemodosimeter **32** on the addition of Hg^{2+} ion and CH_3Hg^+. Reprinted (adapted) with permission from [195]. (**A**) Chemical Scheme, (**B**) proposed fluorescence aggregation

Another chemodosimeter, has been developed by Ou et al. [196] who employed a protection–deprotection strategy to monitor mercury. This approach takes advantage of the distinctly different electronic properties of two different molecules. For example, protected aldehydes and ketones can be deprotected with Hg^{2+} salts. As no other metal ion causes a selective cleavage under

these conditions, the molecular probes are highly selective for Hg^{2+} ions. Thioacetal-modified pyrene sensor **34** was prepared and was shown to be cleaved by Hg^{2+} ions, to form pyrenecarboxaldehyde **34a**, Scheme 14. Compound **34** undergoes an off-on fluorescence response when Hg^{2+} ions are added. The Hg^{2+} ions deprotect the thioacetals to form the aldehyde functional group, confirmed by ^1H NMR as the aldehyde proton appeared at 10.82 ppm. The UV-Vis and fluorescence experiments were used to verify that one equivalent of Hg^{2+} ions were needed to fully convert **34** to **34a**.
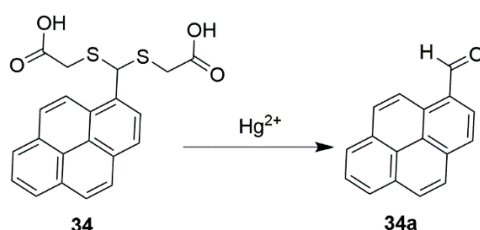
Scheme 14. Chemodosimeter **34**.

The pyridine ring is a versatile moiety and is often found in molecular receptors. Tetrahydrodibenzo phenanthridines, contain a pyridine functional group with five fused six-membered ring systems with connectivity, shown in Figure 15. This arrangement of ring systems are found in natural products and biologically active compounds [197,198]. Two bis(dithioester) substituted phenanthridines, compound **35** and compound **36**, were synthesized by Sundaramurthy et al., who showed that they could coordinate with Hg^{2+} ions [199]. Mono-sulfur derivative **35** demonstrated a strong fluorescence turn on signal in an aqueous solution, in the presence of Hg^{2+} ions, whereas tetra-sulfur derivative **36** showed a strong fluorescence quenching towards Hg^{2+} ions. The binding stoichiometry of both sensors toward Hg^{2+} ions was 1:1, according to the UV-Vis absorption spectra, fluorescence measurements, and computation (DFT) studies. The LoD for the mono-sulfur derivative was found to be as low as 0.91 nM for Hg^{2+} ions, while the bis(dithioester) derivative demonstrated an LoD of 0.04 nM. The spectroscopic changes were also seen in paper-based test strips as seen in Figure 15.
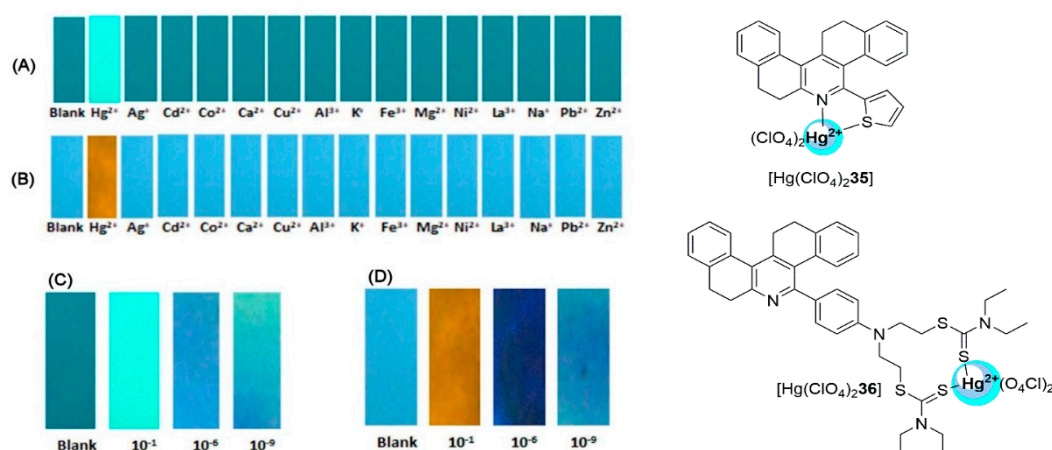
Figure 15. Changes in the fluorescence of probes **35** and **36** in paper strips with different metal ions (**A**) probe **35** (**B**) probe **36**, and at different concentration (nM) of Hg^{2+} ions (**C**) probe **35** and (**D**) probe **36**. Adapted from [199] with permission from the Centre National de la Recherche Scientifique (CNRS) and the Royal Society of Chemistry.

Anthracene-based, reusable fluorescent sensor **37** was synthesized via a one-pot reaction imine condensation by Misra et al. [200]. As anthracene is hydrophobic, it was expected that compound **37** would aggregate when the solvent mixture had a high content of water. By changing the THF:H_2O ratio, it was found that the optimal working condition required 70% water. A strong emission band

around 518 nm was observed (20 μM) with a calculated ϕ of 0.614. As the water content was increased, the molecules came closer together to restrict intramolecular rotation around the imine bond and, therefore, increased the fluorescence emissions, Scheme 15. In solutions where the water content was low, very weak emission bands were observed in the fluorescence spectra (ϕ = 0.002). When $Hg(NO_3)_2$ was added to the aggregates, significant optical quenching was seen in the fluorescence emission, due to the heavy atom effect. This was a consequence of perturbating the intersystem crossing from the first singlet state (S_1) to the lowest triplet state (T_1), thereby, increasing the spin-orbit coupling from the aromatic scaffold of the molecular probe to the external heavy atom [201,202], upon the coordination of the Hg^{2+} ions to **37**, through chelation. Therefore, the Stern–Volmer analysis showed the quenching constant (K_{sv}) to be 2.5×10^5 M^{-1} and the LoD was found to be in the ppb concentration range (3 ppb). Moreover, analysis of municipal water and river water from the local area, using probe **37** detected Hg^{2+} ions.
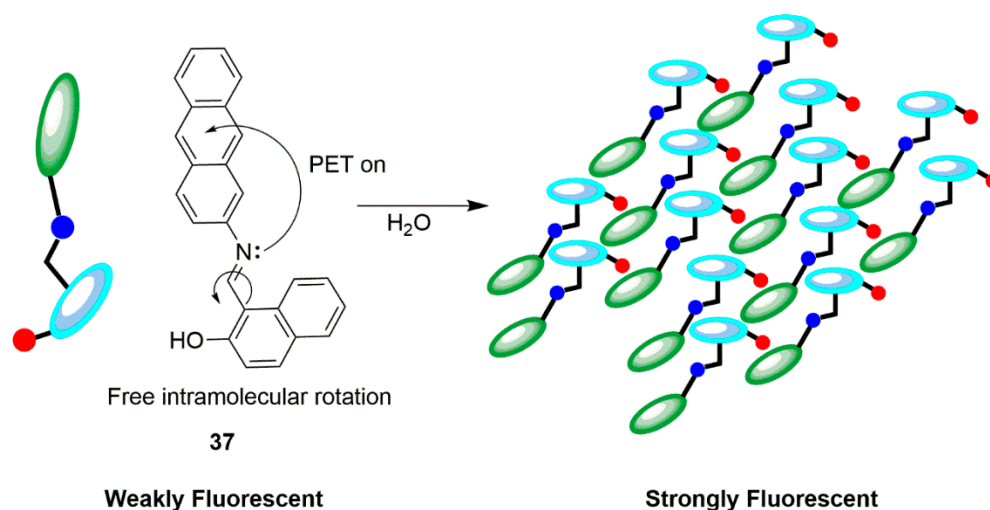

Scheme 15. Proposed aggregation behavior of **37** in water.

The rhodamine fluorophore has been used as a molecular probe for a variety of metal ions over the years and xanthene derivatives have previously been highlighted in this review. Compound **38** was shown to distinguish between Hg^{2+} and Cu^{2+} ions. It was prepared by Gao and Zheng who showed that either in the absence or presence of UV light, a distinction could be made between Hg^{2+} and Cu^{2+} ions, Scheme 16 [203]. Optical studies were carried out in the presence of 16 different metal nitrate salts (Hg^{2+}, Cu^{2+}, Ag^+, K^+, Al^{3+}, Ca^{2+}, Na^+, Ba^{2+}, Co^{2+}, Cd^{2+}, Fe^{3+}, Mg^{2+}, Mn^{2+}, Zn^{2+}, Ni^{2+}, Pb^{2+}) in a IPA:H_2O solvent (25 μM, 8:1, *v/v*). Probe **38** was initially colorless, indicative of the closed lactam moiety. However, on the addition of one equivalent of Hg^{2+} ions, a new band at 557 nm was observed (colorless to pink), indicating that the spirolactam ring was in the open form, which is very common for these molecular probes. Compound **38** shows a very weak emission intensity, but an emission band was seen at 578 nm, when Hg^{2+} ions were added to the solution (λ_{ex} = 550 nm). This phenomenon was not seen in the presence of the other metal cations. Copper(II) is well-known to quench the fluorescence emission, therefore, it was not surprising that an emission signal was not seen on the addition of Cu^{2+} ions, but on the addition of Hg^{2+} ions, a new absorption band was seen at 559 nm and a visible color change from colorless to purple was observed. The coexistence of Hg^{2+} and Cu^{2+} in the solution showed a decrease in the emission intensity of the band at 559 nm, indicating that the presence of Hg^{2+} interfered with Cu^{2+} detection. One way to deliberately make their mixed system monitor one of the ions over the other, is to take advantage of solubility products. Bromide ions were used to precipitate $HgBr_2$ (K_{sp} = 3×10^{-7}), enabling the detection of Cu^{2+} ions.
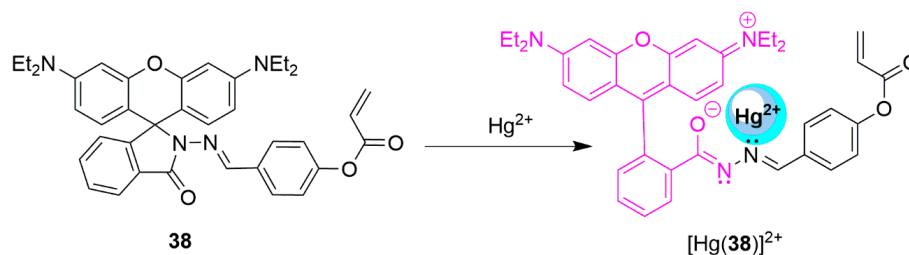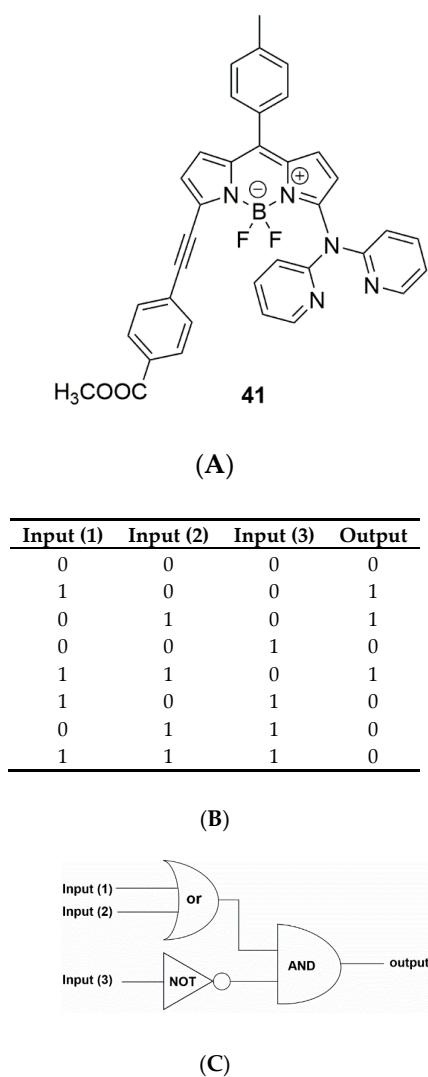
Scheme 16. The coordination of **38** to Hg^{2+} ions.

As mercury is classified as a "soft" metal, mercury ions forms many stable ionic compounds that are insoluble [204,205]. Thermodynamic stability is further enhanced when "soft" Lewis bases are present in the receptor, for example sulfur atoms [206]. The carbonyl group (C=O) in the lactam ring in rhodamine probes could be readily converted to the analogous thio (C=S) group, by using Lawesson's reagent. Zhou, Hu and Yao synthesized thiooxo-rhodamine B hydrazine compounds **39** and **40**, which contain a number of sulfur atoms to help the molecular probe to selectively coordinate to Hg^{2+} over other metal ions [203]. Both molecular probes are colorless but addition of Hg^{2+} ions leads to a significant increase in absorption at 560 nm, due to the spirolactam ring-opening. No optical changes were seen in the presence of the other metals (Na^+, K^+, Mg^{2+}, Ca^{2+}, Al^{3+}, Cr^{3+}, Ba^{2+}, Hg^{2+}, Mn^{2+}, Pb^{2+}, Cd^{2+}, Ni^{2+}, Zn^{2+}, Co^{2+}, Fe^{3+}) in a EtOH/HEPES solution (5 μM 1:1, *v/v* pH 7.4) but Ag^+ and Cu^{2+} ions increased in intensity at 560 nm. Probe **40** selectively detected Hg^{2+} ions via an "off–on" response in solution. The Job's plot and UV-Vis titration data indicated that the stoichiometry between **40** and Hg^{2+} ions was 1:2. This is unsurprising as there is free rotation around the bisthiophene bond, so the two rhodamine units could adapt an anti-conformation with the Hg^{2+} ions bound in each coordination environment. By comparison, compound **39** bound the Hg^{2+} ions in a 1:1 ratio. The association constants for **39** and **40** with mercury were calculated using the Benesi-Hildebrand method and was found to be 4×10^5 M^{-1} and 1.3×10^{11} M^{-2}, respectively. Interestingly, the fluorescence mechanism for the two molecular probes was very different. Molecular probe **39** was shown to exhibit a FRET mechanism, due to overlap between the emission spectra of the bisthiophene donor and the absorption spectra of the rhodamine B acceptor. Compound **40** did not show FRET and the fluorescence emission was due to the ring-opening of the spriolactam. The authors also demonstrated that compounds **39** and **40** could monitor the levels of Hg^{2+} ions in municipal water.
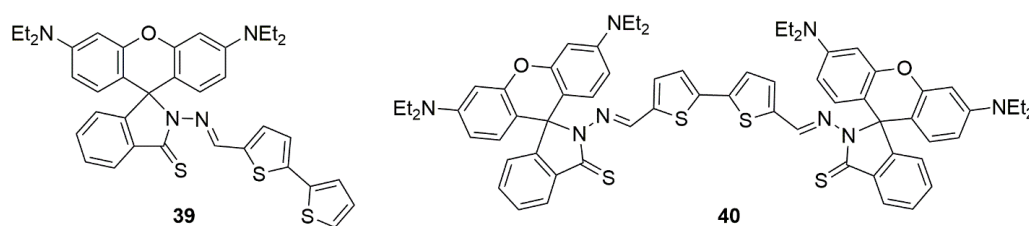
4,4-Difluoro-4-bora-3a,4a-diaza-s-indacene (BODIPY) possesses unique spectroscopic signatures and the BODIPY moiety has been used extensively in molecular probe design [207–209]. Qiu, Zhang, and Yin synthesized a BODIPY-based probe with a dipyridylamino (DPA) receptor (compound **41**), for which the optical response was different for Cu^{2+}, Hg^{2+}, and Pb^{2+} ions [210]. On the addition of the Cu^{2+}, Hg^{2+}, and Pb^{2+} ions, the optical response was different for each metal ion. Optical studies were carried out in the presence of a number of different perchlorate metal salts (Ag^+, Ba^{2+}, Ca^{2+}, Cd^{2+}, Co^{2+}, Cu^{2+}, Fe^{2+}, Hg^{2+}, K^+, Mg^{2+}, Na^+, Ni^{2+}, Pb^{2+}, Zn^{2+}) in a 2.0 μM CH_3CN solution. The presence of Hg^{2+} and Pb^{2+} in the solution, lead to a blue shift in the maximum absorbance peak from 595 nm to 572 nm and a visible color change from blue to purple. The presence of Cu^{2+} ions in the solution led to a blue shift in the maximum absorbance from 595 nm to 512 nm, and a visible color change from blue to fuchsia. Compound **41** showed a single weak emission, when it was excited at 365 nm. The presence of Hg^{2+} and Pb^{2+} ions led to a new emission band at 587 nm and a change from dark red

fluorescence to orange fluorescence. The presence of Cu^{2+} ions led to an emission band at 545 nm and a change from dark red fluorescence to green fluorescence. Competition studies have showed that the presence of Cu^{2+} ions in the solution quenched the Hg^{2+} and Pb^{2+} ions fluorescent responses. The presence of other metal ions did not influence the Cu^{2+} response. Both Hg^{2+} and Pb^{2+} ions could be removed from the binding site of **41**, when EDTA was added to the solution. A Job's plot and ESI-MS data indicated a 1:1 binding stoichiometry, and ^1H NMR data indicated that the probe's fluorescent and colorimetric responses were due to π delocalization between the N-pyridyl and BODIPY groups, caused by the coordination of the metal ions to the BODIPY and DPA groups. As Hg^{2+}, Pb^{2+} and Cu^{2+} produced different emission intensities it was possible to construct OR, NOT, and AND logic circuits, where the inputs were the metal ions and the output was the emission intensity at 587 nm. If the emission intensity was greater than a chosen arbitrary unit (150 au), then "1" was assigned for (i) both Hg^{2+} and Pb^{2+}, (ii) Hg^{2+}, or (iii) Pb^{2+} on their own were present, meaning that the gate was opened. If, Cu^{2+} was present alone, with Hg^{2+} or Pb^{2+} or both Hg^{2+} and Pb^{2+}, it led to a situation whereby the intensity was lower than 150 au, therefore a "0" was assigned, meaning the gate was closed. Therefore, the combinations of the three different metal ions gave rise to different logic gates (OR, NOT, and AND), Figure 16.

(A)

Input (1)	Input (2)	Input (3)	Output
0	0	0	0
1	0	0	1
0	1	0	1
0	0	1	0
1	1	0	1
1	0	1	0
0	1	1	0
1	1	1	0

(B)

(C)

Figure 16. Truth table and logic circuit input (1), (2), and (3) Pb^{2+}, Hg^{2+}, and Cu^{2+} ions (20 μM, CH_3CN), respectively, and output is the fluorescence intensity at 587 nm [210]. (**A**) molecular probe, (**B**) truth table and (**C**) circuit.

Gao and Chen synthesized a Schiff-base probe with coumarin and benzimidazole fluorophores (**42**), which was capable of simultaneously detecting Hg^{2+} and Cu^{2+} ions, by two different mechanisms [211]. Compound **42** produced a fluorescence emission enhancement, when bound to Hg^{2+} ions, whereas, the Cu^{2+} ions quenched the emission band. A weak fluorescence intensity at 426 nm ($\phi = 0.009$) was seen for **42** in a 10 µM HEPES:DMSO (20 mM, 9:1, *v/v*) solution. A significant enhancement was seen in the presence of Hg^{2+} ions ($\phi = 0.152$), whereas in the presence of Cu^{2+} ions, a red shift to 448 nm was seen, but the emission band was reduced in intensity ($\phi = 0.005$). Job's plot analysis and fluorescence titration data both indicated a 1:1 binding ratio for both the Cu^{2+} and Hg^{2+} complexes. The structure of the complexes was supported by HRMS, IR, and NMR studies. The Hg^{2+} ion bound in a tridentate fashion, but the molecular probes underwent hydrolysis via a mercury-promoted hydrolysis (Scheme 17), so the fluorescence emission was due to the coumarin-carboxaldehyde being formed. Fluorescence titration data were used to determine the probe's sensitivity to Hg^{2+} and Cu^{2+} ions, and the Benesi-Hildebrand equation used to calculate the association constants for the probe towards Cu^{2+} ions and Hg^{2+} ions, gave 7×10^4 M^{-1} and 9×10^4 M^{-1}, respectively.
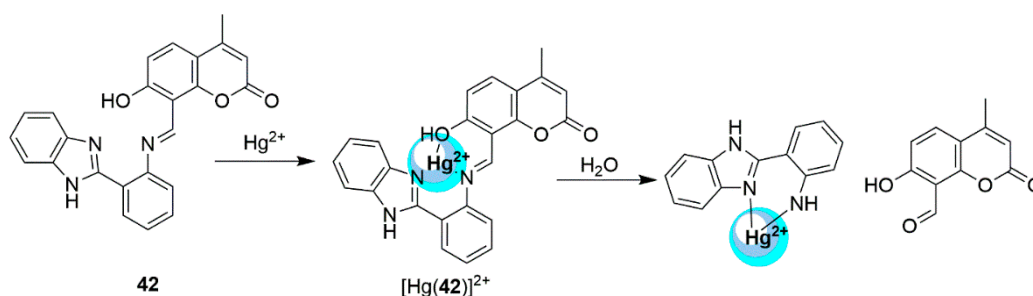
Scheme 17. The coordination and subsequent hydrolysis of molecular probe **42**.

Another example of molecular chemodosimeter that can selectively monitor Hg^{2+} ions is compound **43** [212]. A solution of compound **43** in 10 µM HEPES (10 mM, pH 7) had a maximum absorption band at 315 nm, and when excited at 371 nm, a weak emission band was observed at 450 nm. Interestingly, the authors failed to mention why the excitation wavelength used in their studies was so far removed from the maximum absorption band. An increase in absorption and emission intensity was seen when Hg^{2+} ions were added to **43**. The fluorescence quantum yield of **43** was calculated with respect to rhodamine B and found to be $\phi = 0.027$. The addition of one equivalence of Hg^{2+} led to a ten-fold increase in fluorescent intensity ($\phi = 0.22$), which was accompanied by a change in fluorescence from colorless to blue. No other metal cation showed the same response (Zn^{2+}, Hg^{2+}, Na^+, Pb^{2+}, Co^{2+}, K^+, Ni^{2+}, Cu^{2+}, Al^{3+}, Mn^{2+}, Cr^{3+}, Mg^{2+}, Fe^{3+}, Cd^{2+}). ESI-MS and NMR studies showed that the fluorescence emission was due to the cleavage of the carbonothioate, via a Hg^{2+}-promoted hydrolysis, thereby, forming 7-hydroxy-4-methylcoumarin dye, which was highly fluorescent. This "simple" molecule was used to monitor deliberately spiked tap water with Hg^{2+}, to show that it could be used in a real-world application.

43
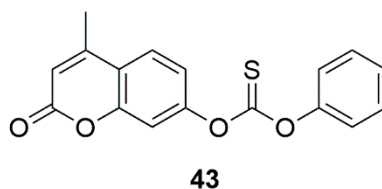
The imine functional group can undergo hydrolysis under acidic conditions [213]. This is a well-known and thoroughly investigated mechanism, whereby the rate determine step is the initial nucleophilic addition to the carbon-nitrogen double bond. It has also been shown that metal ions can accelerate the hydrolysis mechanism via a substrate-metal association, whereby the metal ion is

coordinated to the nitrogen atom, enhancing the substrate for nucleophilic attack [214]. Compound **44** was prepared by Duan et al. [215]. It was shown that compound **44** works as a turn-on sensor through Hg^{2+} promoted hydrolysis, in which the imine is cleaved to form the coumarin aldehyde fluorophore and a 5-aminoisophthalic acid methyl ester. The cleavage did not occur in the presence of other metal ions (Na^+, K^+, Mg^{2+}, Ca^{2+}, Cd^{2+}, Mn^{2+}, Fe^{2+}, Co^{2+}, Ni^{2+}, Cu^{2+}, Zn^{2+}, Ag^+, Pb^{2+}, Hg^{2+}) in a 2×10^{-6} M $CH_3CN:H_2O$ 8:2 (*v/v*) solution at physiological pH (0.1 M $KClO_4$ buffer, pH 7.3). Compound **44** displayed a weak fluorescence signal at 530 nm. The lone pair on the nitrogen atom PET, quenched the emission intensity. On the addition of Hg^{2+} ions, a 20-fold increase in emission was seen at 490 nm. The emission at 490 nm was assigned to the coumarin aldehyde fluorophore, and the ratio between the intensity at 490 nm and 530 nm (I_{490}/I_{530}) was used to detect Hg^{2+} ions, via a ratiometric approach. The LoD of Hg^{2+} was calculated to be in the nanomolar concentration range. Fluorescence was significantly turned on as **44** broke down into two separate molecules, one of which, the coumarin aldehyde is highly fluorescent. It was reasoned that **44** could be used to monitor Hg^{2+} ions in the human breast adenocarcinoma cell (MCF-7) line, which was observed when the cells were incubated with Hg^{2+} ions.


44
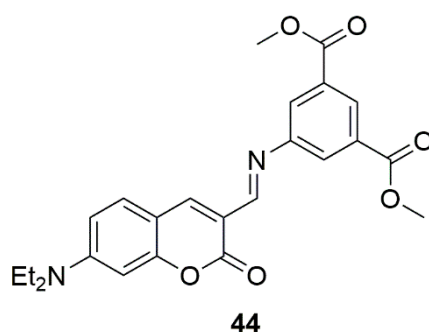
3. Multivariate Analysis

Molecular recognition between low molecular weight fluorescent probes (LMFPs) and metal cations has dominated the field for many years. Sensor arrays, using statistical analysis and pattern-recognition algorithms are now becoming the main approach to measure and monitor a number of analytes in a single experiment, and a recent review written by Jolliffe, highlights some recent examples in fluorescent sensing arrays [216]. Here, we give a couple of recent examples on this new sensing approach, to highlight the direction of research in the field.

Minami et al. used commercially available dyes (alizarin red, bromopyrogallol red, and pyrogallol red) that contained the catechol moiety [217]. The catechol functional groups reacted with 3-nitrophenylbornoic acid (3-NPBA) to form a dynamic covalent bond. The metal ion competed with the boronic acid for the catechol moiety; thus, upon coordination of the metal ion, 3-NPBA was displaced. The metal-dye complex generated different colors, depending on the dye and the metal, Scheme 18.

The coordination of the catechol dyes and 3-NPBA resulted in blue shifts in the absorption spectra, and the addition of metal ions led to a red shift, due to the displacement of 3-NPBA and the formation of a dye-metal complex. FAB-MS and titration isotherms indicated that both the dye:3-NPBA and dye:metal complexes had a 1:1 stoichiometry. Extensive univariant work gave an understanding of the interaction and the K_{assoc} for selected metal ions (Cu^{2+}, Ni^{2+} and Zn^{2+}), which were in the range of 5×10^2 M^{-1} to $> 10^6$ M^{-1}. The array utilized a 384 well microplate for high throughput screening. The response of the sensor array in the presence of 11 metals was investigated (50 mM HEPES buffer solution containing 10 mM NaCl interferant, 40 μM catechol dye, 4 mM 3-NPBA, and 10 μM metals) and was capable of discriminating between Ni^{2+}, Cu^{2+}, Zn^{2+}, Cd^{2+}, Co^{2+}, Fe^{2+}, Hg^{2+}, Al^{3+}, Pb^{2+}, Ga^{3+}, and Ca^{2+}. LDA analysis indicated that 95.2% of variance was sufficient to discriminate between the different metals, and the cross-validation method indicated a 100% correct classification within each cluster, Figure 17A. A potential semi-quantitative analysis to determine the concentration of the

metals was demonstrated using a mixture of Cu^{2+}, Zn^{2+}, and Ni^{2+}, and a regression analysis using a support vector machine (SVM) algorithm (Figure 17B). The results of the semi-quantitative assay, where the three different metals were tested at a concentration range of 0–3.7 ppm with 20 repetitions at each concentration, showed that a plot of the actual vs. predicted concentrations was highly accurate. The concentration range over which the results were obtained ($Ni^{2+} < 30$ ppm, $Cu^{2+} < 2.5$ ppm, $Zn^{2+} < 6$ ppm), the method's potential for high-throughput screening, and the fact that the assay gave no response in the presence of other metals common in environmental water sources, such as K^+, Na^+, Mg^{2+}, indicated that the assay developed by Sasaki and coworkers could be a useful tool for real time testing, in environmental water sources.
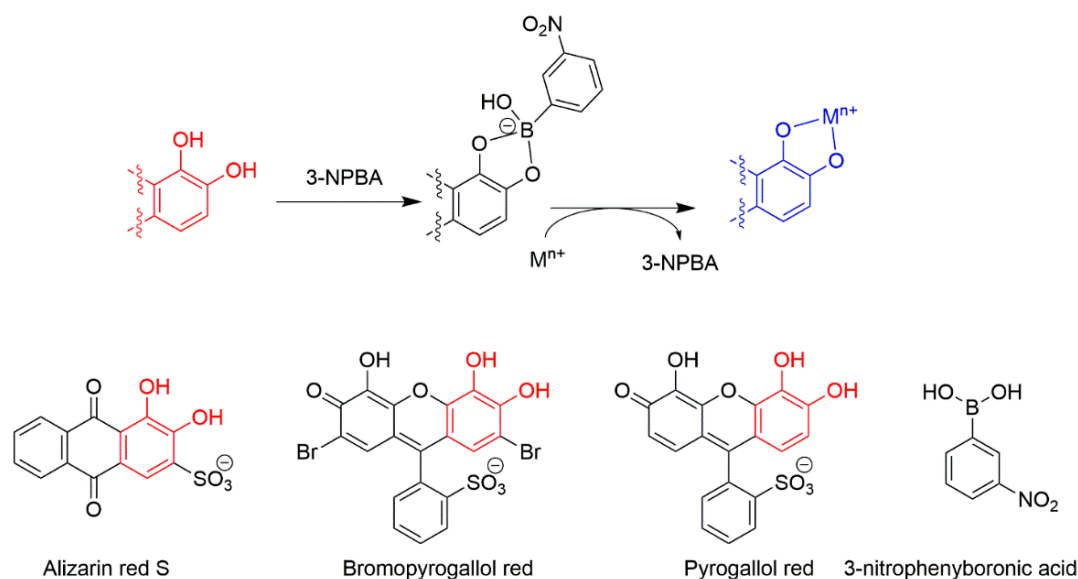
Scheme 18. The displacement approach by which the dyes formed a dynamic bond with the boronic acid derivative which was then displaced upon the coordination of the metal ion.
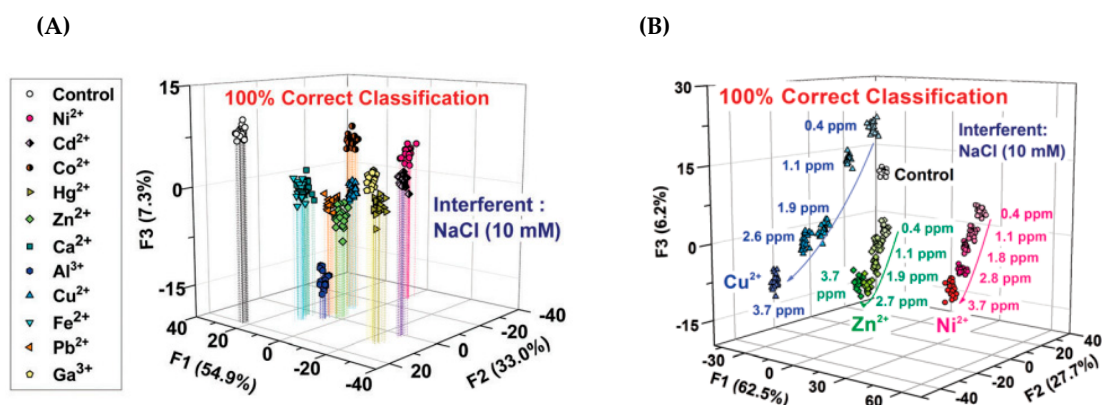
Figure 17. (**A**) Linear discriminant analysis (LDA) score plots for the response of the sensor array to 11 analytes (and control) in a HEPES buffer (50 mM) solution, with sodium chloride (10 mM). The [metal ion] = 10 mM. 20 repetitions were measured for each analyte. (**B**) The cross-validation routine shows 100% correct classification LDA results of the semi-quantitative assay, toward three different metal ions (Cu^{2+}, Zn^{2+} and Ni^{2+}); concentration range of 0–3.7 ppm.%. Adapted from [218] with permission from The Royal Society of Chemistry.

Our group has carried out multivariate pattern recognition approaches to the binding between coumarin–enamine probes (compounds **45a–e**) and ten divalent metal ions [219]. The coordination of the metal ions with compounds **45b–e**, through the nitrogen atom, showed optical responses in a univariant approach, but the data were limited in terms of discrimination. To capture this wealth of information and to be able to carry out the discrimination of metal cations as proposed, a multivariate approach was adopted. A multimode microwell plate reader was utilized, allowing for rapid and automated acquisition of multivariate data. The sensor array comprised compounds **45b** to **45f**. Compound **45a** did not possess a binding site on the aromatic ring system, so it was used as a reference.

45a-e
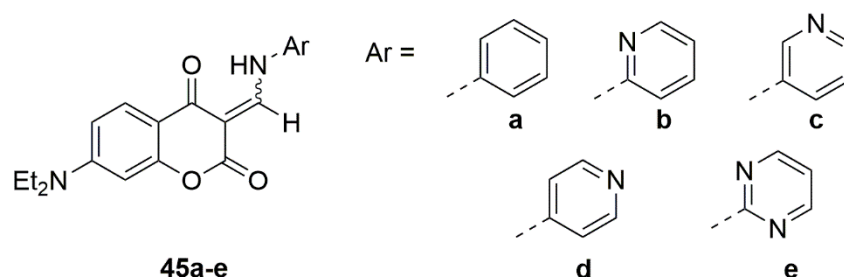
The absorbance response of this array of four sensors at 330, 380, 400, and 430 nm, and fluorescence intensity at 330/450 nm, 330/528 nm, 330/580 nm, 380/450 nm, 380/528 nm, and 380/450 nm ($\lambda_{ex}/\lambda_{em}$) were determined concurrently. The sensing array was exposed to a panel of analytes comprising the chloride salts of—Ca^{2+}, Cd^{2+}, Co^{2+}, Cu^{2+}, Fe^{2+}, Hg^{2+}, Mg^{2+}, Ni^{2+}, Pb^{2+}, and Zn^{2+}, and all measurements were conducted in the same solvent (DMSO) as the univariate analysis for consistency. The sensor array was exposed to each metal multiple times, generating a cluster of 18 replicates for each analyte. This approach generated a very large multivariate data set (4 × sensors by 10 × analytes by 18 × replicates = 720 data points, each described by nine instrumental variables). Linear discriminant analysis (LDA) was used to organize the high-dimensionality data and to extract the most relevant information, ultimately providing the information necessary to classify the ten analytes considered.

The well-established LDA algorithm computed a linear combination of the original variables that maximized the separation between multiple analytes, while minimizing the separation between replicate measurements of the same analyte [218]. In doing so, the algorithm generated a new set of variables, called factors, which were returned in order of decreasing relative information content. Data reduction was then accomplished by retaining only the first two or three LDA factors and dropping the higher-order ones. This produced a transformed dataset, in which each point was associated with a pair or a triplet of numbers, respectively, typically referred to as the factor scores of those points. These factor scores could be used as coordinates in plotting the transformed points in either a two- or three-dimensional plot.

It was shown that, the first two factors obtained from the LDA analysis, out of the ten present in the system, accounted for 80.7% of the total information content of the original system. A two-dimensional score plot (Figure 18) was obtained that showed clear clustering of the data—replicate measurements of samples of each divalent metal ion were classified as similar and grouped together by the LDA analysis. In short, the pattern-based approach was capable of differentiating almost all ten divalent metal cations, using the additional information collected through patterning and multivariate analysis. However, this analysis failed to definitively separate the ten metal ions, this was due to similarities in geometry that was adopted upon the binding of the molecular probe.
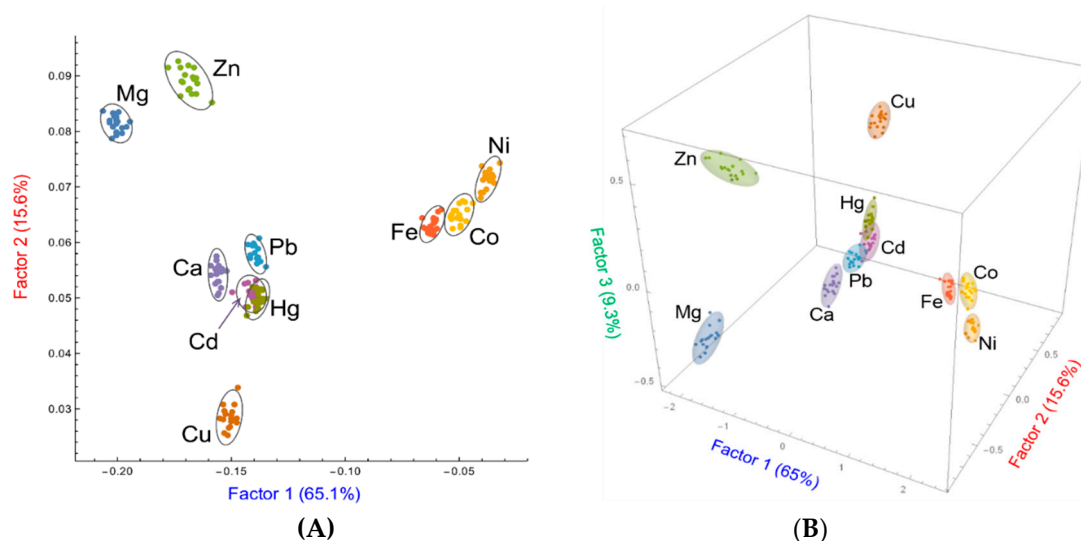
Figure 18. (**A**) Two-dimensional LDA score plot for the analysis of probes **45a–e** binding 10 divalent metal chlorides. (**B**) A three-dimensional LDA score plot captured 90% of all information available from the pattern recognition system, significantly improving on the separation of difficult cases that were imperfectly discriminated, using the two-dimensional results. Confidence ellipsoids were drawn at 95% confidence. Adapted from [218] with permission from The Royal Society of Chemistry.

4. Conclusions and Future Prospects

The chemical sensors that have been highlighted throughout this review showcase recent low molecular weight fluorescent probes designed to target the group 12 triad (Zn^{2+}, Cd^{2+}, and Hg^{2+}). During the last few years there has been a great deal of work on the design, synthesis, and detection of these metal ions. Much of the work presented here is focused on the traditional approach of sensor design, where the spectroscopic response is univariant in nature i.e., one LMFP targets one metal. As small molecule recognition becomes more popular, it is becoming more challenging to prepare novel compounds, but as computer power improves significantly, monitoring and discriminating metal ions in a complex environment seems to be the direction in which the sensor community is moving. Groups still publish their findings on LMFP and, whilst writing this review and taking a closer look at the data, it is clear that there are some general omissions or misleading statements. One of the biggest challenges is to work in 100% aqueous system, however, the systems are often in a mixture of organic-aqueous systems, and more often than not, only a fraction is water. Nevertheless, it has been claimed that a particular probe works in water. Additionally, there is often little or no discussion on the aqueous chemistry of the metal ion which influences the coordination. Moreover, many reports often omit a serious discussion on speciation, in their particular system, claiming that only a 1:1 probe-metal exists, when the data often suggest that other species might exist. More often than not, the counter-anion is omitted and authors make the assumption that it plays no role in binding, but only exists to balance the charge, when many counter ions can form bridging species. This is particularly important if a system is to work in an aqueous system, as anions might not exist in their conjugate base form, depending on the pH, which might influence the speciation. Additionally, care must be taken in reporting equilibrium constants using old linear regression methods, for example, the Benesi–Hilderbrand double reciprocal plot and Job's plot analysis. Even though they are easy to use they are significantly over used and misinterpreted. For example, subtle curvature in the Benesi–Hilderbrand plot is often mistaken as indicative of a 1:1 binding, but in fact it more often than not implies a more complicated equilibria occurring in the system. There are many problems associated with these regression calculations. Computer power has significantly improved over the years and software now exists for non-linear regression analysis to calculate more precise binding constants, including those involving complex equilibria.

References

1. Eggins, B.R. *Chemical Sensors and Biosensors*; John Wiley & Sons: Chichester, UK, 2007.
2. Girigoswami, K.; Akhtar, N. Nanobiosensors and fluorescence based biosensors: An overview. *Int. J. Nano Dimens.* **2019**, *10*, 1–17.
3. Xiong, S.; Deng, Y.; Zhou, Y.; Gong, D.; Xu, Y.; Yang, L.; Chen, H.; Chen, L.; Song, T.; Luo, A. Current progress in biosensors for organophosphorus pesticides based on enzyme functionalized nanostructures: A review. *Anal. Methods* **2018**, *10*, 5468–5479. [CrossRef]
4. Liao, Z.; Wang, J.; Zhang, P.; Zhang, Y.; Miao, Y.; Gao, S.; Deng, Y.; Geng, L. Recent advances in microfluidic chip integrated electronic biosensors for multiplexed detection. *Biosens. Bioelectron.* **2018**, *121*, 272–280. [CrossRef]
5. Kumar, S.; Tripathy, S.; Jyoti, A.; Singh, S.G. Recent advances in biosensors for diagnosis and detection of sepsis: A comprehensive review. *Biosens. Bioelectron.* **2019**, *124–125*, 205–215. [CrossRef]
6. Fothergill, S.M.; Joyce, C.; Xie, F. Metal enhanced fluorescence biosensing: From ultra-violet towards second near-infrared window. *Nanoscale* **2018**, *10*, 20914–20929. [CrossRef]
7. Cheng, F.; Tang, X.L.; Kardashliev, T. Transcription factor-based biosensors in high-throughput screening: Advances and applications. *Biotechnol. J.* **2018**, *13*, e1700648. [CrossRef] [PubMed]
8. Ashrafi, A.M.; Koudelkova, Z.; Sedlackova, E.; Richtera, L.; Adam, V. Electrochemical sensors and biosensors for determination of mercury ions. *J. Electrochem. Soc.* **2018**, *165*, B824–B834. [CrossRef]
9. Aldewachi, H.; Chalati, T.; Woodroofe, M.N.; Bricklebank, N.; Sharrack, B.; Gardiner, P. Gold nanoparticle-based colorimetric biosensors. *Nanoscale* **2018**, *10*, 18–33. [CrossRef] [PubMed]
10. Sher, M.; Zhuang, R.; Demirci, U.; Asghar, W. Paper-based analytical devices for clinical diagnosis: Recent advances in the fabrication techniques and sensing mechanisms. *Expert Rev. Mol. Diagn.* **2017**, *17*, 351–366. [CrossRef]
11. Saidur, M.; Aziz, A.A.; Basirun, W. Recent advances in DNA-based electrochemical biosensors for heavy metal ion detection: A review. *Biosens. Bioelectron.* **2017**, *90*, 125–139. [CrossRef] [PubMed]
12. Liu, Y.; Deng, Y.; Dong, H.; Liu, K.; He, N. Progress on sensors based on nanomaterials for rapid detection of heavy metal ions. *Sci. China Chem.* **2017**, *60*, 329–337. [CrossRef]
13. Lan, L.; Yao, Y.; Ping, J.; Ying, Y. Recent advances in nanomaterial-based biosensors for antibiotics detection. *Biosens. Bioelectron.* **2017**, *91*, 504–514. [CrossRef] [PubMed]
14. Jayanthi, V.S.A.; Das, A.B.; Saxena, U. Recent advances in biosensor development for the detection of cancer biomarkers. *Biosens. Bioelectron.* **2017**, *91*, 15–23. [CrossRef]
15. National Research Council. *Expanding the Vision of Sensor Materials*; National Academemis Press: Washington, DC, USA, 1995; Chapter 6; pp. 73–88. [CrossRef]
16. McNaught, A.D.; Wilkinson, A. *IUPAC Compendium of Chemical Terminology*, 2nd ed.; Blackwell Scientific Publications: Oxford, UK, 2014.
17. Macielag, M.J. *Antibiotic Discovery and Development*; Springer: Berlin/Heidelberg, Germany, 2012; pp. 793–820.
18. Hulanicki, A.; Glab, S.; Ingman, F. Chemical sensors: Definitions and classification. *Pure Appl. Chem.* **1991**, *63*, 1247–1250. [CrossRef]
19. Phan, M.-H.; Peng, H.-X. Giant magnetoimpedance materials: Fundamentals and applications. *Prog. Mater. Sci.* **2008**, *53*, 323–420. [CrossRef]

20. Xu, H.; Li, Y.; Huang, N.-J.; Yu, Z.-R.; Wang, P.-H.; Zhang, Z.-H.; Xia, Q.-Q.; Gong, L.-X.; Li, S.-N.; Zhao, L. Temperature-triggered sensitive resistance transition of graphene oxide wide-ribbons wrapped sponge for fire ultrafast detecting and early warning. *J. Hazard. Mater.* **2019**, *363*, 286–294. [CrossRef]

21. Kobayashi, M. A perspective on steep-subthreshold-slope negative-capacitance field-effect transistor. *Appl. Phys. Express* **2018**, *11*, 110101. [CrossRef]

22. Li, C.; Tan, Q.; Jia, P.; Zhang, W.; Liu, J.; Xue, C.; Xiong, J. Review of research status and development trends of wireless passive LC resonant sensors for harsh environments. *Sensors* **2015**, *15*, 13097–13109. [CrossRef]

23. Balandin, A.A. Low-frequency 1/f noise in graphene devices. *Nat. Nanotechnol.* **2013**, *8*, 549–555. [CrossRef]

24. Suárez, P.L.; García-Cortés, M.; Fernández-Argüelles, M.T.; Encinar, J.R.; Valledor, M.; Ferrero, F.J.; Campo, J.C.; Costa-Fernández, J.M. Functionalized phosphorescent nanoparticles in (bio)chemical sensing and imaging—A review. *Anal. Chim. Acta* **2019**, *1046*, 16–31. [CrossRef]

25. Darr, J.A.; Poliakoff, M. New directions in inorganic and metal-organic coordination chemistry in supercritical fluids. *Chem. Rev.* **1999**, *99*, 495–542. [CrossRef] [PubMed]

26. Carter, S.; Fisher, A.S.; Hinds, M.W.; Lancaster, S.; Marshall, J. Atomic spectrometry update. Review of advances in the analysis of metals, chemicals and materials. *J. Anal. Atom. Spectrom.* **2013**, *28*, 1814–1869. [CrossRef]

27. Shazzo, Y.K.; Karpov, Y.A. Laser sampling in inductively coupled plasma mass spectrometry in the inorganic analysis of solid samples: Elemental fractionation as the main source of errors. *J. Anal. Chem.* **2016**, *71*, 1069–1080. [CrossRef]

28. Chen, S.-H.; Li, Y.-X.; Li, P.-H.; Xiao, X.-Y.; Jiang, M.; Li, S.-S.; Zhou, W.-Y.; Yang, M.; Huang, X.-J.; Liu, W.-Q. Electrochemical spectral methods for trace detection of heavy metals: A review. *TrAC Trends Anal. Chem.* **2018**, *106*, 139–150. [CrossRef]

29. Fen, Y.W.; Yunus, W.M.M. Surface plasmon resonance spectroscopy as an alternative for sensing heavy metal ions: A review. *Sens. Rev.* **2013**, *33*, 305–314.

30. West, M.; Ellis, A.T.; Potts, P.J.; Streli, C.; Vanhoof, C.; Wobrauschek, P. 2016 Atomic Spectrometry update—A review of advances in X-ray fluorescence spectrometry and its applications. *J. Anal. Atom. Spectrom.* **2016**, *31*, 1706–1755. [CrossRef]

31. De Silva, A.P.; Gunaratne, H.N.; Gunnlaugsson, T.; Huxley, A.J.; McCoy, C.P.; Rademacher, J.T.; Rice, T.E. Signaling recognition events with fluorescent sensors and switches. *Chem. Rev.* **1997**, *97*, 1515–1566. [CrossRef]

32. Wu, J.; Liu, W.; Ge, J.; Zhang, H.; Wang, P. New sensing mechanisms for design of fluorescent chemosensors emerging in recent years. *Chem. Soc. Rev.* **2011**, *40*, 3483–3495. [CrossRef] [PubMed]

33. Valeur, B.; Leray, I. Design principles of fluorescent molecular sensors for cation recognition. *Coord. Chem. Rev.* **2000**, *205*, 3–40. [CrossRef]

34. Kang, J.; Huo, F.; Zhang, Y.; Chao, J.; Glass, T.E.; Yin, C. A novel near-infrared ratiometric fluorescent probe for cyanide and its bioimaging applications. *Spectrochim. Acta Part A* **2019**, *209*, 95–99. [CrossRef]

35. Masteri-Farahani, M.; Khademabbasi, K. Heavy atom quenching of CdS quantum dots photoluminescence: Evidences for electron transfer mechanism. *J. Lumin.* **2018**, *204*, 130–134. [CrossRef]

36. Czerwieniec, R.; Yu, J.; Yersin, H. Blue-light emission of Cu(I) complexes and singlet harvesting. *Inorg. Chem.* **2011**, *50*, 8293–8301. [CrossRef] [PubMed]

37. Zu, F.; Yan, F.; Bai, Z.; Xu, J.; Wang, Y.; Huang, Y.; Zhou, X. The quenching of the fluorescence of carbon dots: A review on mechanisms and applications. *Microchim. Acta* **2017**, *184*, 1899–1914. [CrossRef]

38. Birks, J. Excimers. *Rep. Prog. Phys.* **1975**, *38*, 903–974. [CrossRef]

39. Lu, H.; Zheng, Y.; Zhao, X.; Wang, L.; Ma, S.; Han, X.; Xu, B.; Tian, W.; Gao, H. Highly efficient far red/near-infrared solid fluorophores: Aggregation-induced emission, intramolecular charge transfer, twisted molecular conformation, and bioimaging applications. *Angew. Chem. Int. Ed.* **2016**, *55*, 155–159. [CrossRef] [PubMed]

40. Padalkar, V.S.; Seki, S. Excited-state intramolecular proton-transfer (ESIPT)-inspired solid state emitters. *Chem. Soc. Rev.* **2016**, *45*, 169–202. [CrossRef] [PubMed]

41. Rasheed, T.; Bilal, M.; Nabeel, F.; Iqbal, H.M.; Li, C.; Zhou, Y. Fluorescent sensor based models for the detection of environmentally-related toxic heavy metals. *Sci. Total Environ.* **2018**, *615*, 476–485. [CrossRef] [PubMed]

42. Steed, J.W. Coordination and organometallic compounds as anion receptors and sensors. *Chem. Soc. Rev.* **2009**, *38*, 506–519. [CrossRef] [PubMed]

43. Amendola, V.; Fabbrizzi, L.; Mosca, L. Anion recognition by hydrogen bonding: Urea-based receptors. *Chem. Soc. Rev.* **2010**, *39*, 3889–3915. [CrossRef]

44. Hua, Y.; Flood, A.H. Click chemistry generates privileged CH hydrogen-bonding triazoles: The latest addition to anion supramolecular chemistry. *Chen. Soc. Rev.* **2010**, *39*, 1262–1271. [CrossRef]

45. Dougherty, D.A. The cation−π interaction. *Acc. Chem. Res.* **2012**, *46*, 885–893. [CrossRef] [PubMed]

46. Zheng, B.; Wang, F.; Dong, S.; Huang, F. Supramolecular polymers constructed by crown ether-based molecular recognition. *Chem. Soc. Rev.* **2012**, *41*, 1621–1636. [CrossRef]

47. Harada, A.; Takashima, Y.; Nakahata, M. Supramolecular polymeric materials via cyclodextrin–guest interactions. *Acc. Chem. Res.* **2014**, *47*, 2128–2140. [CrossRef] [PubMed]

48. Gale, P.A.; Howe, E.N.; Wu, X. Anion receptor chemistry. *Chem* **2016**, *1*, 351–422. [CrossRef]

49. Schmidt, B.V.; Barner-Kowollik, C. Dynamic macromolecular material design—The versatility of cyclodextrin-based host–guest chemistry. *Angew. Chem. Int. Ed.* **2017**, *56*, 8350–8369. [CrossRef] [PubMed]

50. Zhou, J.; Yu, G.; Huang, F. Supramolecular chemotherapy based on host–guest molecular recognition: A novel strategy in the battle against cancer with a bright future. *Chem. Soc. Rev.* **2017**, *46*, 7021–7053. [CrossRef] [PubMed]

51. Wu, X.; Howe, E.N.; Gale, P.A. Supramolecular transmembrane anion transport: New assays and insights. *Acc. Chem. Res.* **2018**, *51*, 1870–1879. [CrossRef] [PubMed]

52. Zhao, J.; Yang, D.; Yang, X.-J.; Wu, B. Anion coordination chemistry: From recognition to supramolecular assembly. *Coord. Chem. Rev.* **2019**, *378*, 415–444. [CrossRef]

53. Wallace, K.J.; Johnson, A.D.; Jones, W.S.; Manandhar, E. Chemodosimeters and chemoreactands for sensing ferric ions. *Supramol. Chem.* **2018**, *30*, 353–383. [CrossRef]

54. Manandhar, E.; Wallace, K.J. Host–guest chemistry of pyrene-based molecular receptors. *Inorg. Chim. Acta* **2012**, *381*, 15–43. [CrossRef]

55. McEwen, J.J.; Wallace, K.J. Squaraine dyes in molecular recognition and self-assembly. *Chem. Commun.* **2009**, *42*, 6339–6351. [CrossRef] [PubMed]

56. Wallace, K.J. Molecular dyes used for the detection of biological and environmental heavy metals: Highlights from 2004 to 2008. *Supramol. Chem.* **2009**, *21*, 89–102. [CrossRef]

57. Michalke, B.; Willkommen, D.; Drobyshev, E.; Solovyev, N. The importance of speciation analysis in neurodegeneration research. *TrAC Trends Anal. Chem.* **2018**, *104*, 160–170. [CrossRef]

58. Kozlowski, H.; Luczkowski, M.; Remelli, M.; Valensin, D. Copper, zinc and iron in neurodegenerative diseases (Alzheimer's, Parkinson's and prion diseases). *Coord. Chem. Rev.* **2012**, *256*, 2129–2141. [CrossRef]

59. Chasapis, C.T.; Loutsidou, A.C.; Spiliopoulou, C.A.; Stefanidou, M.E. Zinc and human health: An update. *Arch. Toxicol.* **2012**, *86*, 521–534. [CrossRef] [PubMed]

60. Que, E.L.; Domaille, D.W.; Chang, C.J. Metals in neurobiology: Probing their chemistry and biology with molecular imaging. *Chem. Rev.* **2008**, *108*, 1517–1549. [CrossRef] [PubMed]

61. Zeng, X.; Xu, X.; Boezen, H.M.; Huo, X. Children with health impairments by heavy metals in an e-waste recycling area. *Chemosphere* **2016**, *148*, 408–415. [CrossRef] [PubMed]

62. Clemens, S.; Ma, J.F. Toxic heavy metal and metalloid accumulation in crop plants and foods. *Annu. Rev. Plant Biol.* **2016**, *67*, 489–512. [CrossRef] [PubMed]

63. Parrotta, L.; Guerriero, G.; Sergeant, K.; Cai, G.; Hausman, J.-F. Target or barrier? The cell wall of early-and later-diverging plants vs cadmium toxicity: Differences in the response mechanisms. *Front. Plant Sci.* **2015**, *6*, 133. [CrossRef]

64. Nagajyoti, P.C.; Lee, K.D.; Sreekanth, T. Heavy metals, occurrence and toxicity for plants: A review. *Environ. Chem. Lett.* **2010**, *8*, 199–216. [CrossRef]

65. Obrist, D.; Kirk, J.L.; Zhang, L.; Sunderland, E.M.; Jiskra, M.; Selin, N.E. A review of global environmental mercury processes in response to human and natural perturbations: Changes of emissions, climate, and land use. *Ambio* **2018**, *47*, 116–140. [CrossRef] [PubMed]

66. Sundseth, K.; Pacyna, J.; Pacyna, E.; Pirrone, N.; Thorne, R. Global sources and pathways of mercury in the context of human health. *Int. J. Environ. Res. Public Health* **2017**, *14*, 105. [CrossRef] [PubMed]

67. Chen, S.; Pei, R.; Zhao, T.; Dyer, D.J. Gold Nanoparticle Assemblies by Metal Ion−Pyridine Complexation and Their Rectified Quantized Charging in Aqueous Solutions. *J. Chem. Phys. B* **2002**, *106*, 1903–1908. [CrossRef]

68. McCarroll, M.E.; Shi, Y.; Harris, S.; Puli, S.; Kimaru, I.; Xu, R.; Wang, L.; Dyer, D.J. Computational prediction and experimental evaluation of a photoinduced electron-transfer sensor. *J. Chem. Phys. B* **2006**, *110*, 22991–22994. [CrossRef] [PubMed]

69. Hudson, G.A.; Cheng, L.; Yu, J.; Yan, Y.; Dyer, D.J.; McCarroll, M.E.; Wang, L. Computational studies on response and binding selectivity of fluorescence sensors. *J. Phys. Chem. B* **2009**, *114*, 870–876. [CrossRef] [PubMed]

70. Kowalczyk, T.; Lin, Z.; Voorhis, T.V. Fluorescence quenching by photoinduced electron transfer in the Zn^{2+} sensor Zinpyr-1: A computational investigation. *J. Chem. Phys. B* **2010**, *114*, 10427–10434. [CrossRef]

71. Venkataraman, D.; Du, Y.; Wilson, S.R.; Hirsch, K.A.; Zhang, P.; Moore, J.S. A coordination geometry table of the *d*-block elements and their ions. *J. Chem. Educ.* **1997**, *74*, 915–918. [CrossRef]

72. Ebnou, F.; M'Haiham, M.; Ebeid, K.; Carpenter-Warren, C.L.; Slawin, A.M.; Woollins, J.D.; Dhia, M.T.B.; Sanhoury, M.A. Synthesis, characterization, and structural properties of mercury (II), cadmium (II) and zinc (II) tripiperidinophosphine chalcogenide complexes. *Polyhedron* **2019**, *159*, 206–211. [CrossRef]

73. Rajput, G.; Yadav, M.K.; Drew, M.G.; Singh, N. Influence of the ligand frameworks on the coordination environment and properties of new phenylmercury (ii) β-oxodithioester complexes. *Dalton Trans.* **2015**, *44*, 5909–5916. [CrossRef]

74. Ghosh, D.C.; Gupta, K. A new scale of electronegativity of 54 elements of periodic table based on polarizability of atoms. *J. Theor. Comput. Chem.* **2006**, *5*, 895–911. [CrossRef]

75. Crichton, R. *Biological Inorganic Chemistry: A New Introduction to Molecular Structure and Function*; Academic Press: Cambridge, MA, USA, 2019; Chapter 12; pp. 339–362. [CrossRef]

76. Tang, L.; Qiu, R.; Tang, Y.; Wang, S. Cadmium–zinc exchange and their binary relationship in the structure of Zn-related proteins: A mini review. *Metallomics* **2014**, *6*, 1313–1323. [CrossRef] [PubMed]

77. Lane, T.W.; Saito, M.A.; George, G.N.; Pickering, I.J.; Prince, R.C.; Morel, F.M. Biochemistry: A cadmium enzyme from a marine diatom. *Nature* **2005**, *435*, 42. [CrossRef] [PubMed]

78. Lane, T.W.; Morel, F.M. A biological function for cadmium in marine diatoms. *Proc. Natl. Acad. Sci. USA* **2000**, *97*, 4627–4631. [CrossRef] [PubMed]

79. Daeneke, T.; Khoshmanesh, K.; Mahmood, N.; de Castro, I.; Esrafilzadeh, D.; Barrow, S.; Dickey, M.; Kalantar-Zadeh, K. Liquid metals: Fundamentals and applications in chemistry. *Chem. Soc. Rev.* **2018**, *47*, 4073–4111. [CrossRef] [PubMed]

80. McDermott, B.; Koch, C. Preparation of beta brass by mechanical alloying of elemental copper and zinc. *Scr. Metall.* **1986**, *20*, 669–672. [CrossRef]

81. Marshall, S.; Marshall, G. Dental amalgam: The materials. *Adv. Dent. Res.* **1992**, *6*, 94–99. [CrossRef]

82. Shi, G.L.; Li, D.J.; Wang, Y.F.; Liu, C.H.; Hu, Z.B.; Lou, L.Q.; Rengel, Z.; Cai, Q.S. Accumulation and distribution of arsenic and cadmium in winter wheat (Triticum aestivum L.) at different developmental stages. *Sci. Total Environ.* **2019**, *667*, 532–539. [CrossRef] [PubMed]

83. Zhao, F.-J.; Ma, Y.; Zhu, Y.-G.; Tang, Z.; McGrath, S.P. Soil contamination in China: Current status and mitigation strategies. *Environ. Sci. Technol.* **2014**, *49*, 750–759. [CrossRef]

84. Kim, K.-H.; Kabir, E.; Jahan, S.A. A review on the distribution of Hg in the environment and its human health impacts. *J. Hazard. Mater.* **2016**, *306*, 376–385. [CrossRef]

85. Tsakiris, K.A. Saint Ioannis Lampadistis, the first possible case of blindness due to organic mercury poisoning in history. *J. Med. Biogr.* **2018**, *26*, 207–210. [CrossRef]

86. Langford, N.; Ferner, R. Toxicity of mercury. *J. Hum. Hypertens.* **1999**, *13*, 651–656. [CrossRef]

87. Budnik, L.T.; Casteleyn, L. Mercury pollution in modern times and its socio-medical consequences. *Sci. Total Environ.* **2019**, *654*, 720–734. [CrossRef] [PubMed]

88. Kainz, M.; Telmer, K.; Mazumder, A. Bioaccumulation patterns of methyl mercury and essential fatty acids in lacustrine planktonic food webs and fish. *Sci. Total Environ.* **2006**, *368*, 271–282. [CrossRef] [PubMed]

89. EPA United States Environmental Protection Agencey. National Primary Drinking Water Regulations. Available online: https://www.epa.gov/ground-water-and-drinking-water/national-primary-drinking-water-regulations#Inorganic (accessed on 24 April 2019).

90. Guidelines for Drinking-Water Quality. Available online: https://www.who.int/water_sanitation_health/dwq/gdwq0506.pdf (accessed on 24 April 2019).

91.　Levaot, N.; Hershfinkel, M. How cellular Zn^{2+} signaling drives physiological functions. *Cell Calcium* **2018**, *75*, 53–63. [CrossRef] [PubMed]

92.　Huang, L.; Tepaamorndech, S. The SLC30 family of zinc transporters—A review of current understanding of their biological and pathophysiological roles. *Mol. Asp. Med.* **2013**, *34*, 548–560. [CrossRef] [PubMed]

93.　Matsui, C.; Takatani-Nakase, T.; Hatano, Y.; Kawahara, S.; Nakase, I.; Takahashi, K. Zinc and its transporter ZIP6 are key mediators of breast cancer cell survival under high glucose conditions. *FEBS Lett.* **2017**, *591*, 3348–3359. [CrossRef]

94.　Malm, J.; Hellman, J.; Hogg, P.; Lilja, H. Enzymatic action of prostate-specific antigen (PSA or hK3): Substrate specificity and regulation by Zn^{2+}, a tight-binding inhibitor. *Prostate* **2000**, *45*, 132–139.

95.　Weiss, J.H.; Sensi, S.L.; Koh, J.Y. Zn^{2+}: A novel ionic mediator of neural injury in brain disease. *Trends Pharmacol. Sci.* **2000**, *21*, 395–401. [CrossRef]

96.　Tomat, E.; Lippard, S.J. Imaging mobile zinc in biology. *Curr. Opin. Chem. Biol.* **2010**, *14*, 225–230. [CrossRef]

97.　Mocchegiani, E.; Bertoni-Freddari, C.; Marcellini, F.; Malavolta, M. Brain, aging and neurodegeneration: Role of zinc ion availability. *Prog. Neurobiol.* **2005**, *75*, 367–390. [CrossRef]

98.　Leinweber, B.; Barofsky, E.; Barofsky, D.F.; Ermilov, V.; Nylin, K.; Beckman, J.S. Aggregation of ALS mutant superoxide dismutase expressed in Escherichia coli. *Free Radic. Biol. Med.* **2004**, *36*, 911–918. [CrossRef]

99.　Woo, H.; You, Y.; Kim, T.; Jhon, G.-J.; Nam, W. Fluorescence ratiometric zinc sensors based on controlled energy transfer. *J. Mater. Chem.* **2012**, *22*, 17100–17112. [CrossRef]

100.　Kwon, J.E.; Lee, S.; You, Y.; Baek, K.-H.; Ohkubo, K.; Cho, J.; Fukuzumi, S.; Shin, I.; Park, S.Y.; Nam, W. Fluorescent zinc sensor with minimized proton-induced interferences: Photophysical mechanism for fluorescence turn-on response and detection of endogenous free zinc ions. *Inorg. Chem.* **2012**, *51*, 8760–8774. [CrossRef] [PubMed]

101.　Comby, S.; Tuck, S.A.; Truman, L.K.; Kotova, O.; Gunnlaugsson, T. New trick for an old ligand! The sensing of Zn(II) using a lanthanide based ternary Yb(III)-cyclen-8 hydroxyquinoline system as a dual emissive probe for displacement assay. *Inorg. Chem.* **2012**, *51*, 10158–10168. [CrossRef] [PubMed]

102.　Tsikalas, G.K.; Lazarou, P.; Klontzas, E.; Pergantis, S.A.; Spanopoulos, I.; Trikalitis, P.N.; Froudakis, G.E.; Katerinopoulos, H.E. A "turn-on"–turning-to-ratiometric sensor for zinc(II) ions in aqueous media. *RSC Adv.* **2014**, *4*, 693–696. [CrossRef]

103.　Badetti, E.; Wurst, K.; Licini, G.; Zonta, C. Multimetallic architectures from the self-assembly of amino acids and tris (2-pyridylmethyl) amine zinc(II) complexes: Circular dichroism enhancement by chromophores organization. *Chem.-Eur. J.* **2016**, *22*, 6515–6518. [CrossRef] [PubMed]

104.　Wang, D.; Ren, A.-M.; Zou, L.-Y.; Guo, J.-F.; Huang, S. A theoretical investigation of a series of novel two-photon zinc ion fluorescent probes based on bipyridine. *J. Photochem. Photobiol. A* **2017**, *341*, 20–30. [CrossRef]

105.　Panunzi, B.; Borbone, F.; Capobianco, A.; Concilio, S.; Diana, R.; Peluso, A.; Piotto, S.; Tuzi, A.; Velardo, A.; Caruso, U. Synthesis, spectroscopic properties and DFT calculations of a novel multipolar azo dye and its zinc(II) complex. *Inorg. Chem. Commun.* **2017**, *84*, 103–108. [CrossRef]

106.　Zhu, M.-Y.; Zhao, K.; Song, J.; Wang, C.-K. Responsive mechanism and molecular design of di-2-picolylamine-based two-photon fluorescent probes for zinc ions. *Chin. Phys. B* **2018**, *27*, 023302. [CrossRef]

107.　Xia, S.; Shen, J.; Wang, J.; Wang, H.; Fang, M.; Zhou, H.; Tanasova, M. Ratiometric fluorescent and colorimetric BODIPY-based sensor for zinc ions in solution and living cells. *Sens. Actuators B Chem.* **2018**, *258*, 1279–1286. [CrossRef]

108.　Zhao, K.; Song, J.; Zhu, M.-Y.; Zhang, H.; Wang, C.-K. Isomerism and coordination mode effects on two-photon absorption of tris (picolyl) amine-based fluorescent probes for zinc ions. *Chin. Phys. B* **2018**, *27*, 103301. [CrossRef]

109.　Oehme, I.; Wolfbeis, O.S. Optical sensors for determination of heavy metal ions. *Microchim. Acta* **1997**, *126*, 177–192. [CrossRef]

110.　Kimura, E.; Aoki, S. *Zinc Biochemistry, Physiology, and Homeostasis*; Springer: Berlin/Heidelberg, Germany, 2001; pp. 5–18.

111.　Jiang, P.; Guo, Z. Fluorescent detection of zinc in biological systems: Recent development on the design of chemosensors and biosensors. *Coord. Chem. Rev.* **2004**, *248*, 205–229. [CrossRef]

112. Lim, N.C.; Schuster, J.V.; Porto, M.C.; Tanudra, M.A.; Yao, L.; Freake, H.C.; Brückner, C. Coumarin-based chemosensors for zinc(II): Toward the determination of the design algorithm for CHEF-type and ratiometric probes. *Inorg. Chem.* **2005**, *44*, 2018–2030. [CrossRef] [PubMed]

113. Thompson, R.B. Studying zinc biology with fluorescence: ain't we got fun? *Curr. Opin. Chem. Biol.* **2005**, *9*, 526–532. [CrossRef]

114. Maret, W. Zinc coordination environments in proteins as redox sensors and signal transducers. *Antioxid. Redox Signal.* **2006**, *8*, 1419–1441. [CrossRef]

115. Carol, P.; Sreejith, S.; Ajayaghosh, A. Ratiometric and near-infrared molecular probes for the detection and imaging of zinc Ions. *Chem. Asian J.* **2007**, *2*, 338–348. [CrossRef] [PubMed]

116. Dai, Z.; Canary, J.W. Tailoring tripodal ligands for zinc sensing. *New J. Chem.* **2007**, *31*, 1708–1718. [CrossRef]

117. Nolan, E.M.; Lippard, S.J. Small-molecule fluorescent sensors for investigating zinc metalloneurochemistry. *Acc. Chem. Res.* **2008**, *42*, 193–203. [CrossRef]

118. Terai, T.; Nagano, T. Fluorescent probes for bioimaging applications. *Curr. Opin. Chem. Biol.* **2008**, *12*, 515–521. [CrossRef]

119. Sarkar, K.; Dhara, K.; Nandi, M.; Roy, P.; Bhaumik, A.; Banerjee, P. Selective zinc(II)-ion fluorescence sensing by a functionalized mesoporous material covalently grafted with a fluorescent chromophore and consequent biological applications. *Adv. Funct. Mater.* **2009**, *19*, 223–234. [CrossRef]

120. Xu, Z.; Yoon, J.; Spring, D.R. Fluorescent chemosensors for Zn^{2+}. *Chem. Soc. Rev.* **2010**, *39*, 1996–2006. [CrossRef]

121. Pluth, M.D.; Tomat, E.; Lippard, S.J. Biochemistry of mobile zinc and nitric oxide revealed by fluorescent sensors. *Annu. Rev. Biochem.* **2011**, *80*, 333–355. [CrossRef]

122. Carter, K.P.; Young, A.M.; Palmer, A.E. Fluorescent sensors for measuring metal ions in living systems. *Chem. Rev.* **2014**, *114*, 4564–4601. [CrossRef] [PubMed]

123. Lee, M.H.; Kim, J.S.; Sessler, J.L. Small molecule-based ratiometric fluorescence probes for cations, anions, and biomolecules. *Chem. Soc. Rev.* **2015**, *44*, 4185–4191. [CrossRef] [PubMed]

124. Mason, W.T. *Fluorescent and Luminescent Probes for Biological Activity: A Practical Guide to Technology for Quantitative Real-Time Analysis*; Academic Press: London, UK, 1999.

125. Johnson, I. Fluorescent probes for living cells. *Histochem. J.* **1998**, *30*, 123–140. [CrossRef]

126. Krężel, A.; Maret, W. Zinc-buffering capacity of a eukaryotic cell at physiological pZn. *J. Biol. Inorg. Chem.* **2006**, *11*, 1049–1062. [CrossRef] [PubMed]

127. Outten, C.E.; O'halloran, T.V. Femtomolar sensitivity of metalloregulatory proteins controlling zinc homeostasis. *Science* **2001**, *292*, 2488–2492. [CrossRef]

128. Assaf, S.; Chung, S.-H. Release of endogenous Zn^{2+} from brain tissue during activity. *Nature* **1984**, *308*, 734–736. [CrossRef]

129. Zhang, L.; Clark, R.J.; Zhu, L. A heteroditopic fluoroionophoric platform for constructing fluorescent probes with large dynamic ranges for zinc ions. *Chem. Eur. J.* **2008**, *14*, 2894–2903. [CrossRef] [PubMed]

130. Pati, P.B.; Zade, S.S. Selective colorimetric and "turn-on" fluorimetric detection of cyanide using a chemodosimeter comprising salicylaldehyde and triphenylamine groups. *Eur. J. Org. Chem.* **2012**, 6555–6561. [CrossRef]

131. Chakraborty, B.; Halder, P.; Chakraborty, S.; Das, O.; Paria, S. Synthesis, characterization and emission study of zinc(II) and cobalt(II) complexes: Bis(bidentate) iminophenols as zinc(II) selective fluorescence probes. *Inorg. Chim. Acta* **2012**, *387*, 332–337. [CrossRef]

132. Zhao, L.Y.; Mi, Q.L.; Wang, G.K.; Chen, J.H.; Zhang, J.F.; Zhao, Q.H.; Zhou, Y. 1,8-Naphthalimide-based 'turn-on' fluorescent sensor for the detection of zinc ion in aqueous media and its applications for bioimaging. *Tetrahedron Lett.* **2013**, *54*, 3353–3358. [CrossRef]

133. Dugave, C.; Demange, L. Cis−trans isomerization of organic molecules and biomolecules: Implications and applications. *Chem. Rev.* **2003**, *103*, 2475–2532. [CrossRef]

134. Hisamoto, H.; Tohma, H.; Yamada, T.; Yamauchi, K.-I.; Siswanta, D.; Yoshioka, N.; Suzuki, K. Molecular design, characterization, and application of multi-information dyes for multi-dimensional optical chemical sensing. Molecular design concepts of the dyes and their fundamental spectral characteristics. *Anal. Chim. Acta* **1998**, *373*, 271–289. [CrossRef]

135. Natali, M.; Soldi, L.; Giordani, S. A photoswitchable Zn(II) selective spiropyran-based sensor. *Tetrahedron* **2010**, *66*, 7612–7617. [CrossRef]

136. Luo, W.; Liu, M.; Yang, T.; Yang, X.; Wang, Y.; Xiang, H. Fluorescent Zn^{II} Chemosensor Mediated by a 1,8-Naphthyridine Derivative and It's Photophysical Properties. *ChemistryOpen* **2018**, *7*, 639–644. [CrossRef]

137. Park, G.J.; Lee, M.M.; You, G.R.; Choi, Y.W.; Kim, C. A turn-on and reversible fluorescence sensor with high affinity to Zn^{2+} in aqueous solution. *Tetrahedron Lett.* **2014**, *55*, 2517–2522. [CrossRef]

138. Park, G.J.; Na, Y.J.; Jo, H.Y.; Lee, S.A.; Kim, A.R.; Noh, I.; Kim, C. A single chemosensor for multiple analytes: Fluorogenic detection of Zn^{2+} and OAc^- ions in aqueous solution, and an application to bioimaging. *New J. Chem.* **2014**, *38*, 2587–2594. [CrossRef]

139. Erdemir, S.; Malkondu, S. A novel "turn on" fluorescent sensor based on hydroxy-triphenylamine for Zn^{2+} and Cd^{2+} ions in MeCN. *Sens. Actuators B Chem.* **2013**, *188*, 1225–1229. [CrossRef]

140. Burdette, S.C.; Walkup, G.K.; Spingler, B.; Tsien, R.Y.; Lippard, S.J. Fluorescent sensors for Zn^{2+} based on a fluorescein platform: Synthesis, properties and intracellular distribution. *J. Am. Chem. Soc.* **2001**, *123*, 7831–7841. [CrossRef] [PubMed]

141. Burdette, S.C.; Frederickson, C.J.; Bu, W.; Lippard, S.J. ZP4, an improved neuronal Zn^{2+} sensor of the Zinpyr family. *J. Am. Chem. Soc.* **2003**, *125*, 1778–1787. [CrossRef]

142. Nolan, E.M.; Ryu, J.W.; Jaworski, J.; Feazell, R.P.; Sheng, M.; Lippard, S.J. Zinspy sensors with enhanced dynamic range for imaging neuronal cell zinc uptake and mobilization. *J. Am. Chem. Soc.* **2006**, *128*, 15517–15528. [CrossRef] [PubMed]

143. Tomat, E.; Nolan, E.M.; Jaworski, J.; Lippard, S.J. Organelle-specific zinc detection using zinpyr-labeled fusion proteins in live cells. *J. Am. Chem. Soc.* **2008**, *130*, 15776–15777. [CrossRef]

144. Wong, B.A.; Friedle, S.; Lippard, S.J. Solution and fluorescence properties of symmetric dipicolylamine-containing dichlorofluorescein-based Zn^{2+} sensors. *J. Am. Chem. Soc.* **2009**, *131*, 7142–7152. [CrossRef]

145. Du, P.; Lippard, S.J. A highly selective turn-on colorimetric, red fluorescent sensor for detecting mobile zinc in living cells. *Inorg. Chem.* **2010**, *49*, 10753–10755. [CrossRef]

146. Sivaraman, G.; Anand, T.; Chellappa, D. Turn-on fluorescent chemosensor for Zn(II) via ring opening of rhodamine spirolactam and their live cell imaging. *Analyst* **2012**, *137*, 5881–5884. [CrossRef]

147. Wong, B.A.; Friedle, S.; Lippard, S.J. Subtle modification of 2,2-dipicolylamine lowers the affinity and improves the turn-on of Zn(II)-selective fluorescent sensors. *Inorg. Chem.* **2009**, *48*, 7009–7011. [CrossRef] [PubMed]

148. Steed, J.W.; Wallace, K.J. *Advances in Supramolecular Chemistry*; Gokel, G., Ed.; Cerberus: New York, NY, USA, 2003; Volume 9, pp. 221–262.

149. Jung, J.M.; Kang, J.H.; Han, J.; Lee, H.; Lim, M.H.; Kim, K.-T.; Kim, C. A novel "off-on" type fluorescent chemosensor for detection of Zn^{2+} and its zinc complex for "on-off" fluorescent sensing of sulfide in aqueous solution, in vitro and in vivo. *Sens. Actuators B Chem.* **2018**, *267*, 58–69. [CrossRef]

150. Ravitz, S.F. The solubilities and free energies of some metallic sulfides. *J. Phys. Chem.* **1936**, *40*, 61–70. [CrossRef]

151. Fu, Y.; Fan, C.; Liu, G.; Cui, S.; Pu, S. A highly selective and sensitive ratiometric fluorescent chemosensor for Zn^{2+} based on diarylethene with a benzyl-linked 8-aminoquinoline-2-aminomethylpyridine unit. *Dyes Pigm.* **2016**, *126*, 121–130. [CrossRef]

152. Wang, Z.; Cui, S.; Qiu, S.; Zhang, Z.; Pu, S. A highly sensitive fluorescent sensor for Zn^{2+} based on diarylethene with an imidazole unit. *Spectrochim. Acta Part A* **2018**, *205*, 21–28. [CrossRef] [PubMed]

153. Macias-Contreras, M.; Daykin, K.L.; Simmons, J.T.; Allen, J.R.; Hooper, Z.S.; Davidson, M.W.; Zhu, L. Progressive structural modification to a zinc-actuated photoinduced electron transfer (PeT) switch in the context of intracellular zinc imaging. *Org. Biomol. Chem.* **2017**, *15*, 9139–9148. [CrossRef] [PubMed]

154. Simmons, J.T.; Allen, J.R.; Morris, D.R.; Clark, R.J.; Levenson, C.W.; Davidson, M.W.; Zhu, L. Integrated and passive 1,2,3-triazolyl groups in fluorescent indicators for zinc(II) ions: Thermodynamic and kinetic evaluations. *Inorg. Chem.* **2013**, *52*, 5838–5850. [CrossRef]

155. Michaels, H.A.; Murphy, C.S.; Clark, R.J.; Davidson, M.W.; Zhu, L. 2-Anthryltriazolyl-containing multidentate ligands: Zinc-coordination mediated photophysical processes and potential in live-cell imaging applications. *Inorg. Chem.* **2010**, *49*, 4278–4287. [CrossRef] [PubMed]

156. Huang, S.; Clark, R.J.; Zhu, L. Highly sensitive fluorescent probes for zinc ion based on triazolyl-containing tetradentate coordination motifs. *Org. Lett.* **2007**, *9*, 4999–5002. [CrossRef] [PubMed]

157. De Silva, S.A.; Zavaleta, A.; Baron, D.E.; Allam, O.; Isidor, E.V.; Kashimura, N.; Percarpio, J.M. A fluorescent photoinduced electron transfer sensor for cations with an off-on-off proton switch. *Tetrahedron Lett.* **1997**, *38*, 2237–2240. [CrossRef]

158. Walkup, G.K.; Burdette, S.C.; Lippard, S.J.; Tsien, R.Y. A new cell-permeable fluorescent probe for Zn^{2+}. *J. Am. Chem. Soc.* **2000**, *122*, 5644–5645. [CrossRef]

159. Gee, K.R.; Zhou, Z.-L.; Ton-That, D.; Sensi, S.; Weiss, J. Measuring zinc in living cells. A new generation of sensitive and selective fluorescent probes. *Cell Calcium* **2002**, *31*, 245–251. [CrossRef]

160. Yan, J.; Fan, L.; Qin, J.-C.; Li, C.-R.; Yang, Z.-Y. A novel and resumable Schiff-base fluorescent chemosensor for Zn(II). *Tetrahedron Lett.* **2016**, *57*, 2910–2914. [CrossRef]

161. Zhang, G.; Li, H.; Bi, S.; Song, L.; Lu, Y.; Zhang, L.; Yu, J.; Wang, L. A new turn-on fluorescent chemosensor based on diketopyrrolopyrrole (DPP) for imaging Zn^{2+} in living cells. *Analyst* **2013**, *138*, 6163–6170. [CrossRef] [PubMed]

162. Manandhar, E.; Broome, J.H.; Myrick, J.; Lagrone, W.; Cragg, P.J.; Wallace, K.J. A pyrene-based fluorescent sensor for Zn^{2+} ions: A molecular 'butterfly'. *Chem. Commun.* **2011**, *47*, 8796–8798. [CrossRef] [PubMed]

163. Manandhar, E.; Cragg, P.J.; Wallace, K.J. Detection of Zn(II) ions by fluorescent pyrene-derived molecular probes. *Supramol. Chem.* **2014**, *26*, 141–150. [CrossRef]

164. Rosenthal, M.R. The myth of the non-coordinating anion. *J. Chem. Educ.* **1973**, *50*, 331–335. [CrossRef]

165. MacAyeal, J.R. The comprehensive environmental response, compensation, and liability act: The correct paradigm of strict liability and the problem of individual causation. *J. Environ. Law* **1999**, *18*, 217–334.

166. Khairy, M.; El-Safty, S.A.; Shenashen, M. Environmental remediation and monitoring of cadmium. *TrAC Trends Anal. Chem.* **2014**, *62*, 56–68. [CrossRef]

167. Kimblin, C.; Bridgewater, B.M.; Churchill, D.G.; Hascall, T.; Parkin, G. Bis(mercaptoimidazolyl)(pyrazolyl) hydroborato complexes of Zinc, Cadmium, and Cobalt: Structural evidence for the enhanced tendency of Zinc in biological systems to adopt Tetrahedral M[S4] coordination. *Inorg. Chem.* **2000**, *39*, 4240–4243. [CrossRef] [PubMed]

168. Mugesh, G.; Singh, H.B.; Patel, R.P.; Butcher, R.J. Synthesis and structural characterization of monomeric selenolato complexes of zinc, cadmium, and mercury. *Inorg. Chem.* **1998**, *37*, 2663–2669. [CrossRef]

169. Sigel, H.; Martin, R.B. The colourless 'chameleon' or the peculiar properties of Zn^{2+} in complexes in solution. Quantification of equilibria involving a change of the coordination number of the metal ion. *Chem. Soc. Rev.* **1994**, *23*, 83–91. [CrossRef]

170. Wang, Z.; Cui, S.; Qiu, S.; Pu, S. A new fluorescence probe based on diarylethene with a benzothiazine unit for selective detection of Cd^{2+}. *Tetrahedron* **2018**, *74*, 7431–7437. [CrossRef]

171. Maniyazagan, M.; Mariadasse, R.; Jeyakanthan, J.; Lokanath, N.; Naveen, S.; Premkumar, K.; Muthuraja, P.; Manisankar, P.; Stalin, T. Rhodamine based "turn–on" molecular switch FRET–sensor for cadmium and sulfide ions and live cell imaging study. *Sens. Actuators B Chem.* **2017**, *238*, 565–577. [CrossRef]

172. Aich, K.; Goswami, S.; Das, S.; Mukhopadhyay, C.D.; Quah, C.K.; Fun, H.-K. Cd^{2+} triggered the FRET "ON": A new molecular switch for the ratiometric detection of Cd^{2+} with live-cell imaging and bound X-ray structure. *Inorg. Chem.* **2015**, *54*, 7309–7315. [CrossRef]

173. Zhang, L.; Hu, W.; Yu, L.; Wang, Y. Click synthesis of a novel triazole bridged AIE active cyclodextrin probe for specific detection of Cd^{2+}. *Chem. Commun.* **2015**, *51*, 4298–4301. [CrossRef]

174. Teolato, P.; Rampazzo, E.; Arduini, M.; Mancin, F.; Tecilla, P.; Tonellato, U. Silica nanoparticles for fluorescence sensing of Zn(II): Exploring the covalent strategy. *Chemistry* **2007**, *13*, 2238–2245. [CrossRef]

175. Pal, P.; Rastogi, S.K.; Gibson, C.M.; Aston, D.E.; Branen, A.L.; Bitterwolf, T.E. Fluorescence sensing of zinc(II) using ordered mesoporous silica material (MCM-41) functionalized with *N*-(quinolin-8-yl)-2-[3-(triethoxysilyl) propylamino] acetamide. *ACS Appl. Mater. Interfaces* **2011**, *3*, 279–286. [CrossRef]

176. Ding, Y.; Zhu, W.; Xu, Y.; Qian, X. A small molecular fluorescent sensor functionalized silica microsphere for detection and removal of mercury, cadmium, and lead ions in aqueous solutions. *Sens. Actuators B Chem.* **2015**, *220*, 762–771. [CrossRef]

177. Huang, W.-B.; Gu, W.; Huang, H.-X.; Wang, J.-B.; Shen, W.-X.; Lv, Y.-Y.; Shen, J. A porphyrin-based fluorescent probe for optical detection of toxic Cd^{2+} ion in aqueous solution and living cells. *Dyes Pigments* **2017**, *143*, 427–435. [CrossRef]

178. Krishnaveni, K.; Iniya, M.; Jeyanthi, D.; Siva, A.; Chellappa, D. A new multifunctional benzimidazole tagged coumarin as ratiometric fluorophore for the detection of Cd^{2+}/F^- ions and imaging in live cells. *Spectrochim. Acta Part A* **2018**, *205*, 557–567. [CrossRef] [PubMed]

179. Kumar, A.; Ahmed, N. A coumarin–chalcone hybrid used as a selective and sensitive colorimetric and turn-on fluorometric sensor for Cd^{2+} detection. *New J. Chem.* **2017**, *41*, 14746–14753.

180. Roy, S.B.; Mondal, J.; Khuda-Bukhsh, A.R.; Rajak, K.K. A novel fluorene based "turn on" fluorescent sensor for the determination of zinc and cadmium: Experimental and theoretical studies along with live cell imaging. *New J. Chem.* **2016**, *40*, 9593–9608. [CrossRef]

181. Xu, L.; He, M.-L.; Yang, H.-B.; Qian, X. A simple fluorescent probe for Cd^{2+} in aqueous solution with high selectivity and sensitivity. *Dalton Trans.* **2013**, *42*, 8218–8222. [CrossRef] [PubMed]

182. Tuemmler, B.; Maass, G.; Voegtle, F.; Sieger, H.; Heimann, U.; Weber, E. Open-chain polyethers. Influence of aromatic donor end groups on thermodynamics and kinetics of alkali metal ion complex formation. *J. Am. Chem. Soc.* **1979**, *101*, 2588–2598. [CrossRef]

183. Tuemmler, B.; Maass, G.; Weber, E.; Wehner, W.; Voegtle, F. Noncyclic crown-type polyethers, pyridinophane cryptands, and their alkali metal ion complexes: Synthesis, complex stability, and kinetics. *J. Am. Chem. Soc.* **1977**, *99*, 4683–4690. [CrossRef]

184. Weber, V.E.; Vogtle, F. Kristalline 1:1-alkalimetallkomplexe nichtcyclischer neutralliganden. *Tetrahedron Lett.* **1975**, *16*, 2415–2418. [CrossRef]

185. Liu, X.; Li, N.; Xu, M.-M.; Jiang, C.; Wang, J.; Song, G.; Wang, Y. Turn on fluorescent detection for Cd^{2+} based on surfactant controlled squaraine aggregation. *Spectrochim. Acta Part A* **2019**, *208*, 236–242. [CrossRef]

186. Liu, X.; Wang, P.; Fu, J.; Yao, K.; Xue, K.; Xu, K. Turn-on fluorescent sensor for zinc and cadmium ions based on quinolone and its sequential response to phosphate. *J. Lumin.* **2017**, *186*, 16–22. [CrossRef]

187. Song, E.J.; Kang, J.; You, G.R.; Park, G.J.; Kim, Y.; Kim, S.-J.; Kim, C.; Harrison, R.G. A single molecule that acts as a fluorescence sensor for zinc and cadmium and a colorimetric sensor for cobalt. *Dalton Trans.* **2013**, *42*, 15514–15520. [CrossRef]

188. Zhang, Y.-Y.; Chen, X.-Z.; Liu, X.-Y.; Wang, M.; Liu, J.-J.; Gao, G.; Zhang, X.-Y.; Sun, R.-Z.; Hou, S.-C.; Wang, H.-M. A highly sensitive multifunctional sensor based on phenylene-acetylene for colorimetric detection of Fe^{2+} and ratiometric fluorescent detection of Cd^{2+} and Zn^{2+}. *Sens. Actuators B Chem.* **2018**, *273*, 1077–1084. [CrossRef]

189. Zhang, W.J.; Liu, S.G.; Han, L.; Luo, H.Q.; Li, N.B. A ratiometric fluorescent and colorimetric dual-signal sensing platform based on N-doped carbon dots for selective and sensitive detection of copper(II) and pyrophosphate ion. *Sens. Actuators B Chem.* **2019**, *283*, 215–221. [CrossRef]

190. Plácido, J.; Bustamante-López, S.; Meissner, K.; Kelly, D.; Kelly, S. Microalgae biochar-derived carbon dots and their application in heavy metal sensing in aqueous systems. *Sci. Total Environ.* **2019**, *656*, 531–539. [CrossRef]

191. Huang, L.; Yang, Z.; Zhou, Z.; Li, Y.; Tang, S.; Xiao, W.; Hu, M.; Peng, C.; Chen, Y.; Gu, B. A dual colorimetric and near-infrared fluorescent turn-on probe for Hg^{2+} detection and its applications. *Dyes Pigments* **2019**, *163*, 118–125. [CrossRef]

192. Amanulla, B.; Perumal, K.N.; Ramaraj, S.K. Chitosan functionalized gold nanoparticles assembled on sulphur doped graphitic carbon nitride as a new platform for colorimetric detection of trace Hg^{2+}. *Sens. Actuators B Chem.* **2019**, *281*, 281–287. [CrossRef]

193. Manivannan, S.; Seo, Y.; Kang, D.-K.; Kim, K. Colorimetric and optical Hg(II) ion sensor developed with conjugates of M13-bacteriophage and silver nanoparticles. *New J. Chem.* **2018**, *42*, 20007–20014. [CrossRef]

194. Bahta, M.; Ahmed, N. Design and synthesis of 1,4-benzothiazine hydrazide as selective and sensitive colorimetric and turn-on fluorometric sensor for Hg^{2+} detection in aqueous medium. *J. Photochem. Photobiol. A* **2018**, *357*, 41–48. [CrossRef]

195. Chatterjee, A.; Banerjee, M.; Khandare, D.G.; Gawas, R.U.; Mascarenhas, S.C.; Ganguly, A.; Gupta, R.; Joshi, H. Aggregation-induced emission-based chemodosimeter approach for selective sensing and imaging of Hg(II) and methylmercury species. *Anal. Chem.* **2017**, *89*, 12698–12704. [CrossRef] [PubMed]

196. Gao, Y.; Ma, T.; Ou, Z.; Cai, W.; Yang, G.; Li, Y.; Xu, M.; Li, Q. Highly sensitive and selective turn-on fluorescent chemosensors for Hg^{2+} based on thioacetal modified pyrene. *Talanta* **2018**, *178*, 663–669. [CrossRef]

197. Nakanishi, T.; Suzuki, M.; Saimoto, A.; Kabasawa, T. Structural considerations of NK109, an antitumor benzo[c]phenanthridine alkaloid. *J. Nat. Prod.* **1999**, *62*, 864–867. [CrossRef]

198. Takao, N.; Kamigauchi, M.; Okada, M. Biosynthesis of benzo[c]phenanthridine alkaloids sanguinarine, chelirubine and macarpine. *Helv. Chim. Acta* **1983**, *66*, 473–484. [CrossRef]

199. Ponram, M.; Balijapalli, U.; Sambath, B.; Iyer, S.K.; Venkatachalapathy, B.; Cingaram, R.; Sundaramurthy, K.N. Development of paper-based chemosensor for the detection of mercury ions using mono-and tetra-sulfur bearing phenanthridines. *New J. Chem.* **2018**, *42*, 8530–8536. [CrossRef]

200. Shyamal, M.; Maity, S.; Maity, A.; Maity, R.; Roy, S.; Misra, A. Aggregation induced emission based "turn-off" fluorescent chemosensor for selective and swift sensing of mercury(II) ions in water. *Sens. Actuators B Chem.* **2018**, *263*, 347–359. [CrossRef]

201. Rurack, K. Flipping the light switch 'ON'—The design of sensor molecules that show cation-induced fluorescence enhancement with heavy and transition metal ions. *Spectrochim. Acta Part A* **2001**, *57*, 2161–2195. [CrossRef]

202. Shimizu, Y.; Azumi, T. Mechanism of external heavy atom effect on intersystem crossing in fluid solutions. Analysis based on fluorescence decay data. *J. Phys. Chem.* **1982**, *86*, 22–26. [CrossRef]

203. Fang, Y.; Li, X.; Li, J.-Y.; Wang, G.-Y.; Zhou, Y.; Xu, N.-Z.; Hu, Y.; Yao, C. Thiooxo-Rhodamine B hydrazone derivatives bearing bithiophene group as fluorescent chemosensors for detecting mercury(II) in aqueous media and living HeLa cells. *Sens. Actuators B Chem.* **2018**, *255*, 1182–1190. [CrossRef]

204. Jones, M.M.; Vaughn, W.K. HSAB theory and acute metal ion toxicity and detoxification processes. *J. Inorg. Nucl. Chem.* **1978**, *40*, 2081–2088. [CrossRef]

205. Pearson, R.G. Hard and soft acids and bases, HSAB, part II: Underlying theories. *J. Chem. Educ.* **1968**, *45*, 643–648. [CrossRef]

206. Pearson, R.G. Hard and soft acids and bases, HSAB, part 1: Fundamental principles. *J. Chem. Educ.* **1968**, *45*, 581–587. [CrossRef]

207. Shu, T.; Yang, Z.; Cen, Z.; Deng, X.; Deng, Y.; Dong, C.; Yu, Y. A novel ratiometric fluorescent probe based on a BODIPY derivative for Cu^{2+} detection in aqueous solution. *Anal. Methods* **2018**, *10*, 5755–5762. [CrossRef]

208. Sun, W.; Chen, R.; Cheng, X.; Marin, L. Bodipy-based chemosensors for highly sensitive and selective detection of Hg^{2+} ions. *New J. Chem.* **2018**, *42*, 19224–19231. [CrossRef]

209. Zhou, B.; Qin, S.; Chen, B.; Han, Y. A new BODIPY-based fluorescent "turn-on" probe for highly selective and rapid detection of mercury ions. *Tetrahedron Lett.* **2018**, *59*, 4359–4363. [CrossRef]

210. Gu, Z.; Cheng, H.; Shen, X.; He, T.; Jiang, K.; Qiu, H.; Zhang, Q.; Yin, S. A BODIPY derivative for colorimetric fluorescence sensing of Hg^{2+}, Pb^{2+} and Cu^{2+} ions and its application in logic gates. *Spectrochim. Acta Part A* **2018**, *203*, 315–323. [CrossRef] [PubMed]

211. Gao, Y.; Zhang, C.; Peng, S.; Chen, H. A fluorescent and colorimetric probe enables simultaneous differential detection of Hg^{2+} and Cu^{2+} by two different mechanisms. *Sens. Actuators B Chem.* **2017**, *238*, 455–461. [CrossRef]

212. Li, Q.; Hu, Y.; Hou, H.-N.; Yang, W.-N.; Hu, S.-L. A new coumarin-carbonothioate-based turn-on fluorescent chemodosimeter for selective detection of Hg^{2+}. *Inorg. Chim. Acta* **2018**, *471*, 705–708. [CrossRef]

213. Patai, S. *Chemistry of the Carbon-Nitrogen Double Bond*; John Wiley and Sons: Chichester, UK, 1970.

214. Machado, V.G.; Nascimento, M.; Rezende, M. Metal ion catalysis in the hydrolysis of imines. *J. Braz. Chem. Soc.* **1993**, *4*, 76–79. [CrossRef]

215. Jiao, Y.; Liu, X.; Zhou, L.; He, H.; Zhou, P.; Duan, C. A schiff-base dual emission ratiometric fluorescent chemosensor for Hg^{2+} ions and its application in cellular imaging. *Sens. Actuators B Chem.* **2017**, *247*, 950–956. [CrossRef]

216. Smith, D.G.; Topolnicki, I.L.; Zwicker, V.E.; Jolliffe, K.A.; New, E.J. Fluorescent sensing arrays for cations and anions. *Analyst* **2017**, *142*, 3549–3563. [CrossRef]

217. Sasaki, Y.; Minamiki, T.; Tokito, S.; Minami, T. A molecular self-assembled colourimetric chemosensor array for simultaneous detection of metal ions in water. *Chem. Commun.* **2017**, *53*, 6561–6564. [CrossRef]

218. Mallet, A.M.; Davis, A.B.; Davis, D.R.; Panella, J.; Wallace, K.J.; Bonizzoni, M. A cross reactive sensor array to probe divalent metal ions. *Chem. Commun.* **2015**, *51*, 16948–16951. [CrossRef]

219. Jing, X.-Y.; Tang, Y.-Y.; Zhang, D. A Fourier–LDA approach for image recognition. *Pattern Recognit.* **2005**, *38*, 453–457. [CrossRef]